ENERGY LOSS OF CHARGED PROJECTILES IN A DUSTY PLASMA

MAQSOOD-UL-HASAN NASIM

DEPARTMENT OF PHYSICS
QUAID-I-AZAM UNIVERSITY
ISLAMABAD PAKISTAN

1999

This work is submitted as a thesis in
partial fulfillment of
the requirement for the award of the degree of

DOCTOR OF PHILOSOPHY
in
PHYSICS

Department of Physics
Quaid-i-Azam University
Islamabad, Pakistan

CERTIFICATE

Certified that the work contained in this thesis was carried out by **Mr. Maqsood-ul-Hasan Nasim** under our supervision.

Dr. Arshad Majid Mirza
Co-Supervisor
Department of Physics
Quaid-i-Azam University
Islamabad, Pakistan

Prof. Dr. G. Murtaza
Supervisor
Department of Physics
Quaid-i-Azam University
Islamabad, Pakistan

Submitted through

Prof. Dr. M. Zafar Iqbal
Chairman
Department of Physics
Quaid-i-Azam University
Islamabad, Pakistan

To
My Late Parents
And
My Family

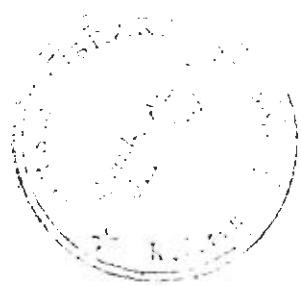

ACKNOWLEDGEMENTS

All praises to ALMIGHTY ALLAH, the most benevolent and merciful, the creator of the universe, who enabled me to complete this thesis.

I think the Holy Prophet MUHAMMAD (peace be upon Him) is for ever a source of guidance and knowledge for humanity as a whole.

First and foremost, I want to express my deepest gratitude to my respectable supervisor Professor G. Murtaza, for his kind and invaluable guidance. His sympathetic attitude and encouraging discussions enabled me in broadening and improving my capabilities not only in physics, but in other aspects of life also.

My immense gratitude goes to Dr. Arshad M. Mirza, my Co-supervisor who graciously extended me every possible help whenever needed. He has stimulated my imagination and has given me insight of research. Special thanks are also due to Dr. M. Zakaullah from whom I learnt a lot and to Dr. M. S. Qaisar (PAEC), Dr. N. A. D. Khatak, Gomal University, D. I. Khan.

I am extremely grateful to Dr. Masud Ahmad, Director, Chairman's Secretariat of PAEC who was very kind and who provided me an opportunity to do this research work.

Very special thanks are due to Prof. P. K. Shukla Ruhr University, Bochum, Germany, and for initiating me in the field of Dusty Plasma and for many fruitful discussions.

I am grateful to Professor M. Zafar Iqbal, Chairman, Department of Physics, for providing the research facilities and moral support.

I also wish to thank all my teachers and friends (especially Zahoor Ahmad and Ziaullah) for their liberal cooperation during the completion of this work.

My heartiest thanks to each member of Plasma Physics Group at Quaid-i-Azam University, and colleagues (M. Salahuddin, Abdul Hamid, M. M. Raja, M. T. Naseem, A. Niaz, S. Tanweer Hassan, S. R. Khan, Mrs. Shadab Kamal) and all liberary staff (especially Mr. Tanweer Ahmad, S. Sajid Hussain and Mr Taj Muhammad) in my office who helped me in one way or other.

I am under great debt to my brother and sister who infused a spirit of steadfastness, patience and perservence to continue this task of research work.

Last but not the least, I wish to record my deepest obligations to my children and my wife for their sustained love and cooperation.

(Maqsood-ul-Hasan Nasim)

Contents

Erratum

- Page (VII) number 7, M. S. Qaisar is deleted.
- Page 15 after Eq.(2.17)

$$\phi_1(\mathbf{X},t)=\frac{2\pi q_t\delta(\mathbf{X}-\mathbf{V_t}t)}{K^2\epsilon(\mathbf{K},\omega)} \text{ Replace with } \frac{8\pi^2 q_t\delta(\mathbf{X}-\mathbf{V_t}t)}{K^2\epsilon(\mathbf{K},\omega)}$$

- Page 15 after Eq. (2.17), Using this space charge density ....the word space be replaced with **test ....**
- Page 17, Eq. (2.21) a word μ is missing.
- Page 17, in Eq. (2.21) $q_t \rightarrow q_t^2$
- Page 18 , in the de nation of K_{max}

$$K_{\max}=\frac{q_t q_\alpha}{m(V_t^2+V_\alpha^2)}$$

- Page 20, in the last term of the Eq. (3.4), $\nabla\cdot\mathbf{E}\rightarrow\nabla\times\mathbf{B}$
- Page 21 correct form of Eq. (3.5) is

$$n_{s1}=n_{s0}\exp\left(-\frac{\phi_1}{T_s}\right)$$

- Page 25, Eq. (3.26), in the denominatoe of this equation K_D^2 be added

$$S=\frac{Z_t^2 N_D Z_d}{2\pi}\int_0^{K_{max}} dK\,K\frac{Y(\varpi)}{\left[K^2+K_D^2+X(\varpi)\right]^2+Y^2(\varpi)} \tag{1}$$

- Page 26 , 2nd line (2.14) be replaced with (3.4).
- Page 27 where $\mu=\cos(\mathbf{K},\mathbf{V}_t)$

  replace $\rho=x\cos\theta_1\rightarrow\rho=X\sin\theta_1$
  replace $x=X\sin\theta_1\rightarrow x=X\cos\theta_1$
  Page 27 in Eq.(3.33) K_D^2 be added in the denominator.

$$S=\frac{Z_t^2 Z_d N_D}{2\pi^2}\int_0^{K_{max}} K^3dK\int_{-1}^{1}\mu d\mu\frac{Y}{\left(K^2+K_D^2+X\right)^2+Y^2} \tag{2}$$

- Page 41, Fig. 4-5.

  Please interchange the vectors **D** and **B**

List of Publications

(The reference number 3-8 and 9 only are included in the thesis)

1. Implosion of Two-gas gas-puff $Z-\theta$ pinch

   Physics Scripta, Vol. **49**, pp. 345-348, 1994.

   M. Salahuddin and **M. H. Nasim**

2. Thermal effects on the dynamics of two-gas gas-puff $Z-\theta$ pinch

   J. Plasma Physics, Vol. **53**, part 2 pp. 135-143,1995.

   M. H. Nasim, M. Salahuddin, and Arshad M. Mirza

3. Energy loss of charged projectiles in dusty plasmas,

   Physics of Plasmas, Vol. **5**, Number 10, pp.3581-87 (1998).

   M. H. Nasim, Arshad M. Mirza, M. S. Qaisar, G. Murtaza and P. K. Shukla.

4. Effect of dust charge fluctuations on energy loss of a test dust charged particulate in a dusty plasma

   Physics of Plasmas, Vol. **6**, Number 5, pp.1409-14 (1999).

   M. H. Nasim, P. K. Shukla, and G. Murtaza

5. Energy loss of a test charge in dusty plasmas: Collective and individual particle contributions

   Physica Scripta, Vol. **59**, pp. 379-388, 1999.

   M. H. Nasim, Arshad M. Mirza, G. Murtaza and P. K. Shukla

6. Energy loss of a test charge in partially ionized dusty plasmas,

   Physics of Plasmas, Vol. **7**, Number 2, 2000 (appear in).

   M. H. Nasim, M. S. Qaisar, Arshad M. Mirza, G. Murtaza and P. K. Shukla

7. Energy loss of a test charge in collisional dusty plasmas,

   Physica Scripta, Vol. **60**, 2000 (appear in).

   M. H. Nasim, M. S. Qaisar, Arshad M. Mirza, G. Murtaza and P. K. Shukla

8. Anisotropy in the energy loss of charged projectiles in plasmas

   Physics of Plasmas, 2000 (Submitted to).

   M. H. Nasim, G. Murtaza and Arshad M. Mirza

Publication in conference proceeding:

9. Energy loss of a dust grain in dusty plasma

   "Proc. 7th National Symposium on Frontiers in Physics", Quaid-i-Azam University , Islamabad, Pakistan, 19-21 November, 1998.

   M. H. Nasim, M. S. Qaisar, Arshad M. Mirza, and G. Murtaza

List of Figures

Chapter 1

Introduction

1.1 Background

Understanding of the slowing down of fast particles (in other words the stopping power of the matter) in matter has significant role in the discovery and knowing of the constituents of matter ever since the beginning of the century. In 1948 Bohr[1] pointed out that a fast positively charged particle traversing matter induces an electronic polarization wake that trails behind the projectile and acts as a restoring force. Bohr gave a rough estimate of the stopping power of the media through which a test particle propagates. The concept of a polarization wake attracted little attention in the years following Bohr's work. In a plasma where, the problem of energy loss of fast particles has been studied by many authors[2, 3, 4] using different approximations. Many applications have been considered over wide ranges of plasma densities and temperatures including conditions of interest for astrophysical plasmas(stellar and interstellar media), solid-state plasmas, cold and hot laboratory plasmas. The energy loss of fast particles under extreme conditions of plasma like in the studies of inertial confinement fusion (ICF) and magnetic confinement fusion (MCF) has also been discussed[5, 6]. In terms of classical mechanics, the rate of energy relaxation of a charged particle in a plasma was given by Spitzer[7], based on the earlier results of Chandrasekhar[8], who studied the analogous problem of energy relaxation of a star moving in the presence of the gravitational perturbations from a cluster of stars. Further description along similar lines were given[9, 10] by considering binary collisions of the charged particles with the electrons

and ions in the plasma.

The study of interaction of the charged particles with matter is relevant in many areas, for example, there has been a growing interest in the energy loss of heavy ions in dense plasmas in view of the potential applications of intense heavy-ion beams[3, 11] (IHIB) and cluster-ion beams [12] (CIB) in the fields of ICF and heavy-ion pumped[13] x-ray lasers. In the CIB one considers the interaction of fluorene-like, carbon-like, or metallic clusters with solids and hot plasma targets. Another important area of interest is in the context of ICF in which the reaction products (such as alpha particles) interact with matter and deposit their energy in the fusion reaction zone, known as self-heating. By estimating the amount of self-heating, the driver energy requirement can be calculated[14].

In low temperature laboratory plasmas such as in plasma processing, plasma coating, radio-frequency discharges[15] and Tokamak edge etc., a large number of very massive micron-sized dust particles/impurities are present. They acquire a negative or positive charge depending upon the ambient plasma condition. These particles move about in the plasma, interact with themselves and with the plasma particles. The space and astrophysical [16, 17] plasmas such as earth ionosphere, molecular cloud, cometary tails, interstellar medium etc., are full of dust particles through which a large number of particles are streaming. These dust particles introduce some new collective effects[18] which can significantly influence the energy loss scenario.

It is well known that the presence of charged dust particles alter[18] the spectra of the usual ion acoustic (IA) and the electrostatic ion- cyclotron (EIC) waves. In addition, the dynamics of charged dust grains provides the possibility of a novel dust-acoustic wave[19] (DAW). In the latter, the restoring force comes from the pressure of the inertialess electrons and ions, while the inertia is provided by the dust mass. The dust ion-acoustic waves (DIAW)[20] and the dust acoustic waves are subjected to a very weak Landau[21] and a non-Landau[22, 23] damping; the latter are caused by the dust charge perturbations. Indeed, both the DIAW and the DAW's have been observed experimentally[24, 25, 26].

To get some idea of these low-frequency modes, dispersion relations for DIAW and DAW are derived in the next section.

1.2 Waves in dusty plasmas

The dispersion relation for DIA waves can be calculated, by treating electrons as a Boltzmann type while ions as a fluid. The Dust provides an immobile neutralizing background. The charge neutrality of the plasma is given as $n_i = n_e + Z_d n_d$, where n_α is the number density of the $\alpha-$species (α equals e for electrons, i for ions and d for dusts) and Z_d is the dust charge state. The subscript 0 (1) will represent the equilibrium (perturbed) quantities. For the DIAW ($V_{ti} < \omega/K < V_{te}$) the dispersion relation is given as

$$\frac{\omega^2}{K^2} = V_{ti}^2 + \frac{T_e/m_i}{\left(1 + K^2\lambda_{De}^2\right)\left(1 - Z_{d0}\frac{n_{d0}}{n_{i0}}\right)}$$

where $V_{t\alpha} = T_\alpha/m_\alpha$ is the thermal velocity, T_α is the temperature(in energy units), $n_{\alpha 0}$ is the equilibrium number density and m_α is the mass of $\alpha-$ species. This will be reduced to the usual ion acoustic waves in the absence of dust particles.

In the low phase velocity ($V_{td} \ll \omega/K \ll V_{ti}, V_{te}$), the number densities of electrons and ions are of Boltzmann type, while the dust is treated as a fluid. The dynamics of dust is governed by the equation of motion and continuity equation. The dispersion relation for DAW will become

$$\frac{\omega^2}{K^2} = V_{td}^2 + \frac{n_{d0}}{n_{i0}} \frac{Z_{d0}T_i/m_d}{\left(1 + K^2\lambda_D^2\right)\left(1 + \frac{T_i}{T_e}\left(1 - Z_{d0}\frac{n_{d0}}{n_{i0}}\right)\right)}$$

where $\lambda_D^2 \left(= \lambda_{De}^2 + \lambda_{Di}^2\right)$ is the effective Debye length. Until now we have assumed that the charge on the dust particle is constant. In reality it is a time dependent variable [27]. In such a situation the dispersion relation for DIAW can be written as

$$\frac{\omega^2}{K^2} = V_{ti}^2 + \frac{T_e/m_i}{\left(1 + K^2\lambda_{De}^2 - iK^2\lambda_{De}^2\frac{\nu_c\beta}{\omega + i\nu_0}\right)\left(1 - Z_{d0}\frac{n_{d0}}{n_{i0}}\right)}$$

and for DAW

$$\frac{\omega^2}{K^2} = V_{td}^2 + \frac{n_{d0}}{n_{i0}} \frac{Z_{d0}T_i/m_d}{\left(1 + K^2\lambda_D^2 - iK^2\lambda_D^2\frac{\nu_c\beta}{\omega + i\nu_0}\right)\left(1 + \frac{T_i}{T_e}\left(1 - Z_{d0}\frac{n_{d0}}{n_{i0}}\right)\right)}$$

where $\nu_c = 4\pi e n_{d0}$ is the dust charge density per dust charge state and ν_0 is the charge relaxation rate given as

$$\nu_0 = |I_{e0}| \frac{e}{C} \left[\left(T_e + e\varphi_{f0} \right)^{-1} + \left(T_i - e\varphi_{f0} \right)^{-1} \right]$$

where C is the capacitance, φ_{f0} is the equilibrium floating potential on the dust particle, I_{e0} is the equilibrium current reaching the grain surface and β is the parameter[28], given as

$$\beta = |I_{e0}| \left[T_e^{-1} + T_i^{-1} \right]$$

In a dusty plasma a large number of neutral dust particles are always present. These dust particles are being charged by the continuous electrons and ions currents on the surface of dust grains (particles). The charging of the dust particles is very fast as compared to the plasma oscillations and collisions between the charged and uncharged dust particles. In the low-phase velocity regimes, incorporating the dust-neutral collisions, the dispersion relations for DIAW and DAW can be modified respectively, as

$$\frac{\omega(\omega + i\nu_d)}{K^2} = V_{ti}^2 + \frac{T_e/m_i}{\left(1 + K^2\lambda_{De}^2\right)\left(1 - Z_{d0}\frac{n_{d0}}{n_{i0}}\right)}$$

and

$$\frac{\omega(\omega + i\nu_d)}{K^2} = V_{td}^2 + \frac{n_{d0}}{n_{i0}} \frac{Z_{d0}T_i/m_d}{\left(1 + K^2\lambda_D^2\right)\left(1 + \frac{T_i}{T_e}\left(1 - Z_{d0}\frac{n_{d0}}{n_{i0}}\right)\right)}$$

where ν_d is the dust-neutral collision frequency. As mentioned earlier, the dust grains are very massive of the order of micron size, and therefore the gravitational potential also becomes important. By using the gravitational force, the dust equation of motion will be modified as

$$m_d \frac{\partial V_{d1}}{\partial t} = -\frac{T_d \nabla n_{d1}}{n_{d0}} + Z_{d0} e \nabla \phi - m_d \nabla \psi,$$

where

$$\nabla^2 \phi = 4\pi e \left(n_{i1} - n_{e1} - Z_{d0} n_{d1} \right)$$

$$\nabla^2\psi \;=\; 4\pi G m_d n_{d1}.$$

Coupling with the dust continuity equation, the dispersion relations for DIAW and DAW can be written respectively, as

$$\frac{\omega^2}{K^2} = V_{ti}^2 - \frac{\omega_J^2}{k^2} + \frac{T_e/m_i}{\left(1+K^2\lambda_{De}^2\right)\left(1-Z_{d0}\frac{n_{d0}}{n_{i0}}\right)}$$

and

$$\frac{\omega^2}{K^2} = V_{td}^2 - \frac{\omega_J^2}{k^2} + \frac{n_{d0}}{n_{i0}}\frac{Z_{d0}T_i/m_d}{\left(1+K^2\lambda_D^2\right)\left(1+\frac{T_i}{T_e}\left(1-Z_{d0}\frac{n_{d0}}{n_{i0}}\right)\right)}$$

where $\omega_J = \sqrt{4\pi G m_d^2 n_d/m_d}$ is the Jean's frequency[29]. It is worth mentioning that Jean's frequency is an analogue of the plasma frequency in which mass is used in the place of charge.

The general form of the dispersion relation, incorporating dust charge fluctuations, dust-neutral collisions and dust gravitational potential is

$$\frac{\omega(\omega+i\nu_d)}{K^2} = V_{ti}^2 - \frac{\omega_j^2}{K^2} + \frac{T_e/m_i}{\left(1+K^2\lambda_{De}^2 - iK^2\lambda_{De}^2\frac{\nu_c\beta}{\omega+i\nu_0}\right)\left(1-Z_{d0}\frac{n_{d0}}{n_{i0}}\right)}$$

for DIA waves

$$\frac{\omega(\omega+i\nu_d)}{K^2} = V_{td}^2 - \frac{\omega_j^2}{K^2} + \frac{n_{d0}}{n_{i0}}\frac{Z_{d0}T_i/m_d}{\left(1+K^2\lambda_D^2 - iK^2\lambda_D^2\frac{\nu_c\beta}{\omega+i\nu_0}\right)\left(1+\frac{T_i}{T_e}\left(1-Z_{d0}\frac{n_{d0}}{n_{i0}}\right)\right)}$$

for DA waves.

In the next section we will discuss the energy loss scenario of dust particles.

1.3 Energy loss scenario

An important process in the interaction of charged particles and plasmas is the phenomenon of the energy loss of the particles which occurs due to localized collisions and due to excitations of collective modes in the plasma. Inside the Debye sphere small-scale collisions of pairs of particles dominate whereas away from the Debye sphere large-scale collective effects such as plasma excitations, become important. For dimensions smaller than the Debye length,

individual particle behavior dominates and the particles interact via two body screening potential. For dimensions larger than the Debye screening length, the plasma acts as a continuous medium in which the charged particles participate in collective behavior such as plasma oscillations. The contribution to the energy loss via individual particle interaction is generally small, yet it must be included in the total energy loss.

1.4 Motivation

The study of dusty plasma is important for at least three different scientific communities of plasma research. Astrophysicist and space theorists were the first who took interest in the study of dusty plasmas because the Heavens are full of dusty plasmas such as planetary rings, comet tails and nebulae. Interest sparked by the space craft such as the voyagers, which revealed the presence of the dust particles immersed in planetary magnetospheric plasmas. The dust particles were seen by Mie scattering of sunlight and detected electrically by their impact upon the space craft. In the last few years industrial plasma processing researchers have discovered that particles suspended in plasmas are a major cause of costly wafer contamination during semiconductor manufacturing. It was found that the plasmas used for deposition and etching can grow particles in the gas phase, or they can release them from vacuum vessel walls. The particles become charged in the plasmas, and they levitate above the wafers, until the fateful moment comes when the plasma is switched off and they fall on the substrate. Much effort has been made to understand particle growth, charging of the dust, levitation and transport in order to devise schemes aimed at avoiding contamination. For basic plasma physics researchers, dusty plasma offers a wide and unexplored territory, such as waves, instabilities and strongly coupled plasma. The presence of dust particles modifies the collective behavior of the plasmas, sometimes only deplete the electrons, while in the low phase velocity, the dust response to new collective electric fields, and new waves and instabilities are born that were previously unknown. Recognizing the great overlap in the physics of these different areas, and the rapid growth of interest in dusty plasmas, motivate us to study the dusty plasma.

A dielectric formulation of the energy-loss rate was studied by Pines and Bohm[30],

Sitenko[31], and other workers for the case of dilute electron-ion plasmas. Neufeld and Ritchie[32] studied the interaction of charged particles with a plasma in early 1950s. They calculated the potential distribution as well as the energy loss of a test charge in an electron plasma by considering fixed background of ions. This work was further extended by incorporating the dynamics of ions[33, 34]. Arista and Ponce[35] evaluated the energy loss using a simplified model to describe long-(short-) wavelength collective-(individual-) excitations for an electron gas. Later[36], the energy loss of a pair of charges in correlated motion was calculated through a degenerate electron gas by using Lindhard's dielectric function. There are several evidences of the presence of correlation effects in connection with the interaction of ion clusters with condensed matters[12, 37, 38, 39].

In this thesis, we have studied[40, 41, 42] the energy loss of dust grains in the dusty plasma by using the linearized Vlasov theory. We have presented a simple derivation of the electrostatic potential and the energy loss of two charged projectiles travelling through dusty plasma. The correlation effects of the two projectiles on the electrostatic (ES) potential and the energy loss mechanism are presented. A comparison has been made for correlated and un-correlated numerical results of the ES potentials and the energy losses.

The dust particles acquire hundred thousands electron charges on its surface. The dust grains are in various sizes and have different charges. Moreover, the dust charge does not remain constant and continuously fluctuates due to various plasma currents that flow onto the dust charge surface. These currents reaching the dust grain surface depend upon the ambient plasma conditions and the floating potential of the dust particle. In this way the dust charge becomes a dynamic variable and fluctuates about an equilibrium charge state. The effect of dust charge fluctuations[28, 43] and dust neutral collisions[44, 45] on the potential perturbations and the energy loss of test charge have been studied both analytically and numerically.

1.5 Layout of thesis

The previous section of this chapter contains the introduction to the energy loss of a test charge in plasma, occurrence of dusty plasma and the wave excitation in it. The next

chapter is devoted to the development of the theoretical background for understanding the dielectric theory and its role in the calculation of potential perturbation and the energy loss mechanism. A brief introduction of the test charge approach and the Debye screening of the test charge in the plasma is also given. In chapter **3** the energy loss of a dust grain is calculated in a multi-component dusty plasma by using linearized Vlasov-Poisson equation. Chapter **4** describes the correlation effect on the potential perturbation and energy loss of test charge moving in the trail of a leading projectile in dusty plasmas. The dust charge as mentioned earlier is a dynamic variable, so it fluctuates about an equilibrium charge state. The effects of dust charge fluctuations on the potential perturbation and energy loss are calculated in chapter **5**. There are always a number of neutral particles present in the dusty plasma. The effect of dust-neutral collisions are discussed in chapter **6**. Chapter **7** summarizes the results and its possible extension to future work.

Chapter 2

Theoretical Background

In this chapter we develope a theoretical background for the calculation of electrostatic potential by using the test charge approach. This potential is used to calculate the energy loss of the test charge.

2.1 Plasma as a dielectric medium

The plasma has been defined as a statistical ensemble of mobile charged particles; these charged particles move randomly in the system, interact with each other through their own electromagnetic forces, and response to the electromagnetic disturbance which may be applied from external sources. A plasma is therefore inherently capable of sustaining rich classes of electromagnetic phenomena.

A proper description of such electromagnetic phenomena may be obtained if we know a plasma response macroscopically to a given electromagnetic disturbance. The function which characterizes these responses is known as plasma response function. All the macroscopic properties of the plasma (as a medium) are contained in these response functions.

If the external disturbance to the plasma is a time dependent electric field $\mathbf{E}$, then the response function appears in the form of an induced displacement current $\mathbf{D}$. The relationship between field-current is the dielectric tensor as $\mathbf{D} = \epsilon\mathbf{E}$. This dielectric tensor is complete in the sense that it contains all the information about the linear electromagnetic properties of the plasma. It is sometimes quite useful to single out certain element of this tensor and

construct another response function known as the dielectric response function. This dielectric response function describes essentially the longitudinal properties of the plasma, and effectively describe the collective behavior of the plasma. In the next section we calculate this dielectric response function (dielectric constant), using Kinetic-Theoretical treatment of the plasma.

2.2 Kinetic-theoretical calculation of the dielectric constant

We calculate the dielectric response function of plasma within a kinetic-theoretical description for an unmagnetized plasma ($\mathbf{B} = 0$). For this purpose, we employ the Boltzmann-Vlasov equation coupled with Poisson's equation.

2.2.1 Vlasov-Poisson system

We define a single particle distribution function $f_\alpha(\mathbf{X}, \mathbf{V}, t)$ for the $\alpha-$species, the number density of plasma particles is given by

$$n_\alpha(\mathbf{X}, t) = n_{\alpha 0} \int f_\alpha(\mathbf{X}, \mathbf{V}, t)\, d\mathbf{V} \tag{2.1}$$

where $\mathbf{X}$ and $\mathbf{V}$ are space and velocity coordinates respectively in three dimensions and $n_{\alpha 0}$ is the equilibrium number density of the plasma particles. The distribution function $f_\alpha(\mathbf{X}, \mathbf{V}, t)$ obeys the Boltzmann-Vlasov equation as

$$(\partial_t + \mathbf{V} \cdot \nabla) f_\alpha - \frac{q_\alpha}{m_\alpha} \nabla\phi \cdot \nabla_v f_\alpha = \left(\frac{\partial f_\alpha}{\partial t}\right)_{coll} \tag{2.2}$$

where q_α is the charge and m_α is the mass of α-species and $\left(\frac{\partial f_\alpha}{\partial t}\right)_{coll}$ is the sum of collisions between the charged particles themselves and between the charged and neutrals particles. The electrostatic potential (ϕ) satisfies the Poisson's equation as

$$
\begin{aligned}
-\nabla^2\phi &= 4\pi\left(\rho_p + \rho_{ext}\right) \\
&= 4\pi\sum_\alpha q_\alpha n_{\alpha 0}\int f_\alpha(\mathbf{X},\mathbf{V},t)d\mathbf{V} + 4\pi\rho_{ext}
\end{aligned}
\tag{2.3}
$$

where ρ_{ext} represents the charge density of external particles such as beam of ions. The set of Vlasov-Poisson equations (2.2) and (2.3) therefore provide a complete kinetic description of a plasma in the fluid limit. In the next section we calculate the dielectric response function of plasma by using the perturbation technique and then calculate the electrostatic potential.

2.2.2 Perturbation analysis

We assume that the plasma is homogeneous and in a stationary state (at $t \to \infty$), the particle distribution function is Maxwellian i.e.;

$$
f_{\alpha 0}(\mathbf{V}) = \left(\frac{m_\alpha}{2\pi T_\alpha}\right)^{3/2}\exp\left(\frac{-m_\alpha V^2}{2T_\alpha}\right), \tag{2.4}
$$

where T_α is the temperature in energy units. We consider a small perturbation in the distribution function $f_{\alpha 1}(\mathbf{X},\mathbf{V},t)$ which causes the perturbation in the electrostatic potential $\phi_1(X,t)$ such that

$$
\begin{aligned}
f_\alpha(\mathbf{X},\mathbf{V},t) &= f_{\alpha 0}(\mathbf{V}) + f_{\alpha 1}(\mathbf{X},\mathbf{V},t) \\
\phi(\mathbf{X},t) &= \phi_0(\mathbf{X}) + \phi_1(\mathbf{X},t)
\end{aligned}
$$

Linearized form of the equations (2.2) and (2.3) for collisionless and field free plasma are

$$
\left(\partial_t + \mathbf{V}\cdot\nabla\right) f_{\alpha 1} - \frac{q_\alpha}{m_\alpha}\nabla\phi_1\cdot\nabla_{\mathbf{v}} f_{\alpha 0} = 0 \tag{2.5}
$$

and

$$
-\nabla^2\phi_1 = 4\pi\sum_\alpha q_\alpha\int f_{\alpha 1}(\mathbf{X},\mathbf{V},t)d\mathbf{V} + 4\pi\rho_{ext} \tag{2.6}
$$

The dielectric response function can be calculated by using the standard integral transform technique. The integral transform (Space-Time Fourier transform) can be defined as

$$\Psi\left(\mathbf{K},\omega\right)=\int d\mathbf{X}\int dt\Psi\left(\mathbf{X},t\right)\exp\left(-i\left[\mathbf{K}\cdot\mathbf{X}-\omega t\right]\right)$$

and the inverse transform as

$$\Psi\left(\mathbf{X},t\right)=\frac{1}{(2\pi)^4}\int d\mathbf{K}\int d\omega\Psi\left(\mathbf{K},\omega\right)\exp\left(i\left[\mathbf{K}\cdot\mathbf{X}-\omega t\right]\right)$$

Taking the Space-Time Fourier transform of equations (2.5) and (2.6), yield

$$f_{\alpha 1}(\mathbf{K},\mathbf{V},\omega)=-\frac{q_\alpha}{m_\alpha}\frac{\mathbf{K}\cdot\nabla_{\mathbf{v}}f_{\alpha 0}}{(\omega-\mathbf{K}\cdot\mathbf{V})}\phi_1\left(K,\omega\right) \tag{2.7}$$

$$K^2\phi_1\left(K,\omega\right)=4\pi\sum_\alpha q_\alpha n_{\alpha 0}\int f_{\alpha 1}(\mathbf{K},\mathbf{V},\omega)d\mathbf{V}+4\pi\tilde{\rho}_{ext} \tag{2.8}$$

where $\mathbf{K}$ is the wave vector, ω is the wave frequency and $\tilde{\rho}_{ext}$ is the Fourier transform of ρ_{ext}. Substituting the value of $f_{\alpha 1}(\mathbf{K},\mathbf{V},\omega)$ into Eq.(2.8) and solving for the potential, we get

$$\phi_1\left(K,\omega\right)=\frac{4\pi\tilde{\rho}_{ext}}{K^2\epsilon\left(K,\omega\right)} \tag{2.9}$$

where $\epsilon\left(K,\omega\right)$ is the dielectric response function [46], which plays a very important role to describe the behavior of the plasma and is written as

$$\epsilon\left(K,\omega\right)=1+\sum_\alpha\frac{\omega_{p\alpha}^2}{K^2}\int d\mathbf{V}\frac{\mathbf{K}\cdot\nabla_{\mathbf{v}}f_{\alpha 0}(\mathbf{V})}{\omega-\mathbf{K}\cdot\mathbf{V}} \tag{2.10}$$

where $\omega_{p\alpha}=\left(4\pi n_{\alpha 0}q_\alpha^2/m_\alpha\right)^{1/2}$ is the plasma frequency of the $\alpha-$species.

If the plasma is in thermodynamic equilibrium, then with the aid of Maxwellian velocity distribution we calculate this response function. If the system is isotropic, we may choose the wave vector along the V_x-axis. Then, the dielectric response function is

$$\epsilon\left(K,\omega\right)\;=\;1+\sum_\alpha\frac{K_{D\alpha}^2}{K^2}\frac{1}{\sqrt{2\pi}}\int_{-\infty}^{\infty}dV_x\frac{KV_x}{KV_x-\omega-i\eta}\exp\left(-\frac{m_\alpha V_x^2}{2T_\alpha}\right)$$

$$
\begin{aligned}
&= 1+\sum_{\alpha}\frac{K_{D\alpha}^2}{K^2}W\left(Z_\alpha\right)\\
&= 1+\sum_{\alpha}\chi_\alpha\left(K,\omega\right)
\end{aligned}
\tag{2.11}
$$

where $K_{D\alpha}=\omega_{p\alpha}/V_{t\alpha}$ is the Debye wave number and is the inverse of Debye length $\lambda_{D\alpha}=\sqrt{T_\alpha/4\pi nq_\alpha^2}$, $V_{t\alpha}=\sqrt{T_\alpha/m_\alpha}$ is the thermal velocity, $Z_\alpha=\omega/\left(KV_{t\alpha}\right)$, η is a small number which is used to ensure the convergence of the contour integration, $\chi_\alpha\left(K,\omega\right)$ is the susceptibility of the plasma particles and $W\left(Z\right)$ is the well known plasma dispersion function[46] defined as

$$
\begin{aligned}
W\left(Z\right) &= \frac{1}{\sqrt{2\pi}}\int_{-\infty}^{\infty}dx\frac{x}{x-Z-i\eta}\exp\left(-\frac{x^2}{2}\right)\\
&= 1+Z\exp(-Z^2/2)\left[i\sqrt{\frac{\pi}{2}}-\int_0^Z dy\exp\left(y^2/2\right)\right]
\end{aligned}
\tag{2.12}
$$

For the purpose of mathematical analysis, it is useful to find series expansion of $W\left(Z\right)$ for small and large arguments.

For $|Z|<1$, $W\left(Z\right)$ can be expressed in a convergent series as

$$
W\left(Z\right)=i\sqrt{\frac{\pi}{2}}Z\exp(-Z^2/2)+1-Z^2+\frac{Z^4}{3}-\cdots\cdots+\frac{(-1)^{n+1}\,Z^{2n+2}}{(2n+1)!!}
\tag{2.13}
$$

where

$$
(2n+1)!!=(2n+1)\,(2n-1)\,(2n-3)\cdots(3)(1)
$$

For $|Z|>1$, $W\left(Z\right)$ can be expressed in an asymptotic series as

$$
W\left(Z\right)=i\sqrt{\frac{\pi}{2}}Z\exp(-Z^2/2)-\frac{1}{Z^2}-\frac{3}{Z^4}-\cdots\cdots-\frac{(2n-1)!!}{Z^{2n}}
\tag{2.14}
$$

To calculate the electrostatic potential we use the test charge particle approach in the next section.

2.3 The test charge approach

The dressed test particle method has proved to be a very powerful tool to calculate the second order statistical function of a plasma. It is useful to calculate the potential due to a point test charge moving with a uniform speed V_t through a Vlasov plasma, which in the absence of the test charge is uniform and field-free. The charge density of the test charge is represented by

$$\rho_t = q_t \delta (\mathbf{X} - \mathbf{V}_t t) \tag{2.15}$$

where q_t is the test charge. This test charge can either be one of the plasma particle or a particle from the external beam, singled out as a test particle. If the test particle is at rest and background plasma is Maxwellian, the potential (ϕ) is a shielded potential. The test charge at rest polarizes the plasma, and acquires a shielding cloud. This shielding cloud is made up of an excess of charge having the opposite sign from q_t and a deficiency of charge having like sign. This shielding of charges is known as Debye screening. The ratio of the charge densities is inversely proportional to the temperatures. The plasma can be thought of as built up of a collection of these dressed test particles.

The potential field around a test charge particle located at the origin (X=0); in vacuum, is given as

$$\phi_C(\mathbf{X}) = \frac{q_t}{X} \tag{2.16}$$

In the plasma the spatial distribution of charged particles is effected by the presence of such a potential field and deviate from a uniform distribution. The space-charge field so induced around the point charge in turn produces an extra potential field, which should be added to the original potential $\phi_C(\mathbf{X})$; a new effective potential $\phi(\mathbf{X})$ is thus constructed as a summation of these two.

2.4 Dynamic Debye screening

As mentioned earlier that the dielectric response function provides a direct measure of the extent to which external test charge is screened by the induced space charge in the plasma. The screening is dynamic in the sense that it depends on the frequency variable as well as the wave vector. So, when the test charge is moving through a plasma with velocity V_t then the space-charge density associated with it is represented by Eq.(2.15), so that its Fourier components are

$$\tilde{\rho}_{ext}(\mathbf{K},\omega) = 2\pi q_t \delta(\omega - \mathbf{K}\cdot\mathbf{V}_t) \tag{2.17}$$

Using this value of space charge density into Eq.(2.9), the perturbed electrostatic potential will become

$$\phi_1(\mathbf{K},\omega) = \frac{2\pi q_t \delta(\omega - \mathbf{K}\cdot\mathbf{V}_t)}{K^2\epsilon(K,\omega)}$$

Carrying out the inverse transformation, we obtain the following result

$$\phi_1(\mathbf{X},t) = \frac{q_t}{2\pi^2}\int d\omega d\mathbf{K}\frac{\exp(i[\mathbf{K}\cdot\mathbf{X} - \omega t])}{K^2\epsilon(K,\omega)}\delta(\omega - \mathbf{K}\cdot\mathbf{V}_t)$$

Performing ω-integration, the ES potential[47, 48] will become

$$\phi_1(\mathbf{X},t) = \frac{q_t}{2\pi^2}\int d\mathbf{K}\frac{\exp(i\mathbf{K}\cdot[\mathbf{X} - \mathbf{V}_t t])}{K^2\epsilon(K,\mathbf{K}\cdot\mathbf{V}_t)} \tag{2.18}$$

The dynamic screening of the test charge for slow (fast) test charge velocity were calculated[49]. However, for a particular case in which the test charge is assumed to be stationary at the origin (i.e.,$\mathbf{V}_t = 0$) immersed in a steady-state electron plasma, the dielectric constant described by the Eq.(2.11), will reduce to

$$\epsilon(K,\omega) = 1 + 1/K^2\lambda_{De}^2$$

Substituting this value of dielectric constant into Eq.(2.18), we will get,

$$\phi_1(\mathbf{X}) = \frac{q_t}{2\pi^2}\int d\mathbf{K}\frac{\exp(i\mathbf{K}\cdot\mathbf{X})}{K^2 + \lambda_D^{-2}}$$

Performing three-dimensional K-integration, we obtain the following result for $\phi_1(\mathbf{X})$

$$\begin{aligned}\phi_1(\mathbf{X}) &= \frac{q_t}{\pi}\int dK \frac{K^2}{K^2+\lambda_D^{-2}}\int_{-1}^{1} d\gamma \exp\left[iKX\gamma\right] \\ &= \frac{q_t}{\pi}\int dK \frac{K^2}{K^2+\lambda_D^{-2}}\frac{\sin(KX)}{KX} \\ &= \frac{q_t}{X}\exp\left(-\frac{X}{\lambda_D}\right)\end{aligned}$$

where $\gamma = \cos(\mathbf{K},\mathbf{X})$. This potential is called Debye-Hückel potential.

$$\phi_D(X) = \frac{q_t}{X}\exp\left(-\frac{X}{\lambda_D}\right) \tag{2.19}$$

The Debye-Hückel potential along-with Coulomb potential is shown in Fig.(2.1). The space-charge distribution induced in the plasma is determined not only from the bare Coulomb potential $\phi_C(\mathbf{X})$, but also from the effective potential in a self-consistent fashion. The calculations along these lines were originally carried out by Debye and Hückel[50] in 1923 in connection with the theory of screening in a strong electrolyte. For distances much smaller than the Debye length, the effective potential is essentially equivalent to the bare Coulomb potential, while for distances larger than the Debye length, the potential field decrease exponentially; the potential field around a test point charge is effectively screened out by the induced space-charge field in the one component plasma (OCP). We extend these calculations to a multi-component dusty plasma case in which a test charge is moving with velocity $\mathbf{V}_t$.

2.5 Energy loss mechanism

The energy loss per unit path length (S) of the test charge particle moving with velocity $\mathbf{V}_t$ along the x-axis, in a reference frame in which the test charge is at rest, is the force $\mathbf{F}$[3] that the test charge particle experiences in its own induced field, i.e.,

$$S = -\frac{dW}{dx} = -\mathbf{F}\cdot\hat{\mathbf{e}}_x\,|_{\mathbf{x}=v_t t}$$

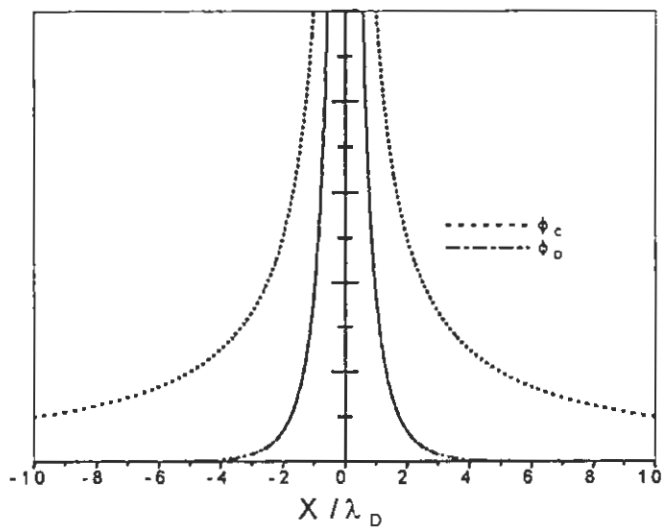

Figure 2-1: Comparison of Coulomb potential (ϕ_C) and Debye potential (ϕ_D) for $\lambda_D = 1$ and $q_t = 1$

$$= q_t \frac{\partial \phi_1}{\partial x} \mid_{\mathbf{x}=V_t t} \tag{2.20}$$

where W is the energy of the test charge and $\hat{\mathbf{e}}_x$ is a unit vector along the x-axis. Using the value of ϕ_1 from Eq.(2.19) into the above equation, we will get

$$\begin{aligned} S &= \frac{q_t}{2\pi^2} \int iKd\mathbf{K} \frac{\exp(i\mathbf{K}\cdot[\mathbf{X}-\mathbf{V}_t t])}{K^2\epsilon(K,\mathbf{K}\cdot\mathbf{V}_t)} \mid_{\mathbf{x}=V_t t} \\ &= \frac{q_t}{2\pi^2} \int Kd\mathbf{K} \frac{i}{K^2\epsilon(K,\mathbf{K}\cdot\mathbf{V}_t)} \end{aligned} \tag{2.21}$$

Since, the energy loss per unit length is a real quantity, therefore

$$\begin{aligned} S &= -\frac{q_t}{2\pi^2} \int Kd\mathbf{K}\, \mathrm{Im}\left[\frac{1}{K^2\epsilon(K,\mathbf{K}\cdot\mathbf{V}_t)}\right] \\ &= -\frac{q_t}{2\pi^2} \int_{-1}^{1} \mu d\mu \int_0^{\infty} dK K \int_0^{2\pi} d\varphi\, \mathrm{Im}\left[\frac{1}{\epsilon(K,K\mu V_t)}\right] \\ &= -\frac{q_t}{\pi} \int_{-1}^{1} \mu d\mu \int_0^{K_{max}} dK K\, \mathrm{Im}\left[\frac{1}{\epsilon(K,K\mu V_t)}\right] \end{aligned} \tag{2.22}$$

where $\mu = \cos(\mathbf{K}, \mathbf{V}_t)$ and $K_{\max}$ is the upper limit of the $K-$integration in order to avoid the logarithmic divergence for large $K-$values. In the last equation we have used dK in spherical co-ordinates. Classically, the maximum wave number[3] may be chosen in the vicinity of the inverse of a distance of closest approach between the test charge and a plasma particle. Hence, we may write

$$K_{\max} = \frac{q_t q_\alpha}{m(V_t + V_{t\alpha})}$$

The $K-$integration in the Eq.(2.22) can be split into $[0, K_{D\alpha}]$ for collective contributions and $[K_{D\alpha}, K_{\max}]$ for individual particle contributions.

While deriving this energy loss, it is necessary to calculate the potential distribution caused by the test charge moving in the multi-component dusty plasma. In the next chapter we discuss the energy loss of a test charge moving through a dusty plasma by employing the dielectric theory:

Chapter 3

Energy Loss Of A Dust Grain

The potential and energy loss of a single test charge particle are calculated both analytically and numerically, in a multi-component dusty plasma using dielectric theory.

3.1 Dusty plasma

Consider a multi-species dusty plasma whose constituents are electrons, singly ionized positive ions, and negatively charged dust grains with fixed charge state Z_{d0} and mass m_d. Since the charge on the dust grain is time dependent due to the continuous accumulation of electron and ion currents from the plasma, the emission of secondary electrons from the surface of the dust grain and photoionization process. Due to the said mechanisms the charge on the dust grain fluctuates around the equilibrium state. However, in this chapter, for simplicity, we ignore the charge fluctuations, which can be justified as long as the characteristic time scale of the charge fluctuation is shorter than the charging time scale. Since the charging is very fast as compared to the plasma oscillations in most of the laboratory plasmas, we can assume that the dust charge to be constant[51, 52]. The dust charge fluctuation will be considered in chapter 5 in some detail. The dusty plasma is characterized by the equilibrium number density n_{j0} mass m_j, charge q_j (equals $-e$ for electrons, e for ions and $-Z_{d0}e$ for dust particles) and the temperature $T_j (j = i, e, d)$, through which a test charge q_t with effective charge $Z_t e$ and mass M_t moves with the velocity $\mathbf{V}_t$ along the x-axis. Moreover, all the plasma particles are assumed to be point particles.

The ES potential and then energy loss per unit path length within the frame work of dielectric theory are calculated in a self-consistent way.

3.2 Self-consistent field approximation

A self-consistent field approximation was proposed by A. Vlasov in 1938 who showed that the electromagnetic field considered in the Maxwell's equations is the total field which is composed of external as well as induced field. The space charge and current densities can be written as

$$\rho = \sum q_j \int f_j(\mathbf{X}, \mathbf{V}, t)\, d\mathbf{V} \tag{3.1}$$

and

$$\mathbf{J} = \sum q_j \int \mathbf{V} f_j(\mathbf{X}, \mathbf{V}, t)\, d\mathbf{V} \tag{3.2}$$

Thus the interaction of plasma particles with fields has been taken into account because the distribution function itself satisfies the Kinetic equation, known as Vlasov equation,

$$(\partial_t + \mathbf{V}\cdot\nabla) f_j(\mathbf{X}, \mathbf{V}, t) + \frac{q_j}{m_j}\left[\mathbf{E} + \frac{1}{c}\mathbf{V}\times\mathbf{B}\right]\cdot\nabla_v f_j = 0 \tag{3.3}$$

with the Maxwell equations in the form

$$\begin{aligned}
\nabla\cdot\mathbf{E} &= 4\pi\sum q_j\int f_j(\mathbf{X},\mathbf{V},t)\,d\mathbf{V} + 4\pi\rho_0 \\
\nabla\times\mathbf{E} &= -\frac{1}{c}\frac{\partial\mathbf{B}}{\partial t} \\
\nabla\cdot\mathbf{B} &= 0 \\
\nabla\cdot\mathbf{E} &= \frac{1}{c}\frac{\partial\mathbf{E}}{\partial t} + \frac{4\pi}{c}\sum q_j\int \mathbf{V} f_j(\mathbf{X},\mathbf{V},t)\,d\mathbf{V} + \frac{4\pi}{c}\mathbf{J}_0
\end{aligned} \tag{3.4}$$

where ρ_0 ($\mathbf{J}_0$) is the equilibrium charge (current) density. The Vlasov-Maxwell (VM) system of equations represents the complete set of self-consistent equations for $\mathbf{E}$, $\mathbf{B}$ and f_α. This set of equations completely describes collisionless plasma while the particles interaction is taken

into account by a self-consistent field. However, in the ES case, $\mathbf{B} = 0$ and the VM system of equations reduce to Vlasov-Poisson (VP) set of equations. The VP set of equations fully described the classical collisionless plasma for the electrostatic case, which can be used to study the dielectric properties of the plasma. In the next section we calculate the dialectic constant by using dielectric theory.

3.3 Dielectric theory

The Vlasov-Poisson system of equations is the one in which the dynamics of the classical collisionless plasma species are described by the Vlasov equations and system of equations is closed by using the Poisson's equation. The linearization of these equations requires that the disturbance of the plasma by the test charge to be so small such that the induced electric field (E_{ind}) is supposed to be linearly proportional to the external perturbation (E_{ext}). This theory is also called dielectric theory because the factor of proportionality between E_{tot} and E_{ext} is the dielectric tensor of the medium.

In the presence of low-phase-velocity (in comparison with the electron and ion thermal velocities) electrostatic disturbances, the number density perturbations of the electrons and positive ions are[53],

$$n_s = n_{s0} \exp\left(q_s \frac{\phi(X)}{T_s}\right), \tag{3.5}$$

where $\phi(X)$ is the electrostatic potential and q_s (equals $-e$ for electrons and e for ions) is the electron/ion charge.

The dynamics of the dust particles is governed by the Boltzmann-Vlasov equation as

$$(\partial_t + \mathbf{V} \cdot \nabla) f_d(\mathbf{X}, \mathbf{V}, t) - \frac{q_d}{m_d} \nabla\phi \cdot \nabla_v f_d = \left(\frac{\partial f_d}{\partial t}\right)_{coll} \tag{3.6}$$

where $f_d(\mathbf{X}, \mathbf{V}, t)$ is the dust particle distribution function, q_d (equals $-Z_{d0}e$, where Z_{d0} is the charge state of the dust particle) is the charge and M_d is the mass of the dust particle. The induced field $-\nabla\phi$ does not contain individual close encounters carried out by the particles by the collisions processes. The close collisions are taken into account by the collision term

$\left(\frac{\partial f_d}{\partial t}\right)_{coll}$.

The collision term is negligible, if the collision frequency is small compared with the plasma frequency ω_{pd}, then the Boltzmann equation reduces to the Vlasov equation. The collisions with neutral dust particles will be discussed in chapter 6.

In the absence of the test charge, the plasma is uniform and field-free. The plasma is slightly perturbed by the test particle, the Vlasov equation can be linearized as

$$(\partial_t + \mathbf{V}\cdot\boldsymbol{\nabla})\, f_{d1} - \frac{q_d}{m_d}\boldsymbol{\nabla}\phi_1 \cdot \boldsymbol{\nabla}_{\mathbf{v}} f_{d0} = 0 \tag{3.7}$$

The induced electrostatic potential ϕ in the plasma by the test charge is the potential of the test charge and the potential it induces in the plasma. Thus ϕ satisfies the Poisson's equation

$$-\nabla^2\phi_1 = 4\pi\rho_p + 4\pi\rho_t \tag{3.8}$$

where $\rho_p = \sum n_j q_j \int f_j d\mathbf{V}$ is the charge density in the plasma and $\rho_t = 4\pi q_t \delta\left(\mathbf{X} - \mathbf{V}_t t\right)$ is the test charge density. The quasi-neutrality condition at equilibrium is

$$n_{i0} = n_{e0} + Z_{d0} n_{d0}, \tag{3.9}$$

where Z_{d0} is the number of equilibrium charges residing on the dust grain surface.

3.3.1 Vlasov-Poisson system in 1-D approximation

A preliminary analysis of the ES potential in a multi-species dusty plasma by assuming that the system remains uniform and unperturbed in the (y, z) plane perpendicular to the direction of motion of test charge (i.e., along x-axis) is discussed. The one dimensional distribution function for dust particles is $f_d\left(x, V_x, t\right)\delta(y)\delta(z)$ which satisfies the Vlasov equation. Notice that, we have used the following normalization of the parameters[40]

$$x \rightarrow x/\lambda_{Dd}, \qquad V \rightarrow V_x/V_{td},$$
$$f(x, V_x, t) \rightarrow V_{td}\; f(x, V_x, t)/n_{do}, \qquad t \rightarrow t\omega_{pd},$$
$$\phi \rightarrow Z_d\; e\phi/T_d, \qquad Z_t = Z_t/N_d Z_d \ll 1$$

where Z_t is the normalized effective charge state of test particle.

the dust plasma frequency is $\omega_{pd} = \sqrt{4\pi Z_d^2 e^2 n_{d0}/m_d}$,

the dust thermal speed is $V_{td} = \sqrt{T_d/M_d}$,

the number of dust particles in Debye sphere are $N_D = n_{do}\lambda_{Dd}^3$

the dust Debye length is $\lambda_{Dd} = \sqrt{T_d/4\pi n_{d0} Z_d^2 e^2}$.

The linearized and dimensionless form of the Vlasov equation is

$$\left(\partial_t + V_x \frac{\partial}{\partial x}\right) f_{d1}(x, V_x, t) + \frac{\partial \phi_1}{\partial x}\frac{\partial f_{d0}}{\partial V_x} = 0, \tag{3.10}$$

the perturbed number density of the electrons and ions can be written as

$$n_{e1} \simeq \left(\frac{K_{De}^2}{K_{Dd}^2}\right)\phi_1(\mathbf{X}), \tag{3.11}$$

$$n_{i1} \simeq -\left(\frac{K_{Di}^2}{K_{Dd}^2}\right)\phi_1(\mathbf{X}), \tag{3.12}$$

and the Poisson's equation is

$$-\frac{\partial^2 \phi_1}{\partial x^2} = Z_t \delta(x - |\mathbf{V}_t| t) + \left(n_{i1} - n_{e1} - \int f_{d1}(x, V_x, t)\, dV\right). \tag{3.13}$$

Calculation of ES potential

The ES potential in 1-D approximation can be solved by using the Space-Time Fourier transform of Eqs.(3.10) – (3.13), and then taking the inverse transform. Fourier component of the perturbed distribution function from Eq.(3.10) is

$$f_{d1}(K_x, V_x, \omega) = \frac{\partial f_{d0}(V)}{\partial V_x}\frac{K_x}{(\omega - K_x V_x)}\phi_1(K_x, \omega), \tag{3.14}$$

and that of the Eq.(3.13) is

$$K^2\phi_1 = 2\pi Z_t \delta(\omega - K_x |\mathbf{V}_t|) + \left(n_{i1}(K_x, \omega) - n_{e1}(K_x, \omega) - \int f_{d1}(K_x, V_x, \omega)\, dV\right) \tag{3.15}$$

Substituting the value of n_{e1}, n_{i1} and f_{d1} in the above equation, we obtain

$$\phi_1(K_x,\omega) = \frac{\delta(\omega - K_x V_t,)}{K_x^2 \epsilon(K_x,\omega)} \tag{3.16}$$

where $\epsilon(K,\omega)$ is the dielectric constant given by

$$\epsilon(K_x,\omega) = 1 + \frac{K_D^2}{K_x^2} + \frac{1}{K_x^2}\int \frac{\partial f_{d0}(V)}{\partial V_x}\frac{K_x}{(\omega - K_x V_x)}dV \tag{3.17}$$

and K_D is the effective normalized wave number, given by

$$K_D^2 = \frac{K_{Di}^2 + K_{De}^2}{K_{Dd}^2} \tag{3.18}$$

If we assume that the distribution function of dust particles at equilibrium is Maxwellian,

$$f_{d0}(V) = \left(\frac{1}{2\pi V_{td}^2}\right)^{1/2} \exp\left[-\frac{1}{2}\left(\frac{V}{V_{td}}\right)^2\right] \tag{3.19}$$

then the integral in the dielectric constant is simply the plasma dispersion function and is given as

$$\begin{aligned}
\int \frac{\partial f_{d0}(V)}{\partial V_x}\frac{K_x}{(\omega - K_x V_x)}dV &= \frac{1}{\sqrt{2\pi}}\int \frac{V\exp\left[-V^2/2\right]}{(V - \omega/K_x)}dV \\
&= W\left(\frac{\omega}{|K|}\right) \qquad (3.20)\\
&\equiv X\left(\frac{\omega}{|K|}\right) + iY\left(\frac{\omega}{|K|}\right) \qquad (3.21)
\end{aligned}$$

where $\mathrm{X}\left(\frac{\omega}{|K|}\right)$ and $\mathrm{Y}\left(\frac{\omega}{|K|}\right)$ are the real and imaginary parts of the plasma dispersion function respectively. The dielectric constant (3.17) can be written as

$$\epsilon(K,\omega) = 1 + \frac{K_D^2}{K_x^2} + \frac{1}{K_x^2}W\left(\frac{\omega}{|K_x|}\right) \tag{3.22}$$

By taking the inverse Fourier transformation of Eq.(3.16), the ES potential will become

$$\phi_1(x,t) = \frac{Z_t}{2\pi}\int \frac{\exp\left(i\left[K_x x - \omega t\right]\right)}{K_x^2 \epsilon(K_x,\omega)}\delta(\omega - K_x V_t)\, dK_x d\omega \tag{3.23}$$

Performing the $\omega-$ integration and making transformation $\xi = x - V_t t$, we obtain the ES potential in a reference frame in which the test charge particles is at rest, is given by

$$\begin{aligned} \phi_1(x) &= \frac{Z_t}{2\pi}\int dK_x \frac{\exp(iK\xi)}{K_x^2 \epsilon(K_x, K_x V_t)} \\ &= \frac{Z_t}{2\pi}\int_0^{K_{max}} dK_x \frac{\exp(iK_x\xi)}{K_x^2 \epsilon(K_x, K_x V_t)} \end{aligned} \tag{3.24}$$

In order to avoid logarithmic divergence at large K in Eq.(3.24), a cutoff parameter K_{max} has been introduced, where $K_{max} = 1/b_{min}$ and $b_{min} = Z_j e^2/M(V_t^2 + V_{td}^2)$ is the minimum impact parameter and M is the reduced mass of the test charge and dust particle. This divergence corresponds to the incapability of the linearized Vlasov theory to treat close encounters between the test charge particle and the plasma species (electrons, ions and dust grains). In the following subsection we shall calculate the energy loss of the test charge in 1-D approximation.

Energy loss of test charge particle in 1-D case

The energy loss per unit path length of the test particle is the force $\mathbf{F}$ that a test charge particle experiences in its own induced field and is given by Eq.(2.22). This energy loss in 1-D approximation can be written as

$$S = -\frac{Z_t^2 N_D Z_d}{2\pi}\int_0^{K_{max}} dK K\, Im\left[\epsilon(K, \mathbf{K}\cdot\mathbf{V}_t)^{-1}\right] \tag{3.25}$$

$$= \frac{Z_t^2 N_D Z_d}{2\pi}\int_0^{K_{max}} dK K \frac{Y(\varpi)}{[K^2 + X(\varpi)]^2 + Y^2(\varpi)} \tag{3.26}$$

Performing the K-integration, we get

$$S = \frac{Z_t^2 N_D Z_d}{4\pi}\left[\arctan\left(\frac{K_D^2 + K_{max}^2 + X(\varpi)}{Y(\varpi)}\right) - \arctan\left(\frac{K_D^2 + X(\varpi)}{Y(\varpi)}\right)\right] \tag{3.27}$$

where $\varpi = \mathbf{K}\cdot\mathbf{V}_t/|K|$ is the normalized dimensionless phase velocity. The expressions for X and Y are very complicated and their analytical results are difficult. However, for very

small or very large arguments their series expansions are given in Eq.(2.13) and Eq.(2.14) respectively. The numerical solutions are discussed in the section (2.14). In the next section potential and energy loss are calculated in 3-D case.

3.3.2 Vlasov-Poisson system in 3-D approximation

In this section we shall study the behavior of the electrostatic potential and energy loss for a three dimensional plasma. The distribution function for the dust particles which satisfies the Vlasov Poisson system of equations is $f_d(\mathbf{X},\mathbf{V},t)$. We normalize the parameters for the 3-D case as $\mathbf{X} \rightarrow \mathbf{X}/\lambda_{Dd}$, $\mathbf{V} \rightarrow \mathbf{V}/V_{td}$, $f_d(\mathbf{X},\mathbf{V},t) \rightarrow V_{td}^3 f_d(\mathbf{X},\mathbf{V},t)/n_{d0}$, and choose the frame in which the test charge is at the origin. The linearized and dimensionless form of the Vlasov equation is

$$\left(\partial_t + \mathbf{V}\cdot\boldsymbol{\nabla}\right) f_{d1}\left(\mathbf{X},\mathbf{V},t\right) + \boldsymbol{\nabla}\phi_1 \cdot \boldsymbol{\nabla}_{\mathbf{v}} f_{d0} = 0, \tag{3.28}$$

and of the Poisson's equation is

$$-\nabla^2\phi_1 = Z_t\delta\left(\mathbf{X}-\mathbf{V}_t t\right) + \left(n_{i1} - n_{c1} - \int f_{d1}\left(\mathbf{X},\mathbf{V},t\right) dV\right) \tag{3.29}$$

while the number densities of electrons and ions are the same as given in the Eqs.(3.11) and (3.12).

Calculation of ES potential

By adopting the same procedure as discussed in section 3.3.1 for 1-D case, the ES potential can be written as

$$\begin{aligned}
\phi_1\left(X,t\right) &= \frac{Z_t}{\left(2\pi\right)^3}\int d\omega d\mathbf{K}\frac{\exp\left(i\left[\mathbf{K}\cdot\mathbf{X}-\omega t\right]\right)}{K^2\epsilon\left(\mathbf{K},\omega\right)}\delta\left(\omega-\mathbf{K}\cdot\mathbf{V}_t\right) \\
&= \frac{Z_t}{\left(2\pi\right)^3}\int d\mathbf{K}\frac{\exp\left(i\mathbf{K}\cdot\left[\mathbf{X}-\mathbf{V}_t t\right]\right)}{K^2\epsilon\left(\mathbf{K},\mathbf{K}\cdot\mathbf{V}_t\right)}
\end{aligned} \tag{3.30}$$

By writing $\mathbf{X}$ and $\mathbf{K}$ in spherical co-ordinates respectively as

$$\begin{aligned}\mathbf{X} &= (X\sin\theta_1\cos\varphi_1,\quad X\sin\theta_1\sin\varphi_1,\quad X\cos\theta_1)\\ \mathbf{K} &= (K\sin\theta\cos\varphi,\quad K\sin\theta\sin\varphi,\quad K\cos\theta)\end{aligned}$$

then

$$\mathbf{K}\cdot\mathbf{X}-V_t t=K\mu\xi+K\rho\sqrt{1-\mu^2}\cos(\varphi-\varphi_1)$$

where $\mu=\cos(\mathbf{K},\mathbf{V}_t)$, $\rho=X\cos\theta_1$, $x=X\sin\theta_1$ and $\xi=x-V_t t$ is the position of the test particle in a reference frame in which the test particle is at rest. The ES potential takes the following form

$$\phi_1(X)=\frac{Z_t}{(2\pi)^2}\int_0^{K_{max}}dK\int_{-1}^{1}d\mu\frac{\exp(iK\xi\mu)}{\epsilon(K,\mathbf{K}\cdot\mathbf{V}_t)}J_0\left(K\rho\sqrt{1-\mu^2}\right)\tag{3.31}$$

where $J_0\left(K\rho\sqrt{1-\mu^2}\right)$ is the zeroth order Bessel function. For numerical calculations real part of $\phi_1(X)$ is used as obtained from Eq.(3.31).

Energy loss of test charge particle in 3-D

The energy loss per unit path length for a test charge particle in 3-D approximation[40] is

$$S = -\frac{Z_t^2 Z_d N_D}{2\pi^2}\int_0^{K_{max}}KdK\int_{-1}^{1}\mu d\mu Im\left[\epsilon(\mathbf{K},\mathbf{K}\cdot\mathbf{V}_t)^{-1}\right]\tag{3.32}$$

$$= \frac{Z_t^2 Z_d N_D}{2\pi^2}\int_0^{K_{max}}K^3dK\int_{-1}^{1}\mu d\mu\frac{Y}{(K^2+X)^2+Y^2}\tag{3.33}$$

Performing the $K-$integration and making transformation $\varpi=\mu V_t$, we obtain

$$S = \frac{Z_t^2 N_D Z_d}{\pi^2}\left(\frac{1}{V_t^2}\right)\int_0^{V_t}\varpi d\varpi Y(\varpi)\left[\ln K_{\max}+\frac{1}{4}\ln\left\{\frac{\left(1+\frac{K_D^2+X(\varpi)}{K_{max}^2}\right)^2+\frac{Y^2(\varpi)}{K_{max}^4}}{(K_D^2+X(\varpi))^2+Y^2(\varpi)}\right\}-\right.$$
$$\left.-\frac{K_D^2+X(\varpi)}{2Y}\left[\arctan\left\{\frac{K_D^2+K_{\max}^2+X(\varpi)}{Y(\varpi)}\right\}-\arctan\left\{\frac{K_D^2+X(\varpi)}{Y(\varpi)}\right\}\right]\right]\tag{3.34}$$

The form of Eq.(3.34) is the same as calculated by Peter and Meyer-ter-Vehn[3]. The effect

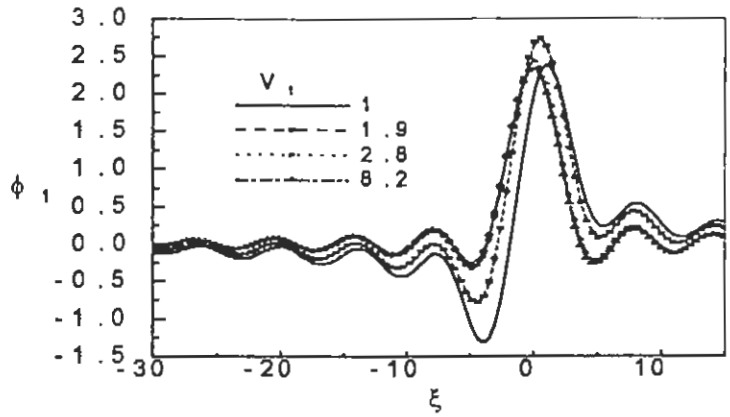

Figure 3-1: The normalized ES potential ($\phi_1 \times 10^2$) vs the normalized axial position $\xi(= x - V_t t)$ for different values of $(0 \leq V_t \leq 10)$, with $K_D = 0.3$ and $Z_t = 0.1$.

of multi-species can be seen by comparing this equation with their Eq.(21). The analytical solution of the energy loss are only possible for limiting case so, we shall numerically calculate the ES potential and energy loss per unit path length of the test charge in the next section.

3.4 Numerical results and discussion

Taking some typical parameters, as given by Barkan et al.[24]: $\lambda_{Dd} = (26-78)\ \mu m$, $\lambda_{De} = 200\ \mu m$, $\lambda_{Di} = 800\ \mu m$, and $Z_{d0} = 10^4$, we numerically solve (3.24). Figure (3.1) displays the variation of normalized ES potential (ϕ_1) in 1-D for a test charge against the normalized axial position ξ ($= x - V_t t$) in the units of λ_{Dd}, for fixed values of normalized effective wave number $K_D = 0.3$ and normalized effective charge state $Z_t = 0.1$ with various values of normalized test charge velocities.

It is evident from the graph that for $V_t \geq V_{td}$, the screened potential follows the Debye Hückel type potential with a strong damped wake-field. As we increase the test charge velocity $V_t \geq 8\ V_{td}$, the Debye-Hückel potential will change to the Coulomb potential. On the other hand, if we fix the values of $V_t = 2.0\ V_{td}$ and $Z = 0.1$, the ES potential (ϕ_1) shows almost the same behavior for all values of $K_D\,(0 < K_D < 1)$ (see, Fig. 3.2). However, the amplitude of the ES potential decreases with the increase in the effective Debye wave

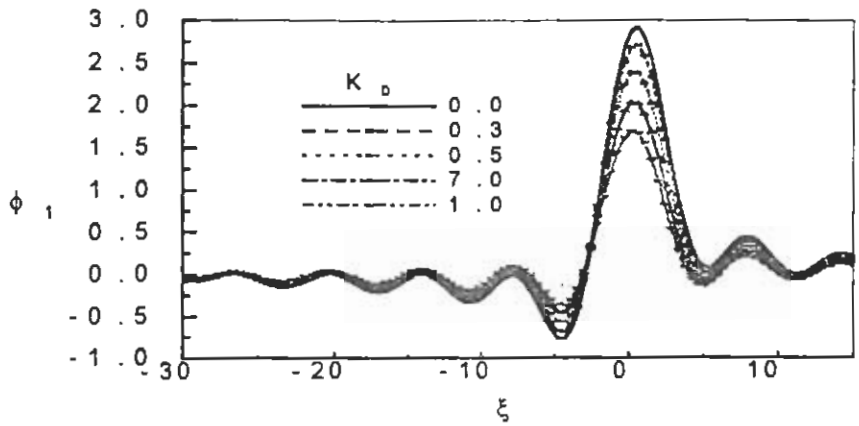

Figure 3-2: The normalized ES potential ($\phi_1 \times 10^2$) vs the normalized axial position $\xi(= x - V_t t)$ for different values of ($0 \leq K_D \leq 1$), with $V_t = 2\ V_{td}$ and $Z_t = 0.1$.

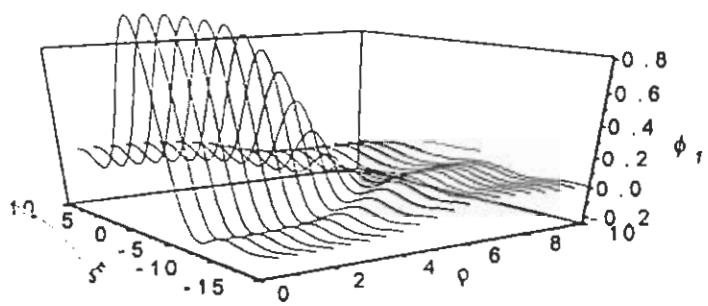

Figure 3-3: The normalized ES potential ($\phi_1 \times 10^3$) vs the normalized axial position $\xi(= x - V_t t)$ and the normalized radial position ρ, with $Z_t = 0.1$, $V_t = 2\ V_{td}$ and $K_D = 0.3$.

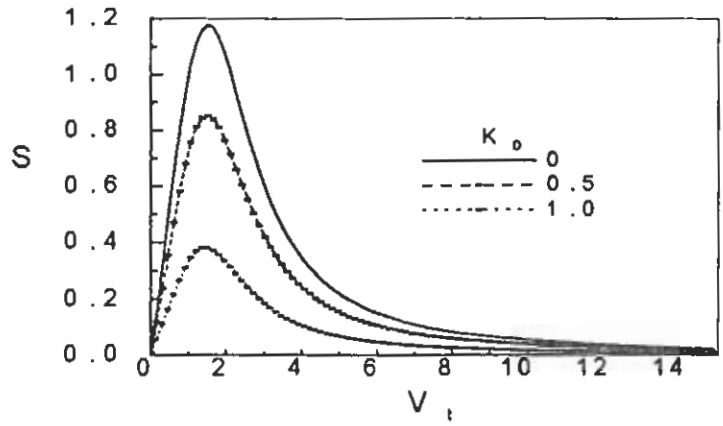

Figure 3-4: The energy loss of a test charge in 1-D case ($S \times 10^3$) vs the normalized test charge velocity V_t for different values of ($0 \leq K_D < 1$), with $Z_t = 0.1$, $Z_d = 10^4$ and $N_D = 200$.

number.

Next for 3-D case, we perform the numerical integration of Eq. (3.31) for different values of normalized axial position (ξ) and radial position (ρ) to obtain the ES potential ϕ_1. A 3-dimensional plot of the potential $\phi_1(\mathrm{X})$ versus ξ in the range $-15 \leq \xi \leq 10$ and ρ in the range $0 \leq \rho \leq 10$ is shown in Fig.(3.3), while keeping the other parameters same as in Fig.(3.1). A damping behavior is depicted from the graph. It is observed that the potential is strongly damped towards the ξ side and weekly damped towards the ρ side.

We perform the numerical integration of Eq.(3.26) and Eq.(3.33) for different values of K_D to obtain the energy loss of the test charge particle per unit path length and plotted for 1-D approximation in Fig.(3.4) and for 3-D case in Fig.(3.5). The enhancement in the energy loss per unit path length for 3-D case is observed.

3.5 Summary

We have analytically and numerically calculated the ES potential and the energy loss of a test charge moving with velocity V_t in a multi-component dusty plasma. A Debye-Hückel potential is observed for test charge velocity greater than the thermal velocity of dust. This shielded potential changes to the Coulomb type potential for very large test charge velocities

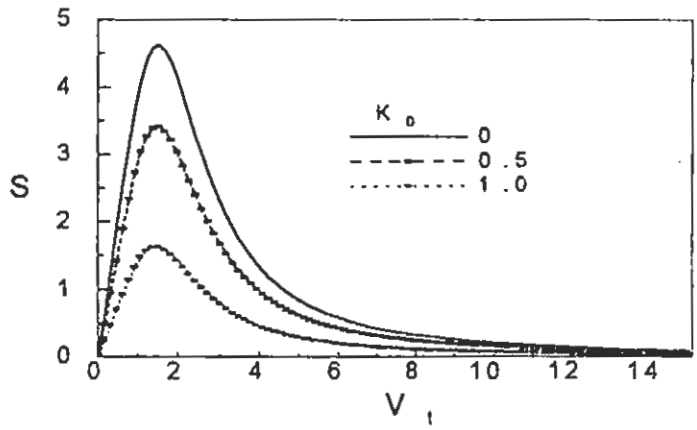

Figure 3-5: The energy loss of a test charge for 3-D case ($S \times 10^3$) vs the normalized test velocity V_t for different values of ($0 \leq K_D < 1$), with $Z_t = 0.1, Z_d = 10^4$ and $N_D = 200$.

($>> 8V_{td}$). The increase in the normalized effective Debye wave number only reduces the amplitude of the ES potential without altering the shape. Actually the increase in the value of K_D results in the increase in the dust Debye length and a decrease in the electron and ion Debye length, so more and more electrons and ions and lesser dust particles are shielded in the Debye sphere. This is in agreement with that the energy loss decreases as we increase the value of K_D. The wake field behind the trail of the moving test charge is strong as compared to the offside (*i.e.*, radial direction). This is quite valid because the maximum perturbation must occur at the position where is the test charge exists.

Chapter 4

Correlation Effect On The Energy Loss

The analytical and numerical results for the slowing down of two heavy projectile ions passing through a multi-component dusty plasma are presented. Within the linear dielectric approach, the electrostatic potential and the stopping power of the two projectiles are computed for different values of K_D (the normalized effective wave number) and R (the separation between the two projectiles) retaining two-ion-correlation effects. The enhancement in the energy loss is observed, and it is compared with that of a single ion projectile case.

4.1 Introduction

The energy loss of single atomic particles in matter has been widely studied for many years, the energy loss of swift ion clusters was the subject of much more interest, concerned with the incidence of swift molecular ions on thin solid films[54, 55, 56]. Molecular effects on the energy loss have was theoretically described[54, 55], as a result of interference effects in the energy dissipated in the material. A relation between the energy loss of ion clusters and the partition rule for the contribution of individual and collective response to the stopping power were found[54, 56]. The energy loss of a pair of charges in correlated motion through a degenerate electron gas was calculated[2] by using Lindhard's dielectric function. It was found that in addition to the usual single projectile stopping power, an additional term arises

from the interference effect of the two correlated projectiles.

In recent years, there has been renewed interest in the field of particle-driven inertial fusion, specific attention has been given to using cluster ion beams (CIB) as very heavy drivers[57, 58, 59]. There are several evidences of the presence of correlation effects in connection with the interaction of ion clusters with condensed matters[12, 37, 38, 39]. Such effects arise due to the collective response of the plasma to the incoming projectiles. The energy loss of fast ions in an electron plasma under the action of the potential distribution induced by the transit of a foregoing similar particle was presented[60], and further extended[61] to non-collinear motion of two such projectiles. The averaging procedure in the configuration space was used to determine the friction force for monochromatic clusters of ions[62]. Recently, Bringa and Arista[4] studied the collective and individual contributions to energy loss of correlated ions for the parameters of the ICF, Z-pinch and tokamak plasmas.

Recently, Otani and Bhattacharjee[63] studied the Debye shielding and particle correlation for strongly correlated dusty plasmas. They used numerical simulations by considering different numbers of dust particles in electron and ion plasmas, and found liquid-like short range correlation functions for two particles averaged over the total number of the dust particles. Later[64], the long-range correlation function for dusty plasma was developed and the numerical results for a broad range of dust densities and plasma temperatures were obtained. The correlations induced by the dust for the electron and ion densities as well as for the dust charges were investigated, and the results exhibited a long-range correlation.

In view of its importance in the dusty plasma, we studied[40] the potential perturbation caused by the two projectiles moving very close to each other in a weakly coupled dusty plasma. A system is said to be weakly coupled as long as its Coulomb potential energy is smaller than its thermal energy. In section 4.2 we will derive the ES potential for two test charged particles for one dimensional (1-D) as well as for three dimensional (3-D) cases. The energy loss of di-correlated test charges are discussed in section 4.3. A comparison has been made for correlated and de-correlated numerical results of the ES potentials and the energy losses.

4.2 Derivation of electrostatic potential for two test charged particles

The dusty plasma is characterized by the equilibrium number density n_{j0} and the temperature $T_j (j = i, e, d)$, through which two point projectile ions (refer as test charges) with effective positive charges $Z_1 e$ and $Z_2 e$ and masses M_1 and M_2 move with the same velocity $\mathbf{V}_t$ along the x-axis. The equilibrium quasi-neutrality is not disturbed by the presence of these test charged particles. Assuming the axial symmetry of the problem, the test charged particles trajectories $X_\alpha (\alpha = 1, 2)$ can be written as $\mathbf{X}_1(t) = V_t t \, \hat{e_x}$ and $\mathbf{X}_2(t) = V_t (t - \tau) \, \hat{e_x}$, where τ is the delay time of the second projectile. The charge density of the two test charges is given as

$$\rho_{t1} = q_{t1} \delta (\mathbf{X} - \mathbf{V}_t t) \tag{4.1}$$

and

$$\rho_{t2} = q_{t2} \delta (\mathbf{X} - \mathbf{V}_t (t - \tau)) \tag{4.2}$$

In this case the linearized and dimensionless form of the Poisson's equation (3.29) will be modified as

$$-\nabla^2 \phi_1 = Z_1 \delta (\mathbf{X} - \mathbf{V}_t t) + Z_2 \delta (\mathbf{X} - \mathbf{V}_t (t - \tau)) + n_{i1} - n_{e1} - \int f_{d1} (\mathbf{X}, \mathbf{V}, t) \, d\mathbf{V} \tag{4.3}$$

whereas the dynamics of the negatively charged dust is governed by the Vlasov equation (3.7) and number densities of electrons and ions by the Eq. (3.5). Choosing the reference frame in which both the test charged particles are at rest, and that the leading test charge is at the origin and following the procedure used in the subsection (3.3.1), the ES potential (ϕ_1) in 1-D approximation is given as

$$\phi_1 (x) = \frac{1}{2\pi} \int dK_x \frac{\exp [iK_x (x - V_t t)]}{K^2 \epsilon (K_x, K_x V_t)} (Z_1 + Z_2 \exp(-iK_x |\mathbf{V}_t| \tau)) \tag{4.4}$$

and for 3-D is given as

$$\begin{aligned}\phi_1(\mathbf{X}) &= \frac{1}{(2\pi)^3}\int d^3K \frac{\exp\left[i\mathbf{K}\cdot(\mathbf{X}-\mathbf{V}_t t)\right]}{K^2\epsilon\left(K,\mathbf{K}\cdot\mathbf{V}_t\right)}\left(Z_1+Z_2\exp(-i\mathbf{K}\cdot\mathbf{V}_t\tau)\right)\\ &= \frac{1}{(2\pi)^2}\int_0^{K_{max}} dK\int_{-1}^{1} d\mu \frac{\exp\left(iK\xi\mu\right)}{\epsilon\left(K,\mathbf{K}\cdot\mathbf{V}_t\right)}\\ &\quad\times J_0\left(K\rho\sqrt{1-\mu^2}\right)\left[Z_1+Z_2\exp(-i\mathbf{K}\cdot\mathbf{R})\right]\end{aligned} \tag{4.5}$$

where $\epsilon(K,\omega)$ is the dielectric constant given in Eq (3.22) and $\mathbf{R}=\mathbf{V}_t\tau$ is the separation between the two projectiles. In the large velocity limit ($V_t \geq V_{td}$), the main result is that a single test charge couples to the plasma electrostatic modes (collective degrees of freedom), exciting a conical wake behind the test charge itself. A second test charge that moves in such a trail will be correlated to the leading projectile by means of excited oscillations. The phase factor $\exp(-i\mathbf{K}\cdot\mathbf{R})$ arises from the presence of the second test charged particle and represents the two-ion correlated motion. Under the linear approximation, the electrostatic potential distributions created by two test charged particles is the superposition of the potential distribution associated with these test charges.

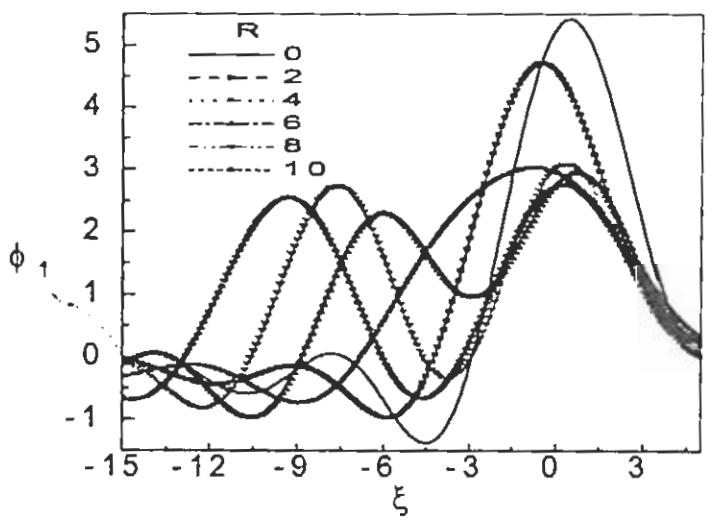

Figure 4-1: The normalized induced ES potential for two projectiles ($\phi_1 \times 10^{-2}$) vs the normalized axial position $\xi(=x-V_t t)$ for different values of $(0 \leq R \leq 10)$, with $K_D = 0.3$, $Z_1 = Z_2 = 0.1$ and $V_t = 2$.

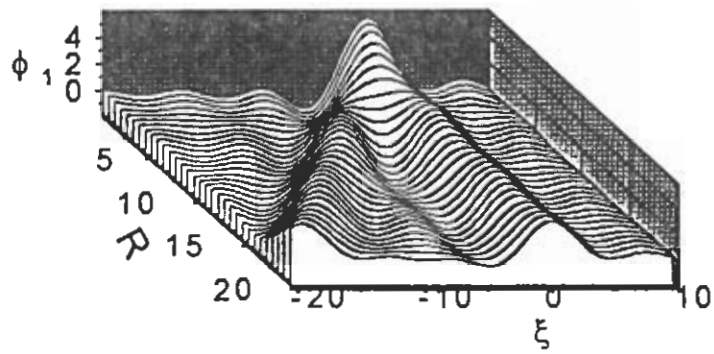

Figure 4-2: The normalized induced ES potential for two projectiles ($\phi_1 \times 10^{-2}$) vs the normalized axial position $\xi(= x - V_t t)$ and the separation R ($0 \leq R \leq 10$), with $K_D = 0.3$, $Z_1 = Z_2 = 0.1$ and $V_t = 2$.

In Fig. (4.1), we have plotted the total ES potential induced by the two projectiles retaining two ion correlation effect versus ξ for a wide range of separation $0 \leq R \leq 10$ between the projectiles while other parameters are the same as in Fig. (3.1). It is evident from Fig. (4.1), that when there is no separation between the two projectiles ($R = 0$), the ES potential distribution is similar to the potential for a single projectile but having charge equal to the sum of the two projectile charges. It can also be seen from the graph that while the potential peaks for both the projectiles remain inside the Debye sphere ($R \leq 5$), there appears only one peak showing superposition of the ES potential of the two projectiles. But when the projectiles are separated by a distance greater than the Debye radius ($R > 5$), the two peaks tend to appear separately, indicating the de-correlated behavior of the two projectiles. The two similar peaks are formed for the two projectiles separated by a distance larger than the sum of shielding length of the two projectiles. These results are more pronounced in Fig. (4.2). From Fig.(4.3) one notices the same type of deformation of the static Debye screening with different values of the amplitude keeping K_D in the range $0 < K_D < 1$ and a constant separation ($R = 7$) between the two projectiles.

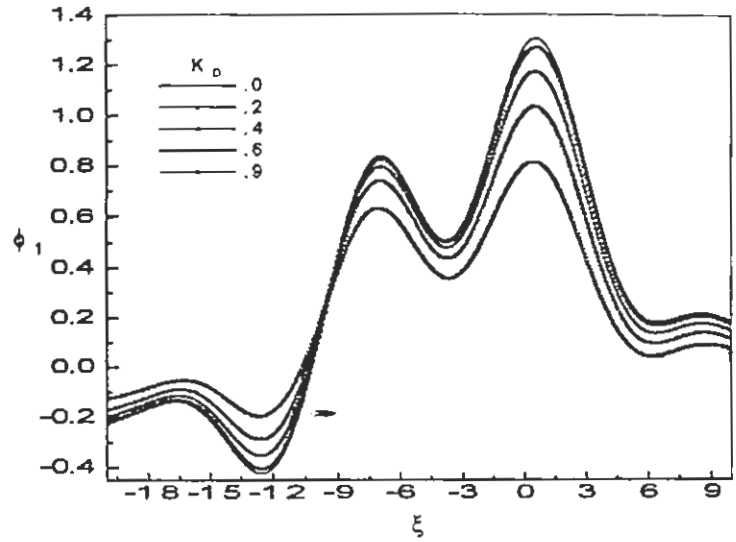

Figure 4-3: The normalized induced ES potential for two projectiles (ϕ_1) vs the normalized axial position $\xi(= x - V_t t)$ for different values of $(0 \leq K_D \leq 1)$, with $R = 7$, $Z_1 = Z_2 = 0.1$ and $V_t = 2$.

4.3 Energy loss of di-correlated test charge particles

The energy loss (or the stopping power) of the test charge is the force **F** experienced by the test charges in its own induced field. The energy loss of the second test charge which follows the trail of the leading test charge can be calculated by differentiating the electrostatic potential caused by the leading one. The total stopping power is the sum of the two contributions when one test charge moves in the electrostatic potential of the other and is expressed[3] as

$$S_{stop} = -\frac{dW}{dx} = -\mathbf{F}\cdot\hat{e_x} = Z_1 e\frac{\partial\phi}{\partial x}\mid_{x=V_t t} + Z_2 e\frac{\partial\phi}{\partial x}\mid_{x=V_t(t-\tau)}, \tag{4.6}$$

The energy loss of the two ions travelling in a plasma in a reference frame in which both the ions are stationary in 1-D approximation is given as

$$S_{stop} = S_1 + S_2 + S_R^{cor}$$

where $S_\alpha\,(\alpha = 1, 2)$ is the energy loss for a single projectile when the two test charges have a very large separation, and S_R^{cor} is the correlation contribution to energy loss of two projectile and are given by

$$S_\alpha = \frac{Z_d N_D Z_\alpha^2}{2\pi} \int_0^{K_{max}} dK Im\left(\frac{-1}{K\epsilon(K, \mathbf{K}\cdot\mathbf{V}_t)}\right), \tag{4.7}$$

and

$$S_R^{cor} = \frac{Z_d N_D Z_1 Z_2}{\pi} \int_0^{K_{max}} dK Im\left(\frac{-1}{K\epsilon(K, \mathbf{K}\cdot\mathbf{V}_t)}\right) \cos(KR) \tag{4.8}$$

The numerically calculated values of S_{stop} are plotted in Fig.(4.4) versus the projectile velocity V_t for different values of $0 \leq R \leq 5$ and $K_D = 0.3$, while other parameters remain the same as in Fig. (3.1). As long as the mutual separation between the projectiles is of the order of or smaller than the effective screening length, $\lambda_{eff} \approx V_t/\omega_{pd}$, there have a correlated motion. This modified motion can be explained by assuming that when $R < \lambda_{eff}$, the response function to the two projectiles is that it would manifest in the presence of a single projectile having a total charge almost equal to the sum of two charges. The value at $R = 0$ corresponds to the energy loss of a single projectile with charge equal to the sum of the charges of the two projectiles. It is observed that the phase factor(wake field) causes a periodic change to the energy loss rate. This can be explained as R is greater than the effective screening length $(\lambda_{eff1} + \lambda_{eff2})$, the one projectile moves in the wake field of the leading projectile. This wake filed attracts either the similar charges or opposite charges causing to increase/decrease the number of particles in the Debye sphere. When $R \rightarrow \infty$, the correlated part S_R^{cor} vanishes and the energy loss comes out to be the sum of two independent projectiles.

In the next subsections, we shall present the expressions for the energy loss of the two test charges moving along the same path (collinear) and parallel to each other (non collinear) for 3-D calculations.

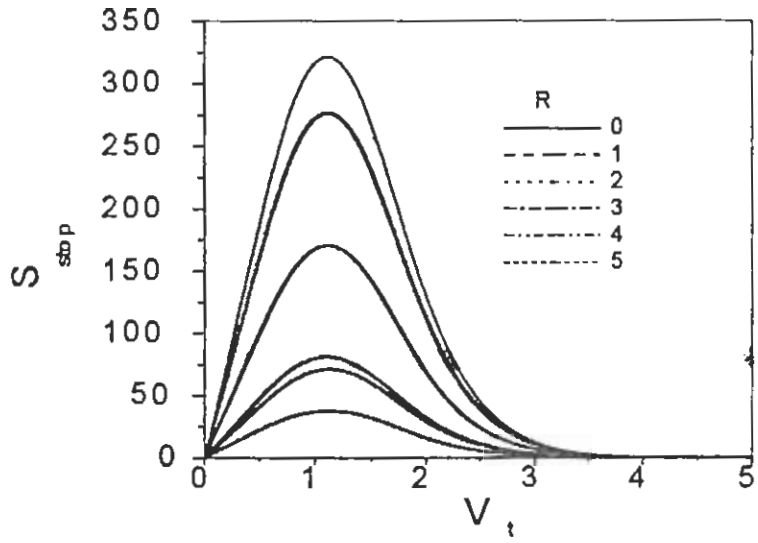

Figure 4-4: The energy loss of two projectiles for 1-D case (S_{stop}) vs the normalized projectile velocity V_t for different values of ($0 \leq R \leq 5$), with $Z_1 = Z_2 = 0.1$, $Z_d = 10^4$ and $N_D = 200$.

4.3.1 When the two projectiles are collinear

Considering two collinear test charges separated by a distance R and moving with an equal velocity V_t in the 3-D case, the total energy loss $S_{stop}(= S_1^{sp} + S_2^{sp} + S_R^{cor})$ is

$$S_{stop} = \frac{Z_d N_D}{(2\pi)^3} \int_0^{K_{max}} K dK Im\left(\frac{-1}{K^2 \epsilon\left(K, \mathbf{K}\cdot\mathbf{V}_t\right)}\right)\left(Z_1^2 + Z_2^2 + 2\ Z_1 Z_2 \exp(-i\mathbf{K}\cdot\mathbf{R})\right). \tag{4.9}$$

The two terms S_α^{sp} represent the energy loss of a single test charge (see e.g, 3.32), and are given by

$$S_\alpha^{sp} = \frac{Z_d N_D Z_\alpha^2}{(2\pi)^2} \int_0^{K_{max}} K dK \int_{-1}^{1} \mu d\mu Im\left(\frac{-1}{\epsilon\left(K, \mathbf{K}\cdot\mathbf{V}_t\right)}\right). \tag{4.10}$$

The term S_R^{cor} is the contribution from the correlation of the two projectiles, and is given by

$$S_R^{cor} = 2\frac{Z_d N_D Z_1 Z_2}{2\pi^2} \int_0^{K_{max}} K dK \int_0^{1} \mu d\mu Im\left(\frac{-1}{\epsilon\left(K, \mathbf{K}\cdot\mathbf{V}_t\right)}\right) \cos\left(K\mu R\right) \tag{4.11}$$

The energy loss of two collinear projectiles is plotted versus projectile velocities for different separations between the projectiles ($0 < R < 20$) with $Z_1 = Z_2 = 0.1$ $N_D = 200$

and $Z_d = 10^4$ in Fig. (4.5). It is evident from the graph that as the separation between the projectiles increases, the value of S_R^{cor} decreases for all projectile velocities. The value at $R = 0$ corresponds to the single projectile with a charge equal to the sum of the two charges. The contribution from the correlated term becomes lesser and lesser as the separation R increases. Further, when the separation between the two projectiles becomes larger than the Debye length of single projectile ($R > 5$), both projectiles behave like independent projectiles with a negligible correlation effect. The contribution to the S_{stop} from the correlation term vanishes for $R > (\lambda_{eff1} + \lambda_{eff2})$.

4.3.2 When the two projectiles are moving parallel

For the two non-collinear parallel projectiles, R can be resolved into two components B and D (along and perpendicular to the projectile velocity respectively) as shown in Fig.(4.5). We study the energy loss

$$S_{stop} = S_\alpha^{sp} + S_I^{cor}$$

of both the projectile ions moving with the same velocity V_t, separated by a fixed distance R. The terms S_α^{sp} are the same as given above while S_I^{cor} is the interference term and is given as

$$S_I^{cor} = \frac{Z_d N_D Z_1 Z_2}{2\pi^2} \int_0^{K_{max}} K dK \int_{-1}^{1} \mu d\mu Im\left(\frac{-1}{\epsilon\left(K, \mathbf{K}\cdot\mathbf{V}_t\right)}\right) \cos(K\mu B) J_0\left(DK\sqrt{1-\mu^2}\right) \tag{4.12}$$

We have plotted S_{stop} versus V_t for fixed value of R by varying B, $0 \leq B \leq R$ and D $(=\sqrt{R^2 - B^2})$ in Fig.(4.7). It is worth mentioning here that when $D = 0$, the two projectiles are collinear whereas, when $B = 0$, the projectiles are parallel. It is seen from the graph that when the two projectiles are parallel we have greater S_{stop} than when they are collinear. It shows that the wake field for horizontal separation is smaller than that for the vertical separation. The behavior of the two projectiles is significantly different from the predictions of a single projectile theory, if their mutual separation is of the order of or smaller than the screening length ($\lambda_{eff} \simeq V_t/\omega_{pd}$). We further note that for fast projectile, λ_{eff} is larger than the corresponding static screening length i.e., the Debye length $\lambda_D \simeq V_{td}/\omega_{pd}$. This modified

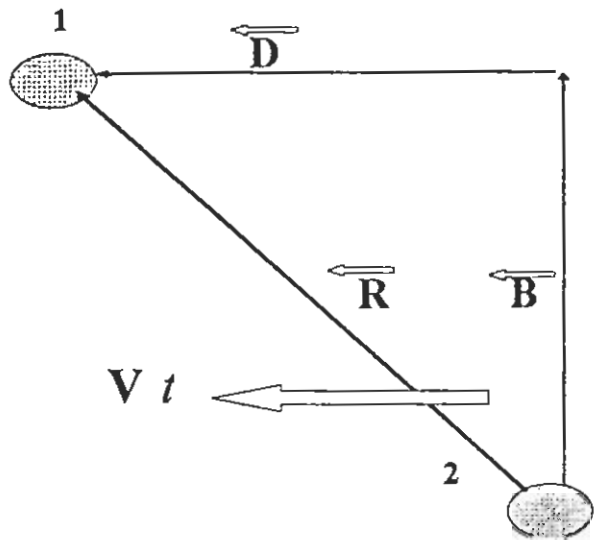

Figure 4-5: The schematic represenation of the separation R between the two projectiles moving with the same velocity V_t along x-axis. The R is resolved into parallel (D) and perpendicular(B) components. .

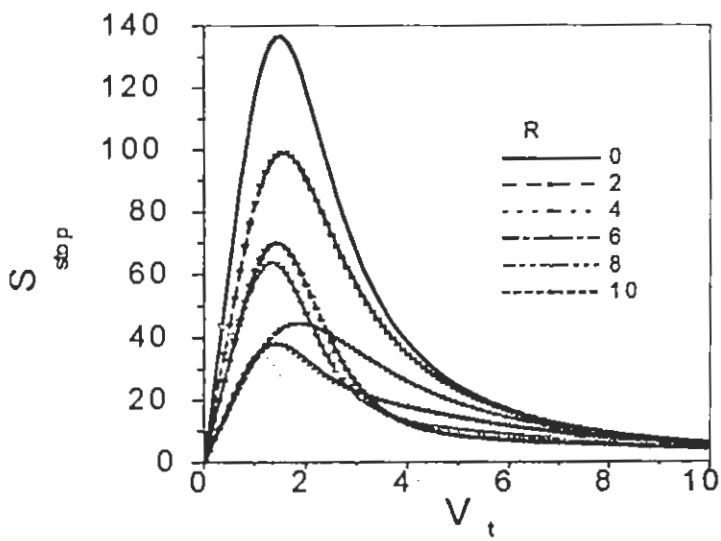

Figure 4-6: The energy loss of two collinear projectiles for the 3-D case (S_{stop}) vs the normalized projectile velocity V_t for different values of $(0 \leq R < 20)$, with $Z_1 = Z_2 = 0.1, Z_d = 10^4$ and $N_D = 200$.

interaction can easily be explained by assuming that when $R \leq \lambda_{eff}$, the plasma response to two projectiles is like that of a single projectile having a total charge almost equal to sum of two charges $(Z_1 e + Z_2 e)$. In Fig. (4.8) we plotted the S_{stop} for different alignment $0 \leq \theta \leq \pi/2$, with $R = 3, 5, 7$; between the two projectiles $(a) < \lambda_D$, $(b) \approx \lambda_D$ and $(c) > \lambda_D$ respectively. There is greater enhancement in the energy loss for collinear $(\theta = 0)$ projectiles than non-collinear $(\theta = \pi/2)$.

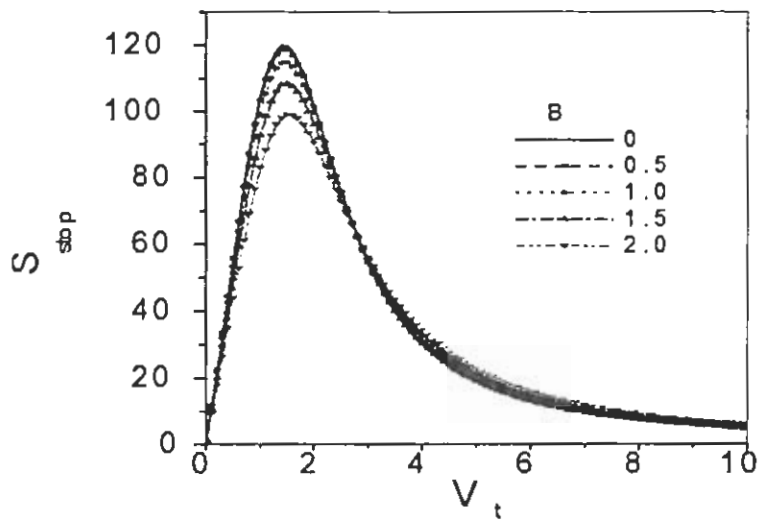

Figure 4-7: The energy loss of two non-collinear projectiles for the 3-D case (S_{stop}) vs the normalized projectile velocity V_t for different values of $(0 \leq B \leq 2)$ and keeping fixed $R = 2$, $Z_1 = Z_2 = 0.1, Z_d = 10^4$ and $N_D = 200$.

4.4 Numerical results and discussion

We have numerically investigated the two-ion correlation effects in the limit of fast projectile velocity (V_t) in a multi-species dusty plasma. Their influence on the stopping power increases as the projectile velocity is increased. The ES potential distribution and the energy loss of two heavy projectiles in a classical, collisionless and non-isothermal multi-species dusty plasma have been studied numerically within the framework of a linearized dielectric theory. A Debye-Hückel type of potential with a long trail of wake field extended to several Debye

lengths is observed for different projectile velocities. The wake field is slowly damped for larger projectile velocities. A similar pattern of the potential is observed for projectile velocities greater than $3V_{td}$. We have extended the calculation for two collinear as well as for two non-collinear projectiles. It is observed that as long as the separation between the two projectiles remains less than the Debye length of dust particles, the two projectiles behave as a single projectile with charge almost equal to the sum of the charges of the two projectiles, having larger Debye length.

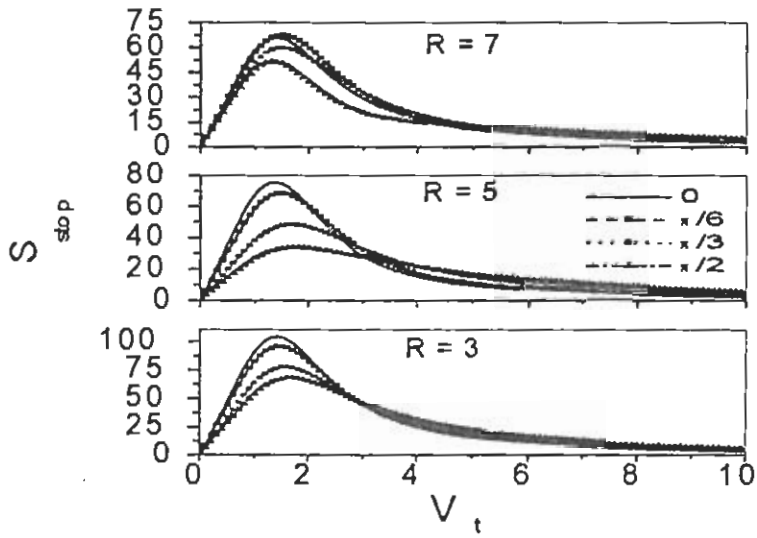

The same as Fig. 4.7 execpt for different orientations $(0 \leq \theta \leq \pi/2)$ (a) $R = 3$ (inside), (b) $R = 5$ (at), (c) $R = 7$ (outside) the Debye sphere

We have calculated energy loss of two di-correlated projectile ions as well. The enhancement with energy loss of the two di-correlated projectile ions is observed as compared to that of a single projectile. The interferente contribution to the potential and the energy loss of two correlated projectiles has also been calculated numerically. Furthermore, we have only examined the collective behavior of the ES potential and the energy loss. When a projectile is moving in the trail of the leading one an enhancement in the energy loss is seen as it is moving parallel to the leading projectile at equal distance. This shows that the maximum perturbation occurs behind the projectile as compared to the off-side and becomes minimum to the normal position.

Chapter 5

Effect of Dust charge fluctuations

The energy loss of a test charged particle in an unmagnetized dusty plasma is calculated by employing the dusty dielectric response function which accounts for the dust charge fluctuation. It is found that the dust charge fluctuation introduces a new contribution to the energy loss, which enhances it for fast charge relaxation rates and reduces it for slow rates. In the energy loss curves drawn against the test charge velocity, some peaks are observed. These peaks diminish for large charge relaxation rates. Possible explanation for these peaks is also given. Moreover, collective and individual particle contributions to potential and energy loss are also discussed.

5.1 Charging of dust grain

The charging of the dust grain is due to various plasma currents that flow onto the dust charge surface. These currents reaching the dust grain surface depend upon the ambient plasma conditions and the floating potential of the dust particle. These currents arise from a variety of circumstances, like collection of electrons and ions, photoelectron emissions by UV radiation, ion sputtering, secondary electron emission etc. The plasma particles may be attracted or repelled, depending upon their sign and the floating potential. The charge on the dust grain is negative due to higher mobility of electrons than that of ions, if secondary currents are negligibly small, otherwise, it may be either negative or positive depending upon the amount of secondary currents. In the present calculations, we have ignored the

secondary electron emission current as well as the photoemission current which are found to be negligibly small for low energy plasmas. This assumption is quite valid in the context of some experiments[65, 66] Various models [67] are found in the literature which describe the charging of dust grains. We will describe only a continues charging process based on the probe theory.

5.1.1 Orbital-motion limited currents

For the case of isolated dust grains, the charge on the dust is easily calculated for spherical grains of radius a. Since the grain is electrically floating, it collects electrons and ions. The floating potential acquired by a charged dust grain in a plasma is analogous to the floating potential of a similar shaped probe in a plasma. In other words, mostly the dust charging mechanisms are based on electrostatic probe theories in plasmas[68]. These theories determine the electron and ion currents reaching to the probes. The currents are termed as orbital-motion limited (OML) when the size of the dust grain is smaller than the effective Debye length. In the OML theory, the currents to the particles are calculated by assuming that only those electrons and ions are collected whose collisionless orbits intersect the probe's surface.

The dust charging equation is[18]

$$\left(\partial_t + \mathbf{v}_d \cdot \nabla\right) Q_d = I_e + I_i, \tag{5.1}$$

where Q_d is the dust charge, $\mathbf{v}_d$ is the dust velocity, $I_e(I_i)$ is the electron (ion) current [18, 65, 66, 27, 69, 70] given as

$$\begin{aligned} I_e &= -\pi a^2 e \left(\frac{8T_e}{\pi m_e}\right)^{1/2} n_e \exp\left[\frac{e}{T_e}\left(\phi_f - \phi\right)\right] \\ I_i &= \pi a^2 e \left(\frac{8T_i}{\pi m_i}\right)^{1/2} n_i \left[1 - \frac{e}{T_i}\left(\phi_f - \phi\right)\right] \end{aligned} \tag{5.2}$$

where T_s is temperature in the energy units, m_s is the mass, n_s is the number density of $s-$species ($s = i, e$) and $\phi_f - \phi$ is the potential difference between the dust floating potential $\left(\phi_f\right)$ and plasma potential (ϕ). The equilibrium currents can be determined by setting the

relation $\partial_t Q_d = 0$, and then dust grain is at equilibrium floating potential ϕ_{f0}. Treating the dust grain as a spherical capacitor having capacitance C, then the equilibrium charge Q_{d0} is $C\phi_{f0}$.

If we compare the dust charging time τ_d with the time scale of thermal motions of the dust particles, the latter being of the order of the inverse dust particle frequency i.e., ω_{pd}^{-1}, where $\omega_{pd} = (4\pi Z_{d0}^2 e^2 n_{d0}/m_d)^{1/2}$, then $\tau_d \ll \omega_{pd}^{-1}$ in a laboratory plasma, assuming micron-sized dust particles. Since the charging process in laboratory plasma[71, 72] as well as in numerical simulations[73] is very fast, the dust charge can be assumed to remain constant. However, for space plasmas, we may have $\tau_d \geq \omega_{pd}^{-1}$ and thus, the charging equation becomes relevant when the characteristic time scale is of the order of the charging period [74].

5.1.2 Dust charge perturbation

In contrast to an ordinary electron-ion plasma a dusty plasma contains sufficiently large number of dust grains, in which the dust charge perturbation $Q_{d1}\,(= Z_{d1}e)$, which arises due to the wave motion induced oscillations in the electron and ion currents that flow onto the grain surface, is a new dynamical variable. The perturbation of the dust charge in the presence of such disturbances is[69]

$$\frac{\partial}{\partial t} Z_{d1} e = I_{e1} + I_{i1} \tag{5.3}$$

where I_{s1} is the first order perturbed currents of s-species and are given as

$$\begin{aligned} I_{e1} &= -|I_{e0}| \left(\frac{e\phi_{f1}}{T_e + e\phi_0} + \frac{n_{e1}}{n_{e0}} \right) \\ I_{i1} &= -|I_{e0}| \left(\frac{e\phi_{f1}}{T_i - e\phi_0} - \frac{n_{e1}}{n_{e0}} \right) \end{aligned} \tag{5.4}$$

where $\phi_{f1} = Z_{d1}e/C$ is the perturbation in the floating potential of the dust grain and $|I_{s0}|$ is the equilibrium current reaching the dust grain surface of s-species. The electron equilibrium current can be written as

$$|I_{e0}| \simeq -\pi a^2 e \sqrt{\frac{8T_e}{\pi m_e}} n_{e0} \left[1 + \frac{e}{T_e}\phi_{f0} \right]$$

Moreover, $|I_{e0}| = -|I_{i0}|$ implies that

$$\left(\frac{T_e}{m_e}\right)^{1/2} n_{e0}\left[1+\frac{e}{T_e}\phi_{f0}\right] = \left(\frac{T_i}{m_i}\right)^{1/2} n_{i0}\left[1-\frac{e}{T_i}\phi_{f0}\right] \tag{5.5}$$

Using this relation into Eq.(5.3), we get

$$(\partial_t + \nu_0)\, Z_{d1} e = |I_{e0}|\left(\frac{n_{i1}}{n_{i0}} - \frac{n_{e1}}{n_{e0}}\right) \tag{5.6}$$

where ν_0 is the charge relaxation rate originating from the variation in the effective collision cross-section due to perturbation on the charge on the grain surface as experienced by the unperturbed particles and is given as

$$\nu_0 = |I_{e0}|\frac{e}{C}\left[\frac{1}{T_e + e\phi_{f0}} + \frac{1}{\left(T_i - e\phi_{f0}\right)}\right] \tag{5.7}$$

The number densities of electrons and ions can be approximated by the Boltzmann distributions, if we ignore a small contribution arising from the Landau damping. This is quite valid assumption for low phase velocity (compared with the thermal speed of electron and ion), used in calculating the dust charge perturbations. However, these Landau terms shall be retained in the dielectric constant. Thus, taking n_{s1} from Eq. (3.5), the Fourier component of the dust charge fluctuation is

$$Z_{d1}(K,\omega) = -i\frac{\beta}{\omega + i\nu_0}\phi\,(K,\omega)\,, \tag{5.8}$$

where $\beta = |I_{e0}|\,(1/T_i + 1/T_e)$. In the next section we will calculate the dielectric constant when the charge on the dust grain does not remain constant but fluctuates.

5.2 Calculation of dielectric constant

The plasma under consideration is composed of electrons, singly ionized positive ions and micron sized negatively charged dust grains with charge state $Q_d\,(= Q_{d0} + Q_{d1})$. As mentioned earlier the test charge having charge $Z_t e$ with velocity $\mathbf{V}_t$ propagating through the

plasma along the x-axis. The dynamics of the charged particles are governed by the linearized form of the Vlasov equation (2.5). Due to the presence of dust charge fluctuations $(Z_{d1}e)$, the Poisson's equation will be modified as

$$-\nabla^2\phi = 4\pi Z_t e\delta\left(\mathbf{X}-\mathbf{V}_t t\right) + 4\pi e\left(n_{i1} - n_{e1} - Z_{d0}\int f_{d1}\left(\mathbf{X},\mathbf{V},t\right)d\mathbf{V} - Z_{d1}n_{d0}\right) \tag{5.9}$$

where n_{d0} is the equilibrium dust number density calculated from the unperturbed Maxwellian distribution function $f_{d0}\left(V\right)$, as

$$n_{d0} = \int f_{d0}\left(V\right)d^3V$$

while n_{s1} is the perturbed density calculated from the distribution function $f_{s1}\left(X,V,t\right)$ as

$$n_{s1} = \int f_{s1}\left(\mathbf{X},\mathbf{V},t\right)d^3V$$

By adopting the procedure used in the subsection (3.3.1), the ES potential in a stationary frame can be calculated as

$$\phi\left(X\right) = \frac{Z_t e}{\left(2\pi\right)^2}\int_0^{K_{max}} dK\int_{-1}^{1} d\mu\frac{\exp\left(iK\xi\mu\right)}{\epsilon\left(K,\mathbf{K}\cdot\mathbf{V}_t\right)}J_0\left(K\rho\sqrt{1-\mu^2}\right) \tag{5.10}$$

where the dielectric constant $\epsilon\left(K,\omega\right)$ is given as

$$\epsilon\left(K,\omega\right) = 1 + \sum_{j=i,e,d}\frac{K_{Dj}^2}{K^2}W\left(\frac{\omega}{K\sqrt{2}v_{tj}}\right) - i\frac{\omega_c}{\omega+i\nu_0}$$

where $v_{tj} = \sqrt{T_j/m_j}$ is the thermal speed of j-th species $(j = e,i,d)$, and $W\left(\varpi\right) = X\left(\varpi\right) + iY\left(\varpi\right)$ is the plasma dispersion function, defined in the Eq.(2.12).

In the low phase velocity $(\omega/K \simeq v_{td} \ll v_{ti},\ v_{te})$, the plasma dispersion function for s-species can be approximated by the Eq.(2.13). Retaining only the leading term, the modified dielectric constant[28] is given as

$$\epsilon\left(K,\omega\right) = 1 + \frac{K_D^2}{K^2} + i\,\frac{LD}{K^2} + \frac{K_{Dd}^2}{K^2}W\left(\frac{\omega}{K\sqrt{2}v_{td}}\right) - i\frac{\omega_c}{\omega+i\nu_0} \tag{5.11}$$

where $K_D = \left(\lambda_{Di}^{-2} + \lambda_{De}^{-2}\right)^{1/2}$ is the inverse of effective Debye radius of the dusty plasma, $LD = \sqrt{\pi/2}\omega/K\left[1/(\lambda_{De}^2 v_{te}) + 1/(\lambda_{Di}^2 v_{ti})\right]$ the effective Landau damping rate, $\lambda_{Dj} = v_{tj}/\omega_{pj}$ the Debye length of the j-th species, and $\omega_{ps} = (4\pi e^2 n_{s0}/m_s)^{1/2}$ the plasma frequency of the s-th species, $K_{Dd} = (4\pi n_{d0} Z_{d0}^2 e^2/T_d)^{1/2}$ the Debye wave number of the dust particle, and ω_c is the dust charging frequency and can be written as

$$\begin{aligned} \omega_c &= \beta\nu_c/K^2 \\ &= |I_{e0}|\ \frac{4\pi e n_{d0}}{K^2}\left(\frac{1}{T_i} + \frac{1}{T_e}\right). \end{aligned} \tag{5.12}$$

where $\nu_c = 4\pi e Z_{d0} n_{d0}/Z_{d0}$ is the dust charge density per dust charge state.

5.3 Calculation of energy loss

The energy loss per unit path length defined in the section (3.3.1) can be written as

$$S = -\frac{Z_t^2 e^2}{2\pi^2}\int_0^{K_{max}} K^3 dK \int_{-1}^{1} \mu d\mu\, \mathrm{Im}\,\frac{-1}{\epsilon\,(K,\omega)}$$

Using the value of dielectric constant from Eq.(5.11) into the above Equation, we get

$$S = -\frac{Z_t^2 e^2}{2\pi^2}\int_0^{K_{max}} K^3 dK \int_{-1}^{1} \mu d\mu \frac{K_{Dd}^2 Y + LD - K^2 A}{\left[K^2 + K_D^2 + K_{Dd}^2 X - K^2 B\right]^2 + \left[K_{Dd}^2 Y + LD - K^2 A\right]^2} \tag{5.13}$$

where

$$\begin{aligned} A &= \frac{K\mu V_t \omega_c}{(K\mu V_t)^2 + \nu_0^2} \\ B &= \frac{\nu_0 \omega_c}{(K\mu V_t)^2 + \nu_0^2} \end{aligned}$$

Now we shall study some limiting cases of very fast (slow) charge relaxation rates.

5.3.1 Fast charge relaxation rate

If the charge relaxation rate is very high i.e., $\nu_0 \gg \omega \simeq K \cdot V_t$ then the dielectric constant will reduce to

$$\epsilon(\mathbf{K},\omega) \approx 1 + \frac{K_D^2}{K^2} + i\,\frac{LD}{K^2} + \frac{K_d^2}{K^2}\,W\left(\frac{\omega}{K\sqrt{2}v_{td}}\right) - \frac{\omega_c}{\nu_0}, \tag{5.14}$$

Using the imaginary part of the inverse dielectric constant given in the above Equation, the energy loss per unit path length S is

$$S = -\frac{Z_t^2 e^2}{2\pi^2}\int_0^{K_{\max}} K^3 dK \int_{-1}^{1} \mu d\mu \frac{K_d^2 Y + LD}{\left[K^2 + K_D^2 + K_d^2 X - K^2\omega_c/\nu_0\right]^2 + \left[K_d^2 Y + LD\right]^2}. \tag{5.15}$$

Performing the $K-$integration and making a transformation $\varpi = \mu V_t$, we get

$$\begin{aligned} S \;=\; & \frac{Z_t^2 Z_d}{\pi^2}\left(\frac{1}{V_t^2}\right)\int_0^{V_t} \varpi d\varpi Y(\varpi)\left[\ln K_{\max} + \frac{1}{4}\ln\left\{\frac{\left(1 + \frac{K_D^2 + X(\varpi)}{K_{\max}^2} - \frac{\nu_c\beta}{K_{\max}^2\nu_0}\right)^2 + \frac{Y^2(\varpi)}{K_{\max}^4}}{\left(K_D^2 + X(\varpi) - \nu_c\beta/\nu_0\right)^2 + Y^2(\varpi)}\right\} - \right. \\ & - \frac{K_D^2 + X(\varpi) - \nu_c\beta/\nu_0}{2Y}\left[\arctan\left\{\frac{K_D^2 + K_{\max}^2 + X(\varpi) - \nu_c\beta/\nu_0}{Y(\varpi)}\right\} - \right. \\ & \left.\left. - \arctan\left\{\frac{K_D^2 + X(\varpi) - \nu_c\beta/\nu_0}{Y(\varpi)}\right\}\right]\right] \end{aligned} \tag{5.16}$$

This is the modified form of the energy loss per unit path length for dusty plasma with dust charge fluctuations, previously calculated for electron /electron-ion plasmas[3, 28].

5.3.2 Slow charge relaxation rate

If the charge relaxation rate is very slow i.e., $\nu_0 \ll \omega \simeq K \cdot V_t$ then there are very few collisions between the dust grain and electrons/ions, the dielectric constant will reduce to

$$\epsilon(\mathbf{K},\omega) \approx 1 + \frac{K_D^2}{K^2} + i\,\frac{LD}{K^2} + \frac{K_{Dd}^2}{K^2}W\left(\frac{\omega}{K\sqrt{2}v_{td}}\right) - \frac{i\omega_c}{\omega}. \tag{5.17}$$

The imaginary part of the inverse dielectric function is

$$Im\frac{1}{\epsilon(K,K.V_t)} = -K^2\frac{K_{Dd}^2Y + LD - K^2\frac{\omega_c}{K\varpi}}{[K^2+K_D^2+K_{Dd}^2X]^2 + \left[K_{Dd}^2Y + LD - K^2\frac{\omega_c}{K\varpi}\right]^2}, \tag{5.18}$$

the energy loss per unit path length thus can become,

$$S = S_1 + S_2,$$

where

$$S_1 = -\frac{Z_t^2e^2}{2\pi^2}\int_0^{K_{max}} K^3dK\int_{-1}^{1}\mu d\mu\frac{K_{Dd}^2Y + LD}{[K^2+K_D^2+K_{Dd}^2X]^2 + \left[K_{Dd}^2Y + LD - K^2\frac{\omega_c}{K\varpi}\right]^2}, \tag{5.19}$$

and

$$S_2 = -\frac{Z_t^2e^2}{2\pi^2}\int_0^{K_{max}} K^3dK\int_{-1}^{1}\mu d\mu\frac{-K^2\frac{\omega_c}{K\varpi}}{[K^2+K_D^2+K_{Dd}^2X]^2 + \left[K_{Dd}^2Y + LD - K^2\frac{\omega_c}{K\varpi}\right]^2}, \tag{5.20}$$

The expression for S_1 gives energy loss similar to the earlier results [3, 28], while S_2 represents the energy gain which is a new contribution. This shows that for slow charge relaxation rate there is an additional negative contribution to the energy loss. It means that the dust grain act as sink of electrons and ions reaching on it and less number of particles can be shielded resulting into a decrease in the collective response of the plasma to the test charge. In the next section we will find the numerical results for the ES potential and energy loss per unit length.

5.4 Numerical results and discussion

Choosing some typical parameters: $n_{i0} = 10^9\ cm^{-3}$; $n_{e0} = 9.8\times10^8\ cm^{-3}$; $n_d = 10^5\ cm^{-3}$; $T_i = 0.11$ eV; $T_d = 0.1$ eV; $T_e = 1.0$ eV; $Z_{d0} = Z_t = 200$; $m_d = 10^8m_p$ where m_p is the

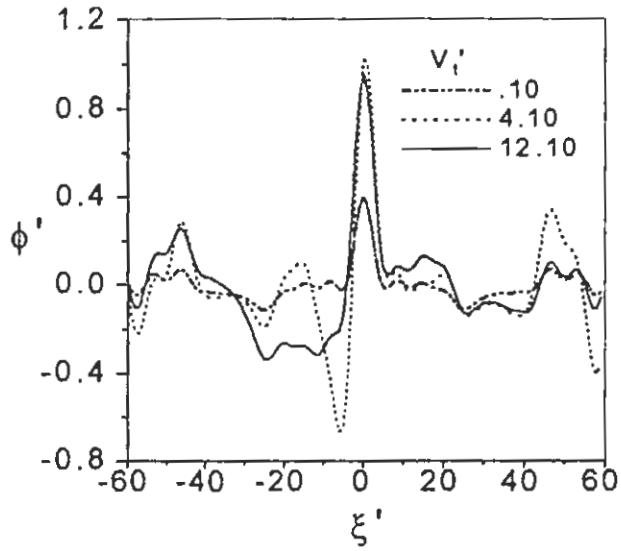

Figure 5-1: The normalized ES potential $\phi'(= Z_{d0}e\phi/T_d)$ of a test charge vs the normalized axial position ξ' $(= x - V_t t$ in the units of $\lambda_{Dd})$ for different values of normalized test charge velocity V_t' (in the units of V_{td}) $(0 < V_t' \leq 12)$, with $T_e = 1.0$ eV, $T_i = 0.11$ eV, $T_d = 0.1$ eV, $n_i = 10^9$ cm^{-3}, $n_d/n_i = 10^{-5}$, $Z_d = Z_t = 200$, with effective normalized Debye wave number $K_D = 0.32$ (in the units of λ_{Dd}^{-1}) and without the dust charge fluctuation.

mass of proton, we numerically solve Eq. (5.10) for ES potential and Eq. (5.13) for energy loss. It may be noted here that the values of these parameters lie within the range of some experimental values[24, 71]. The dimensionless variables are denoted by a prime.

The $K-$integration in the Eqs.(5.10) & (5.13) can be separated in collective $(0 < K < K_c)$ and individual $(K_c < K < K_{\max})$ terms according to Bohm and Pines theory [30]. The value of K_c separating both regimes is usually taken as the Debye wave number K_D. In the present calculation it is the effective wave number.

5.4.1 Collective response

In this section we will calculate the collective response of the plasma to the ES potential and energy loss by using the normalized value of the K $(= K/K_{Dd})$. So the K-integration is performed in the range $(K \in [0, 1])$.

Figure (5.1) displays the variation of normalized ES potential $\phi'(= Z_{d0}e\phi/T_d)$ against

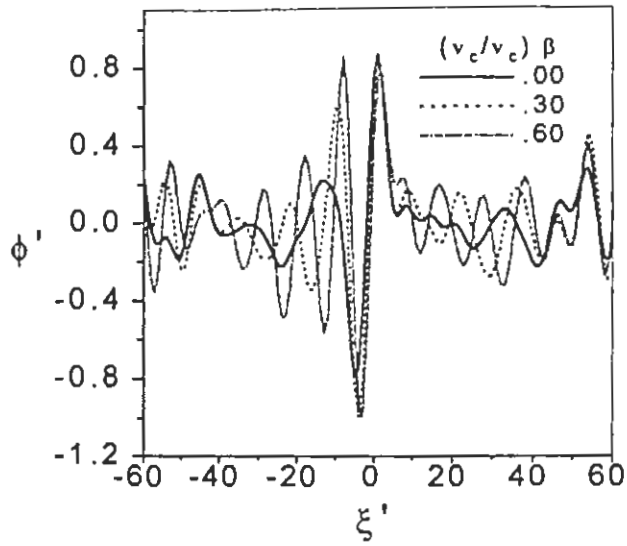

Figure 5-2: The normalized ES potential of a test charge (ϕ') vs the normalized axial position ξ' $(= x - V_t t)$ for different values of $(0 \leq (\nu_c/\nu_0)\beta \leq 0.6)$, with $V_t' = 3$ and other parameters are the same as in Fig. 1. A comparison of potential is made with no charge fluctuations (i.e., $\beta = 0$) for collision dominated plasma.

the normalized axial position ξ' $(= x - V_t t$ in the units of λ_{Dd}) with various values of the normalized test charge velocity V_t' $(= V_t/V_{td})$ without dust charge perturbation. One can observe a static Coulomb potential for the test charge velocity $V_t \left(= \frac{\omega}{|K|}\right) \ll V_{td}$ and a screened Debye-Hückel type ES potential for $V_{td} \leq V_t \leq V_{ti}$. In the latter case, we observe that when the test charge velocity approaches the dust acoustic speed (C_d), the amplitude of the potential grows due to resonance. At this point, the test charge will substantially loose its energy, while for larger velocities ($V_t \gg v_{sd}$) almost the same static behavior is exhibited.

Very fast charge relaxation rate

Substituting Eq.(5.14) into Eq.(5.10), we numerically calculate the ES potential (ϕ') versus the axial position (ξ') for different values of $\frac{\nu_c\beta}{\nu_0}$ ($0 \leq \frac{\nu_c\beta}{\nu_0} \leq 0.6$). The results are displayed in Fig.(5.2), keeping other parameters the same as in Fig. (5.1). It is seen that with the increase of dust charge fluctuation the amplitude of ES potential enhances. The $\frac{\nu_c\beta}{\nu_0} = 0$ curve corresponds to the no charge fluctuation case. One also observes larger amplitude of

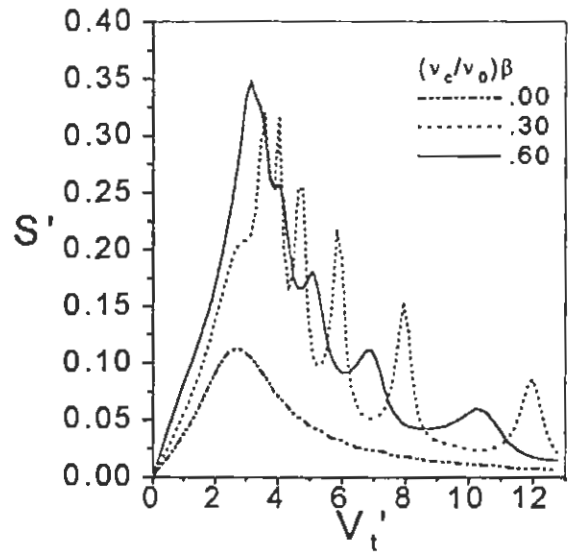

Figure 5-3: The energy loss of a test charge (S') in the units of $Z_t^2 e^2/2\pi^2$ vs the normalized test charge velocity V_t' for different values of $(0 \leq (\nu_c/\nu_0)\beta < 0.6)$, keeping other parameters fixed as in Fig. 1. A comparison of energy loss is made with the no charge fluctuation (i.e., $\beta = 0$) for collision dominated plasmas.

ES potential (without changing the Debye length of the plasma) for relatively slower charge relaxation rates. We cannot detect any appreciable contribution in the low phase velocity regime (comparing with the thermal motions of electron and ion) arising from the Landau damping of the electron and ion plasma.

We have also numerically calculated the value of S' and plotted (in Fig. (5.3)) it against the test charge velocity (V_t') for different values of $\nu_c\beta/\nu_0$, while other parameters are the same as in Fig. (5.1). The enhancement in the energy loss is observed as compared with the case having no charge fluctuations. For smaller values of the charge relaxation rate (but $\nu_0 \gg \omega$), greater enhancement in the energy loss is observed. Also, for smaller values of $\nu_c\beta/\nu_0$, some peaks are observed in the energy loss curves. Perhaps these peaks were due to excitations of some collective modes, which are only due to the dust charge fluctuations. These peaks diminish and move towards lower velocity regimes for higher values of $\nu_c\beta/\nu_0$.

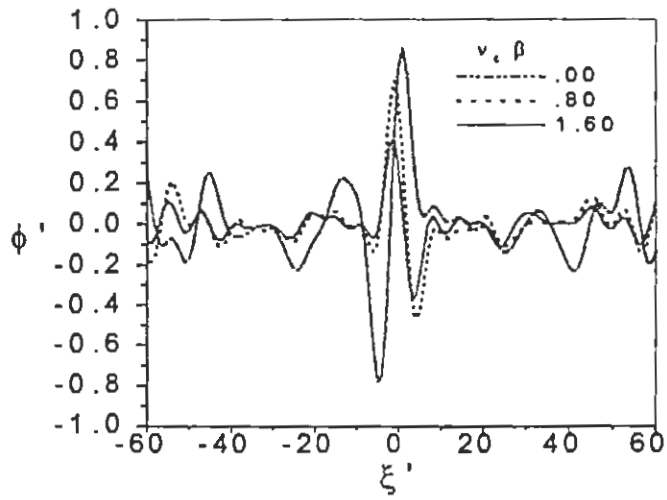

Figure 5-4: The normalized ES potential of a test charge (ϕ') vs the normalized axial position ξ' $(= x - V_t t)$ for different values of $(0 \leq \nu_c\, \beta \leq 1.6)$, with $V_t' = 3$ and the other parameters are the same as in Fig.1. A comparison of the potential is made with the no charge fluctuation (i.e., $\beta = 0$) case for collisionless plasmas.

Very slow charge relaxation rate

Inserting Eq. (5.18) into Eq.(5.10), we numerically calculate the value of ϕ' and plot it versus ξ' for different values of $\nu_c\beta$ ($0 \leq \nu_c\beta \leq 1.6$). The results are displayed in Fig. (5.4), keeping other parameters the same as in the Fig. (5.1). It is seen that for very slow charge relaxation rate, the dust charge fluctuation causes large damping in the ES potential.

The energy loss per unit path length S $(= S_1 + S_2)$ is numerically calculated. The values of S' versus the test charge velocity V_t' for different values of $\nu_c\beta$ $(0 \leq \nu_c\beta \leq 0.09)$ are graphically shown in Fig. (5.5). It is seen that without the charge relaxation rate, the dust charge fluctuations cause an increase rather than a decrease in the energy of a test charged dust particulate in a multi-component dusty plasma for smaller test charge velocity; and that the energy loss per unit path length is smaller than that for the no charge fluctuation case. Furthermore, the contribution from S_2 is large for smaller test charge velocity than for larger velocities.

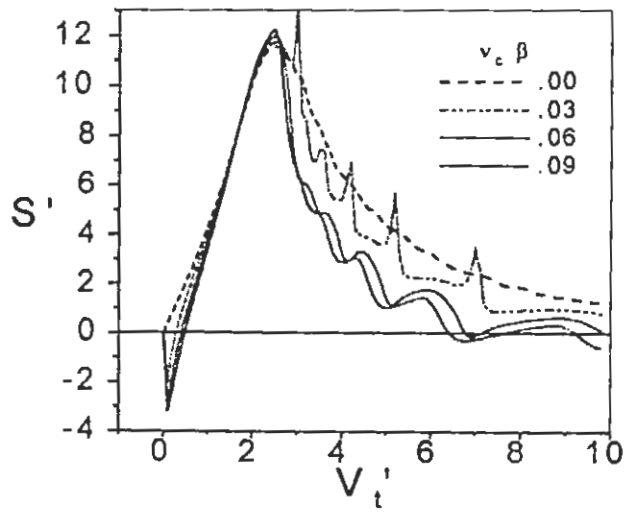

Figure 5-5: The energy loss of a projectile ($S' \times 10^{-2}$) in the units of $Z_t^2 e^2/2\pi^2$ vs the normalized projectile velocity V_t' for different values of ($0 \leq \nu_c\beta \leq 0.09$), keeping other parameters fixed as in Fig.1. A comparison of energy loss is made with no charge fluctuations (i. e., $\beta = 0$) for collisionless plasmas.

5.4.2 Discussion on the results of collective response

The energy loss per unit path length of the test charged particulate provides force that the test charge experiences in its own induced field, which produces acceleration of other dust grains. The energy loss rate may increase when the test charge velocity becomes comparable to the dust sound speed and a dust acoustic wave is excited due to resonant exchange of energy.

It is further found that the dust charge fluctuation has a significant effect on the induced electrostatic potential and the energy loss of a test charged particulate. The charge fluctuation enhances the energy loss when the charge relaxation rate is very high and reduces it when the rate is low, as compared with no-charge fluctuation case. The energy loss curves drawn against the test charge velocity exhibit some peaks in the dust charge fluctuation case. These peaks, however, diminish for higher values of the charge relaxation rates.

The occurrence of the peaks may be attributed to a number of effects. For example, they may appear due to exchange of energy of the test charged particulate with some other

collective modes such as unstable ion waves[69], Kelvin-Helmholtz instability[75] and some other electrostatic instabilities[76], brought about by the dust charge fluctuations. In other words, these peaks represent enhanced energy loss of test charged particulate when its velocity matches the phase velocities of the excited waves. The identification and investigation of these collective modes is, however, not the subject of the present investigation.

Another possible explanation for the peaks is the enhancement of the dust charge due to the accumulation of more electrons and ions resulting from the perturbation. Initially, when the fast electrons make contact with the dust particulate, the latter acquires higher negative charge state which then, on arrival of slower ions, relaxes to an equilibrium when the electron and ion currents match. In this manner, the charge state of dust particulate undergoes fluctuations. This periodic rise and fall of the dust charge results in the peaking and lowering of the energy loss rate. This notion is further supported by the observation that the peak heights reduce in size when the charge relaxation rate becomes large. One also observes that for small charge relaxation rate, the test charged particulate gains energy instead of loosing in the limit of small test charge velocities.

In the dust charge fluctuation case, the charge on the dust particulate does not remain constant, and any fluctuation in the dust charge produces fluctuations in the electrostatic force for the field free plasma. The fluctuation on the force, in turn, produces fluctuations in the energy loss rates. This may be an explanation for the appearance of peaks. However, this nonlinear effect ($-Z_1 e\nabla\phi$) does not enter in our linear analysis.

The energy loss mechanism discussed here may provide a possible explanation for the crystal formation in which low energy dust particulates arrange themselves into some lattice pattern, or the low energy dust particulate condensate into heavier particulate in space and laboratory plasmas. It may also explain the transport of the dust grain in planetary rings in which slower dust grains gain energy instead of loosing.

The behavior of the ES potential is found similar to that of the energy loss. When the test charge velocity ($V_t = \frac{\omega}{|K|}$) is less than the dust thermal velocity (v_{td}), a static Coulomb potential is observed, whereas for larger velocities the potential becomes Debye-Hückel. On phase velocity becoming comparable to the dust sound speed (v_{sd}), the potential is observed to acquire a large amplitude. For test charge velocities greater than the dust sound speed

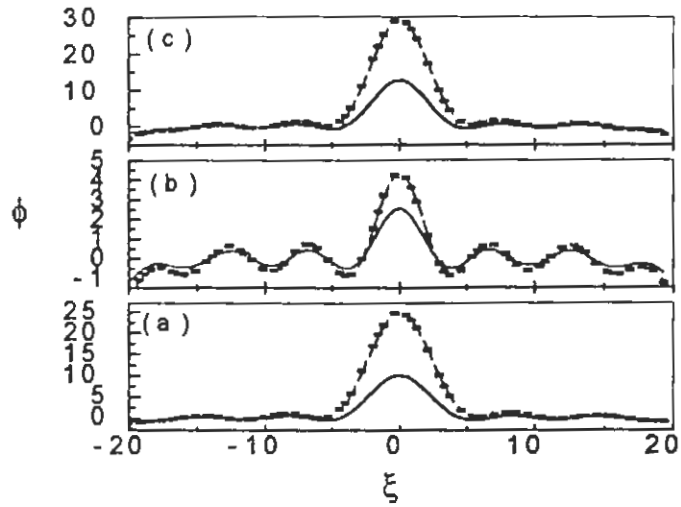

Figure 5-6: The collective response (a), individual particle interaction (b) and total (c) $\phi \times 10^{-5}$ versus ξ for $v_0 = 1.1\omega_{pd}$, $V_t = 0.01 v_{td}$, with (line with square) and without dust charge fluctuation (solid line), for large charge relaxation rate limit (line with circle) with effective normalized Debye wave number $K_D = 0.32$ and with $Z_t = 0.01$.

($v_{sd} \leq V_t \leq 12 v_{td}$), Debye-Hückel potential is observed. However, when the test charge velocity becomes too large ($12 v_{td} < V_t < v_{ti}$), the Debye-Hückel potential changes back to the Coulomb type.

Further, we do not observe a measurable contribution from the electron and ion plasma Landau damping, to the ES potential and energy. In the low phase regimes, however, the dust Landau damping does make a significant contribution.

5.4.3 Individual particle interaction

Taking some experimental parameters as, given by Barkan *et al.*[24]: $\lambda_{Dd} = (26 - 78)\ \mu m$; $\lambda_{De} = 200\ \mu m$; $\lambda_{Di} = 800\ \mu m$; $n_{e0} \simeq n_{i0} = 10^9\ cm^{-3}$; $n_{d0} = 10^5\ cm^{-3}$; $T_i = 0.15\ eV$; $T_d = 0.1\ eV$; $T_e = 1.0\ eV$; $Z_t = Z_d = 10^4$; $m_d = 10^8\ m_p$, and m_p is the mass of proton, we numerically solve Eq.(5.10) & Eq. (5.13) taking the $K-$integration $1 < K < K_{max}$, for very fast (slow) charge relaxation rate[43]

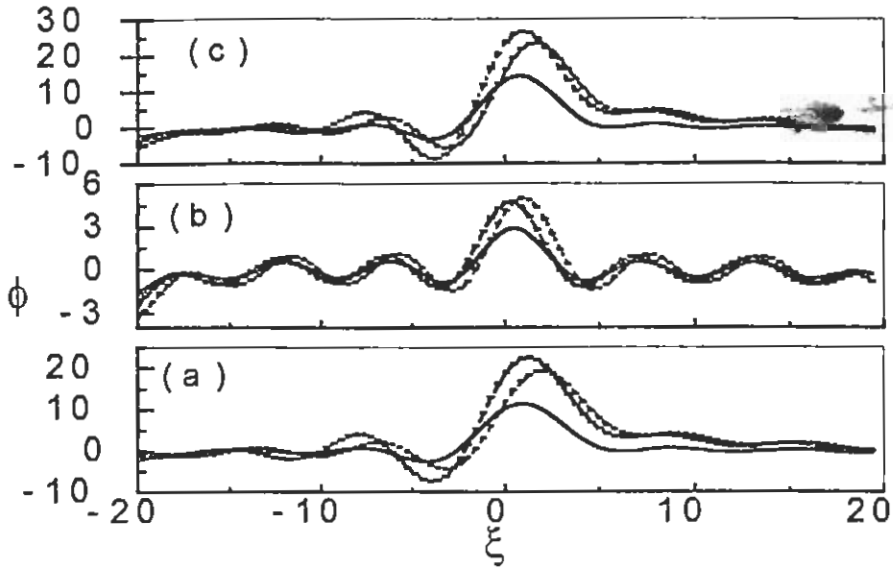

Figure 5-7: The same as Fig. 5.6 except for $V_t = 1.1 v_{td}$.

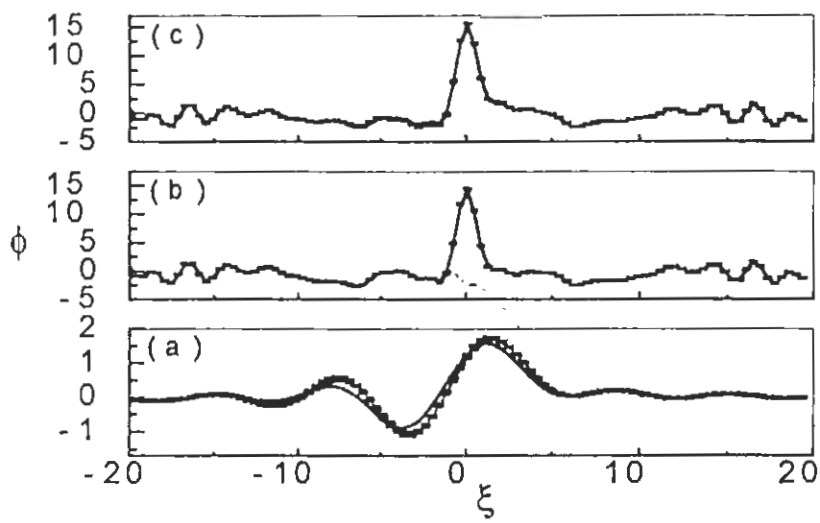

Figure 5-8: The same as Fig. 5.6 except for $V_t = 2.0 v_{td}$.

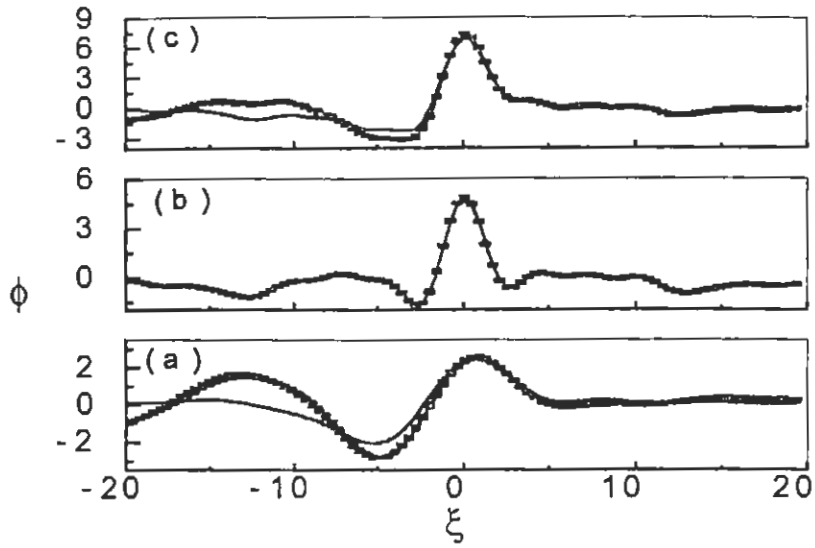

Figure 5-9: The same as Fig. 5.6 except for $V_t = 3.3v_{td}$.

Very fast charge relaxation rate

The parts (a) of figures $(5.6 - 5.9)$ display the variation of the collective response $(K \in [0,1])$ of the plasma to the normalized ES potential ϕ $(= Z_{d0}e\phi/T_d)$ against the normalized axial position ξ $(= x - V_t t)$ in the units of λ_{Dd}, for various normalized test charge velocities V_t $(= V_t/v_{td})$ and charge relaxation rates, by using the exact (as given by 5.11) and approximated dielectric constant (using 5.14). The results are compared with that of no dust charge fluctuations. The parts (b) and (c) of these figures show the individual contribution of particles $(K \in [1,\infty])$ to the ES potential and the total ES potential respectively.

It is observed that for a slow test charge $(V_t \simeq 0)$, the collective as well as the individual interactions of the particles result in a Coulomb type ES potential with and without dust charge fluctuations. The ES potential will be shielded and become Debye–Hückel type for higher test charge velocities $(V_t > v_{td})$ as shown in Fig. $(5.7 - 5.9)$. A damped wake field is formed behind the test charge. For large test charge velocity the ES potential shows similar behavior for both with and without dust charge fluctuations. The individual interaction of particles show an oscillatory field beyond the Debye sphere. Figures $(5.6 - 5.9)$ display the ES potential of a test charge due to collective response of plasma, individual particle

interactions as well as their sum.

The energy loss of a test charge in a stationary referential frame is calculated numerically by substituting Eq. (5.13) into Eq.(5.12) and is plotted (see e.g., Figs. 5.10 – 5.12) versus normalized test charge velocity V_t for charge relaxation rates $\nu_0 = 1.1\ \omega_{pd}$, $10\ \omega_{pd}$ and $50\ \omega_{pd}$, keeping other parameters the same as in Fig. (5.6). These results are compared with those for a constant dust charge and the exact dielectric constant (using 5.11). It is evident from the figures (5.10 – 5.12) that the dust charge fluctuation enhances the energy loss. We observe a number of peaks in the energy loss for the dust charge fluctuation. Perhaps the peaks were caused due to excitations of some other collective modes which are only present for dust charge fluctuations case. The excitation of these modes diminishes as we increase the charge relaxation rate ($\nu_0 \geq 50\ \omega_{pd}$) as shown in Fig. (5.12).

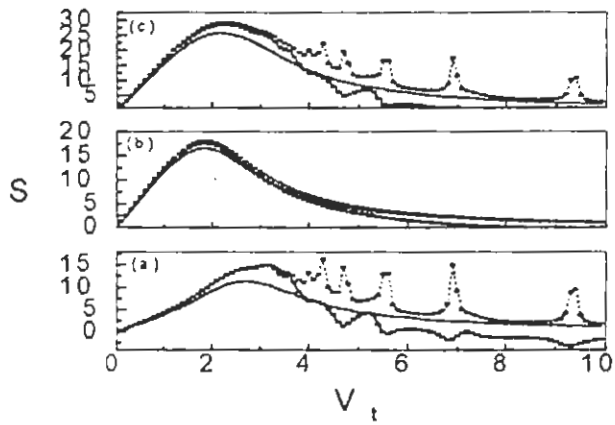

Figure 5-10: The collective response (a), individual particle interaction (b) and total (c) energy loss ($S \times 10^{-4}$) versus normalized test charge velocity $V_t = 0.01\ v_{td}$, for the normalized charge relaxation rate $\nu_0 = 1.1\ \omega_{pd}$, with (line with square) and without dust charge fluctuation (solid line), for large charge relaxation rate limit (line with circle) with effective normalized Debye wave number $K_D = 0.32$ andwith effective normalized charge state $Z_t = 0.01$.

Very slow charge relaxation rate

Using the modified as well as actual dielectric constant in Eq. (*), we have numerically calculated the normalized ES potential and plotted it versus normalized axial position (ξ)

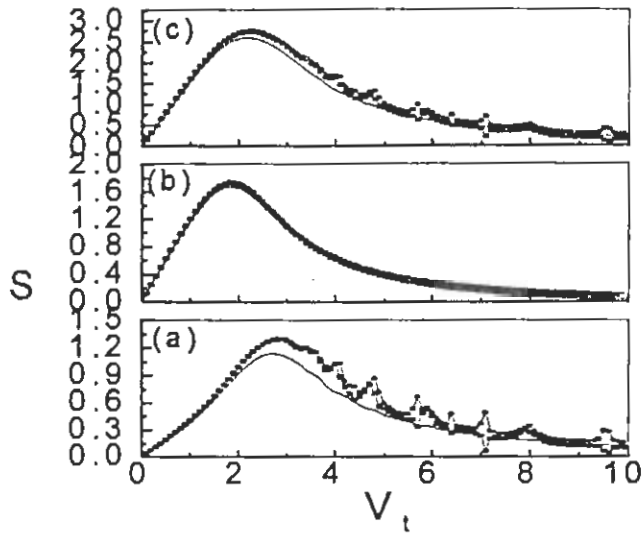

Figure 5-11: The same as the Fig.(5.10) , execpt $\nu_0 = 10\ \omega_{pd}$.

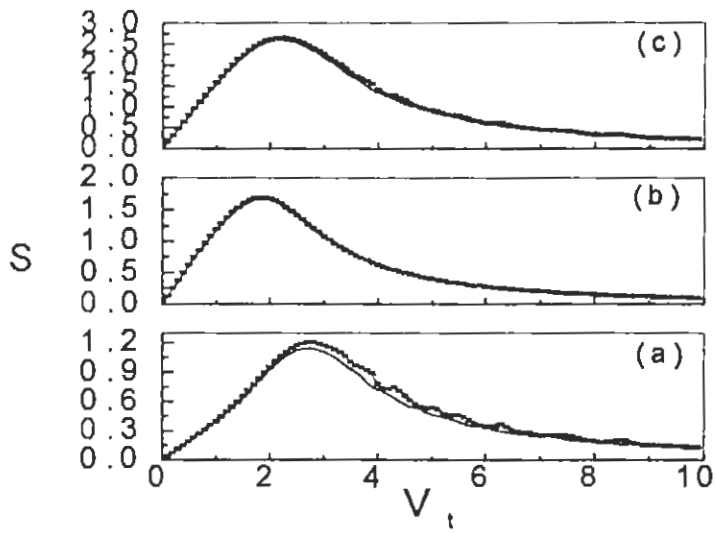

Figure 5-12: The same as the Fig. (5.10), execpt $\nu_0 = 50\ \omega_{pd}$.

for different test charge velocities $V_t = 0.01 v_{td}$, $1.1 v_{td}$ and $3.3 v_{td}$ with $\nu_0 = 0.1\ \omega_{pd}$, keeping other parameters the same as in Fig. (5.6). The dust charge fluctuations seems to act as a sink term for other charge species (i.e., electrons and positive ions). For small test charge velocity, we observe *i*) a Coulomb type ES potential with no dust charge fluctuation *ii*) a potential well with dust charge fluctuation. In the latter case, we also observe a very weak ES potential for a small charge relaxation rate. While an oscillatory potential is observed for individual particle interaction case, a damped wake field may be seen when the collective response of the plasma is taken into account (see e.g., Fig. 5.13). For higher test charge velocity ($V_t > v_{td}$) case, a shielded potential with a large Debye sphere for collective response and with a small Debye sphere for individual response is observed. The charge fluctuations produce oscillations beyond the Debye sphere. In the limit of higher test charge velocities, we found a good agreement of electrostatic potential obtained by using approximated and exact dielectric constants. These results are exhibited in Figs. (5.13 – 5.15).

The collective as well as individual particle contribution to energy loss along with total energy loss of a test charge is numerically calculated and shown graphically in Fig. (5.16) for small test charge velocity limit and in Fig. (5.17) without any velocity limit for both the cases of with and without dust charge fluctuations, keeping other parameters the same as in Fig. (5.6). It is observed that for small charge relaxation rate ($\nu_0 < \omega = \mathbf{K} \cdot \mathbf{V}_t$) the test charge gains energy instead of loosing. The dielectric constant for small test charge velocity limit does not show any change in the results. It may be concluded that for slow charge relaxation rate, the dust charge fluctuations cause a potential well in which the test charge is trapped (and gains energy).

5.4.4 Discussion on the results of individual contribution

For fast charge relaxation rate ($\nu_0 > \omega = \mathbf{K} \cdot \mathbf{V}_t$) , a shielded potential occurs for large test charge velocities ($V_t > v_{td}$) and a Coulomb type potential for small test charge velocities ($V_t \leq v_{td}$). This behavior is the same for both the collective and the individual particle contributions. On the other hand, for small charge relaxation rates ($\nu_0 < \omega = \mathbf{K} \cdot \mathbf{V}_t$) and for small test charge velocities ($V_t < v_{td}$) a potential well is formed. The individual particle

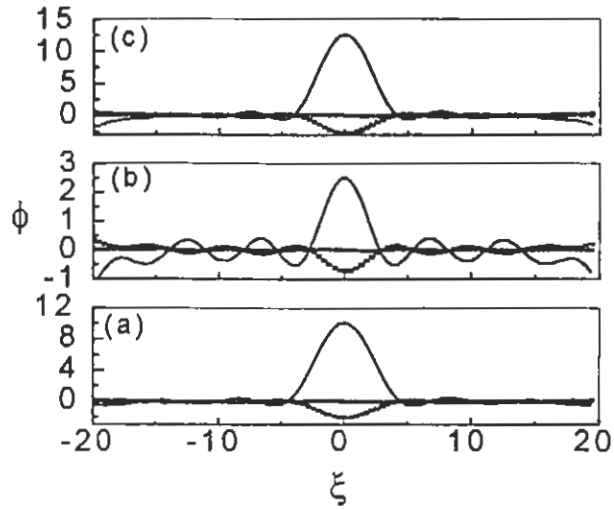

Figure 5-13: The collective response (a), individual particle interaction (b) and total (c) $\phi \times 10^{-5}$ versus ξ for $\nu_0 = 0.1\omega_{pd}$, $V_t = 0.01\ v_{td}$, with (line with square) and without dust charge fluctuation (solid line), for small charge relaxation rate limit (line with circle) with effective normalized Debye wave number $K_D = 0.32$ and with effective normalized charge state $Z_t = 0.01$.

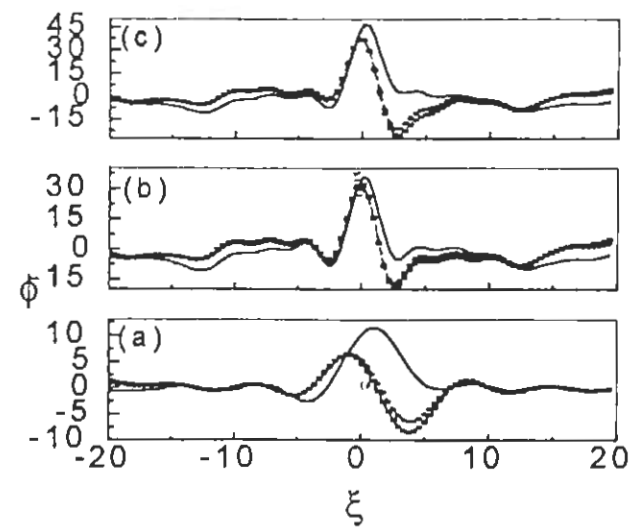

Figure 5-14: The same as Fig. (5.13) execpt for $V_t = 1.1\ v_{td}$.

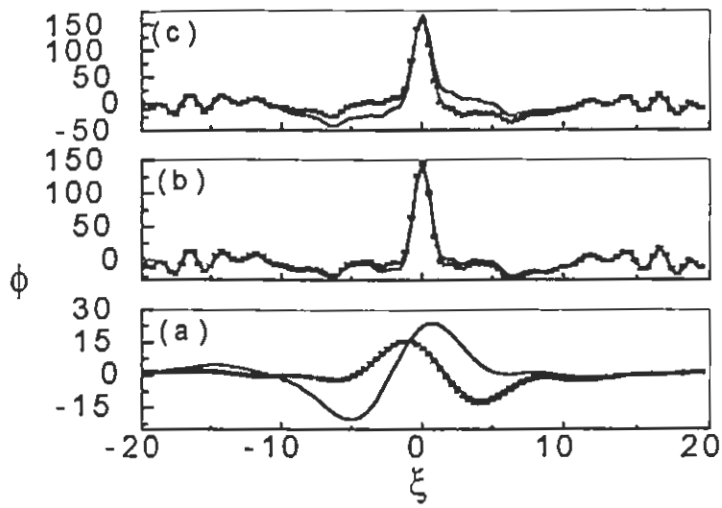

Figure 5-15: The same as Fig.(5.13) execpt for $V_t = 3.3\ v_{td}$.

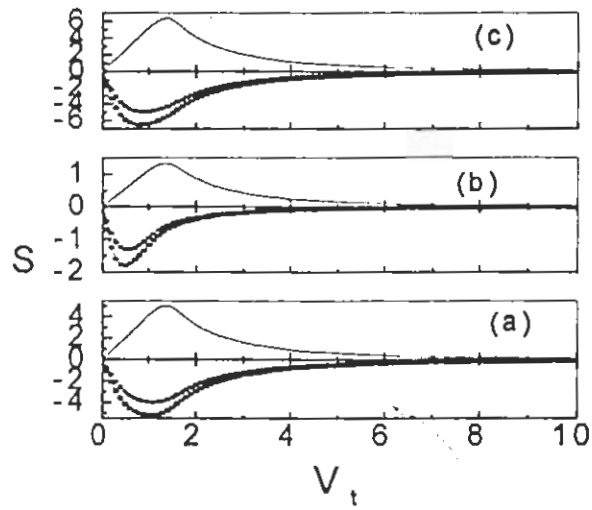

Figure 5-16: The collective response(a), individual particle interaction (b) and total (c) normalized energy loss ($S \times 10^{-4}$) versus normalized test charge velocity V_t ($= V_t/v_{td}$), for the normalized charge relaxation rate $\nu_0 = 0.1\ \omega_{pd}$, with (line with square) and without dust charge fluctuation (solid line), for small charge relaxation rate limit (line with circle) with effective normalized Debye wave number $K_D = 0.32$ and with effective normalized charge state $Z_t = 0.01$, for small test charge velocity limit.

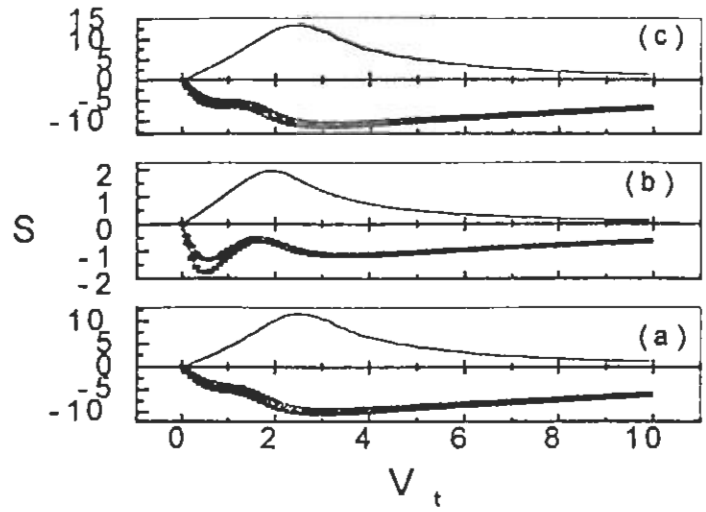

Figure 5-17: The same as Fig. (5.16), execpt without any test charge velocity limit.

interaction causes oscillations beyond the Debye sphere but a static potential inside the Debye sphere, which changes to a Debye–Hückel type potential as we increase the test charge velocity. The main feature of the individual particle interaction is a shielded potential with a small Debye sphere.

In the presence of charge fluctuations, a test charge gains energy instead of loosing, for small charge relaxations rates (less than the plasma oscillations). This is perhaps due to charging of the dust grains and trapping of electrons and ions inside a potential well. On the other hand, an enhancement in the energy loss is observed for large charge relaxation rates. This might be due to the dust grain having acquired a large constant charge. We also observe some peaks in the energy loss curves for relatively higher velocities in the collective response of the plasmas. These might have arisen due to excitations of some other collective modes which are not present for constant dust charge as well as for individual response of the plasma. The said modes diminish for large charge relaxation rates ($\nu_0 > 50\omega_{pd}$). The perturbations due to dust charge fluctuations are damped and become a constant dust charge case with higher charge state of the dust.

Chapter 6

Collisional Effects on the energy loss

The energy loss of a test charge in an unmagnetized dusty plasma is estimated for different dust parameters (such as dust charge state, dust number density, dust charge fluctuation and dust-neutral collisions) using Krook and BGK-type collisional models. We find that higher the dust-charge-state more pronounced is the wake-field (which extends up-to several Debye lengths). Similar behavior occurs with the variation of the dust number density. For large dust-neutral collisions a weakly damped large amplitude wake-field is observed which jumps ahead of the test charge position for higher collision frequencies. A critical test charge velocity is determined for a particular dust-neutral collision frequency below which the test charge gains energy instead of loosing. The dust neutral collisions are also found to enhance the energy loss for test charge velocities greater than the dust acoustic speeds in contrast with the dust charge fluctuations which enhances the energy loss only for test charge velocities smaller than the dust acoustic speeds.

6.1 Introduction

Since there is always a large number of neutral particles present in a dusty plasma, it is instructive to examine the effect of dust-neutral collisions on the potential perturbation caused by the test charge and consequently the effect on the energy loss per unit path length by the test charge. Recently, attempts have been made to investigate the effect of dust–neutral collisions on the dust-acoustic waves (DAW) in partially ionized dusty plasma[77] and in

strongly coupled dusty plasmas[78]. Their effect was also investigated on the damping of surface waves[79] and on the dynamics of neutrals in both low and high–frequency electromagnetic modes[80]. A wide variety of acoustic modes[81] and the boundary effects[82] thereon were also studied in a collisional dusty plasma. The neutral particles may also exist in low–temperature dusty plasmas, which on collision, will provide a drag force on the low–frequency modes.

Stenflo et al.[83] calculated the effect of the electron-neutral collisions on the potential of a slowly moving (as compared to the electron thermal motion) test charge by using the Bhatanagar, Gross, Krook (BGK) collisional model. The energy loss of a test charge was also investigated[44, 45] in a partially ionized dusty plasma and it was found that a slow test charge gains energy and can thus accelerate up to the thermal speed of the ambient plasma. There is, however, a need to investigate collisional effects on the electrostatic (ES) potential as well as on the energy loss of the test charge particles as they propagate through a multi-component dusty plasma having different dust parameters such as dust-charge state, dust-number density, dust-charge fluctuations and dust-neutral collisions.

In this chapter, we study the effect of dust-neutral collisions on the electrostatic potential and energy loss per unit path length of a charged projectile propagating through a multi-component dusty plasma by using the Krook and the BGK collision models. Moreover, we investigate the effect of charge state and number density of the dust particles on the potential perturbations and on the energy loss of the test charge. Finally, we compare the effects of the dust charge fluctuations with that of the collision frequency.

6.2 The collisional operator

For low-frequency, large-scale phenomena, collisions may become dominant, and a proper treatment of the close collisions must be given. We use simple models to incorporate the dust-neutral collisions proposed by Krook [84] known as Krook model and Bhatanagar, Gross and Krook[85], known as BGK model. These models have been used to estimate the effect of collision on plasma wave propagation. For some problems, the conclusions derived from it agree qualitatively with those obtained from more sophisticated collision operators

When it is desirable to take only some limited account of collisional effects, one may use the simple relaxation model in which the collisional operator can be written as

$$(\partial f_d/\partial t)_c = -\nu_{d0}\,(f_d - f_{d0})\,,$$

where f_{d0} is the equilibrium velocity distribution function and ν_{d0}^{-1} is the relaxation rate for the dust velocity distribution. This is known as Krook model. This relaxation model provides a very simple collision term which tends to drive f_d toward some equilibrium distribution f_{d0} at a rate governed by the relaxation time ν_{d0}^{-1}. There are some examples one can cite where the model leads to almost identical results obtained by using the more complicated models.

Writing $f_d = f_{d0} + f_{d1}$, the linearized form of the Krook collisional operator becomes

$$(\partial f_d/\partial t)_c = -\nu_{d0} f_{d1}. \tag{6.1}$$

Although this model does not conserve the number density, yet it is simple enough to use in the situation where one needs a rough estimation.

In the BGK model, on the other hand, the rate of change of the dust distribution function f_d due to collisions is given by

$$(\partial f_d/\partial t)_c = -\nu_{d0}\,(f_d - f_M)$$

where f_M is a suitable Maxwellian distribution and ν_{d0} is an empirical collision frequency, which can depend on velocity if desired, but is usually left constant. In BGK model the term $-\nu_{d0} f_d$ represents the rate of loss of particles, due to collisions, from a small element of phase space, while $\nu_{d0} f_M$ represents the corresponding rate of gain of particles as the end product of collisions.

Assuming that f_M has the same density as f_d, the zero mean velocity, and the temperature equal to the ambient temperature, the linearized form of the suitable maxwellian distribution f_M is[86]

$$f_M = \frac{n_{d1}}{n_0} f_{d0},$$

where n_0 is the number density of neutral dust particles. On linearization, we have

$$(\partial f_d/\partial t)_c = -\nu_{d0}\left(f_{d1} - \frac{n_{d1}}{n_0} f_{d0}\right). \tag{6.2}$$

In the next section we will calculate the dielectric constant by using Krook as well as BGK collisional operators. The effect on the ES potential perturbation as well as on the energy loss will also be discussed.

6.3 Calculation of dielectric constant

The plasma under consideration is composed of electrons, singly ionized positive ions and micron sized negatively charged dust grains with charge q_j. As mentioned earlier a test charge having charge $Z_t e$ with velocity $\mathbf{V}_t$ passes through the plasma along z-axis. The electrons and ions are assumed to follow the Boltzmann distribution as given in Eq.(3.5) Due to the presence of dust-neutral collisions the Vlasov-Boltzmann equation can be written as

$$\left(\frac{\partial}{\partial t} + \mathbf{v}\cdot\nabla\right) f_{d1} + \frac{Z_{d0}e}{m_d}\nabla\phi\cdot\nabla_{\mathbf{v}} f_{d0} = \left(\frac{\partial f_d}{\partial t}\right)_c \tag{6.3}$$

where $f_{d1}(\mathbf{v}) << f_{d0}(\mathbf{v})$ is a small perturbation in the equilibrium distribution $f_{d0}(\mathbf{v})$ which is assumed to be a Maxwellian. The equations are closed by using the Poisson equation(3.8). By adopting the procedure used in the subsection (3.3.1), the ES potential in a stationary frame can be calculated as

$$\phi(\mathbf{X}, t) = \frac{Z_t e}{2\pi^2}\int d\mathbf{K} d\omega \frac{\delta(\omega - \mathbf{K}\cdot\mathbf{V}_t)}{K^2\epsilon(\mathbf{K},\omega)} \exp\left[i\mathbf{K}\cdot\mathbf{X} - \omega t\right] \tag{6.4}$$

Performing the ω-integration in Eq.(6.4), we will get

$$\phi(\mathbf{X}, t) = \frac{Z_t e}{2\pi^2}\int d\mathbf{K} \frac{\exp\left[i\mathbf{K}\cdot(\mathbf{X} - \mathbf{V}_t t)\right]}{K^2\epsilon(K, \mathbf{K}\cdot\mathbf{V}_t)} \tag{6.5}$$

Writing $\mathbf{X}$ and $\mathbf{K}$ in spherical co-ordinates and performing the azimuthal integration as in subsection (3.3.2), we have the ES potential as

$$\phi(X,t) = \frac{Z_t e}{\pi} \int_0^{K_{max}} dK \int_{-1}^{1} d\mu \frac{\exp(iK\xi\mu)\, J_0\left(K\rho\sqrt{1-\mu^2}\right)}{\epsilon(\mathbf{K}, \mathbf{K}\cdot\mathbf{V}_t)}, \tag{6.6}$$

where $J_0\left(K\rho\sqrt{1-\mu^2}\right)$ is the zeroth order Bessel function, $\xi = x - V_t t$ is the instantaneous position of the test particle in the reference from in which the test particle is at rest, $\mu = \cos(\mathbf{K}, \mathbf{V}_t)$ and $\epsilon(K,\omega)$ is the dielectric constant given as

$$\epsilon(\mathbf{K},\omega) = 1 + \chi_i(\mathbf{K},\omega) + \chi_e(\mathbf{K},\omega) + \chi_d(\mathbf{K},\omega) + \chi_z(\mathbf{K},\omega) \tag{6.7}$$

where $\mathbf{K}$ and ω are the wave vector and frequency respectively and χ_j is the susceptibility of the particle species j (j equals e for the electrons, i for the ions, and d for the dust grains) and χ_z is the susceptibility due to dust charge fluctuations. For low phase velocity ($\omega/K \ll v_{ti}, v_{te}$), the dielectric susceptibility of the electrons and positive ions are obtained from Eq.(2.13) for small argument of the plasma dispersion function *i.e.*,

$$\chi_s \simeq \frac{K_{Ds}^2}{K^2}\left[1 + i\sqrt{\frac{\pi}{2}}\frac{\omega}{K v_{ts}}\right], \tag{6.8}$$

where $K_{Dj} = \left(4\pi n_{j0} q_j^2/T_j\right)^{1/2}$ is the Debye wave number, $v_{tj} = (T_j/m_j)^{1/2}$ is the thermal velocity, n_{j0} the equilibrium number density, m_j the mass, q_j the charge ($-e$ for electronic charge, e the ionic charge and $-Z_{d0}e$ the dust charge), and T_j the temperature (in energy units) of jth species.

The susceptibility of negatively charged dust particles with the dust–neutral collisions approximated by Eq.(6.1) is given as

$$\chi_d = \frac{K_{Dd}^2}{K^2}\left[1 + CG(C)\right]. \tag{6.9}$$

where $C = (\omega + i\nu_{d0})/\sqrt{2}Kv_{td}$, and ν_{d0} is the dust-neutral collision frequency which may depend upon the velocity, but is usually left constant as it is here in our case. The Dawson

integral $G(C)$ is given by[87]

$$G(C) = -2\int_0^C \exp\left(z^2 - C^2\right) dz + i\sqrt{\pi}\exp(-C^2),$$

so that the Eq.(6.9) can be re-written as

$$\chi_d = \frac{K_{Dd}^2}{K^2}\left[1 - 2C\exp\left(-C^2\right)\int_0^C \exp\left(z^2\right) dz + \sqrt{\pi}C\exp(-C^2)\right]. \tag{6.10}$$

By using (6.8) and (6.10) into (6.7), we obtain

$$\epsilon\left(\mathrm{K},\omega\right) = 1 + \frac{K_D^2}{K^2} + i\frac{1}{K^2}L_D + \frac{K_{Dd}^2}{K^2}\left[1 + CG(C)\right], \tag{6.11}$$

where $L_D = \sqrt{\pi/2}\,(\omega/K)\left[(K_{De}^2/v_{te}) + (K_{Di}^2/v_{ti})\right]$ is the Landau damping of electrons and ions and $K_D = \sqrt{K_{De}^2 + K_{Di}^2}$ the effective Debye wave number.

Using BGK collision operator in the linearized Boltzmann-Vlasov equation, the dust susceptibility can be approximated by

$$\chi_d = \frac{K_{Dd}^2}{K^2}\left(\frac{1 + CG(C)}{1 + i\left(\nu_{d0}/Kv_{td}n_0\right)G(C)}\right). \tag{6.12}$$

It may be noted that the BGK collisions introduce an additional term in the denominator of χ_d. The Krook's model simply modifies the angular frequency $\omega \rightarrow \omega + i\nu_{d0}$ in C.

The dielectric constant in this case becomes

$$\epsilon\left(\mathrm{K},\omega\right) = 1 + \frac{K_D^2}{K^2} + i\frac{1}{K^2}L_D + \frac{K_{Dd}^2}{K^2}\left(\frac{1 + CG(C)}{1 + i\left(\nu_{d0}/n_0\right)G(C)}\right). \tag{6.13}$$

Knowing the above we can estimate the energy loss per unit path length of the test particle from Eq.(2.20) as

$$S = \frac{Z_t^2 e^2}{2\pi^2}\int_0^{K_{\max}} KdK\int_{-1}^{1}\mu d\mu Im\left[\epsilon^{-1}\left(\mathrm{K},\mathrm{K}\cdot\mathrm{V_t}\right)\right]. \tag{6.14}$$

In the next section, we will numerically calculate the ES potential and the energy loss per

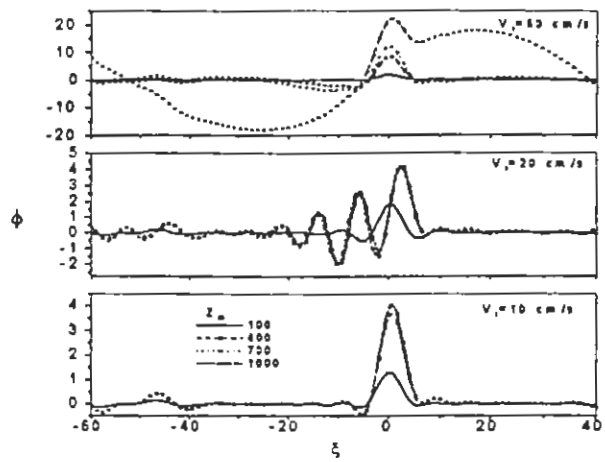

Figure 6-1: The normalized ES potential ϕ ($\times 10^{-5}$) versus the normalized axial position $\xi\,(=z-V_t t)$ with $n_{i0}=10^8\ cm^{-3}$, $n_{d0}=10^5\ cm^{-3}$; $T_e=2.0$ eV;$T_i=0.3$ eV;$T_d=0.1$ eV, for different dust charge states $Z_{d0}=100$ (solid line), 400 (dashed line), 700 (dotted line), 1000 (dashed dotted line) and test charge velocity (a) $V_t=10$ cm/s (b)$V_t=20$ cm/s (c)$V_t=60$ cm/s.

unit length for different dust-parameters.

6.4 Numerical Results

We have normalized the parameters $X\rightarrow X/\lambda_{Dd}$, $\mathrm{V}\rightarrow \mathrm{V}/V_{td}$, $t\rightarrow t\omega_{pd}$, $\phi\rightarrow Z_{d0}e\phi/T_d$, $f(\mathrm{X},\mathrm{V},t)\rightarrow V_{td}^3 f(\mathrm{X},\mathrm{V},t)/n_{d0}$, $Z=Z_t/N_d Z_{d0}$, and $\nu_{d0}\rightarrow \nu_{d0}/\omega_{pd}$, where $N_d=n_{d0}\lambda_{Dd}^3$ is the number of dust particles in the Debye sphere and numerically solve Eqs.(6.6) and (6.11) for the ES potential and the energy loss, respectively, by taking some typical parameters: $T_d=0.03-0.1\ eV$, $T_i=0.3\ eV$, $T_e=2.0\ eV$, $n_{i0}=10^8\ -10^9 cm^{-3}$and $m_d=10^8 m_p$, where m_p is the mass of proton. Various values of the dust charge state Z_{d0} $(10^2<Z_{d0}<10^3)$ and the number density n_{d0} $(10^3<n_{d0}<10^4)$, which satisfy the charge neutrality condition $(n_{i0}=n_{e0}+Z_{d0}n_{d0})$, are taken. We have studied the effect of the dust charge state, the dust number density and the dust–neutral collision frequency on the ES potential and energy loss per unit length, which are discussed in the following subsections:

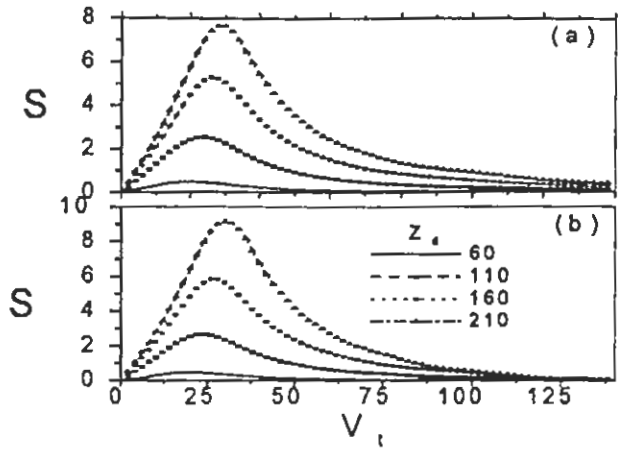

Figure 6-2: The energy loss per unit path length $(-dE/dx)$ versus test charge velocity V_t with $n_{i0} = 10^9\ cm^{-3}$, $n_{d0} = 10^5\ cm^{-3}$; $T_e = 2.0$ eV;$T_i = 0.3$ eV;$T_d = 0.03$ eV, for different dust charge states $Z_{d0} = 60$ (solid line), 110 (dashed line), 160 (dotted line), 210 (dashed dotted line) and (a) without dust charge fluctuation (b) with dust charge fluctuation.

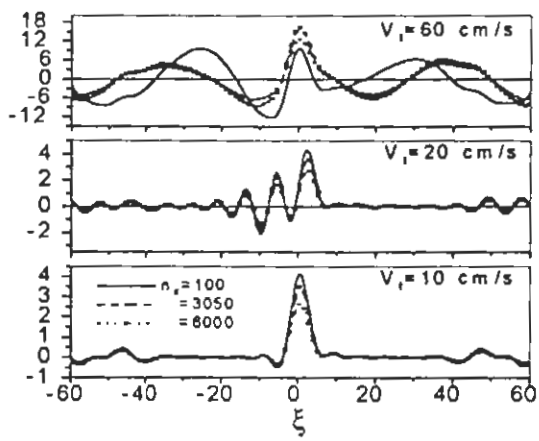

Figure 6-3: Same as Fig. (6.1), except $Z_{d0} = 10^3$ is fixed and different values of n_{d0} $(10^2 < n_{d0} < 6 \times 10^3)$.

6.4.1 Effect of the dust charge state

We calculate the effect of the dust charge on the ES potential and the energy loss of the test charge. The dust charge value can vary over a wide range depending upon the charging source and nature. Further, the dust charge, being a dynamical variable, can also fluctuate about its equilibrium value. In the present discussion, however, we shall consider only the equilibrium charge state, ignoring its fluctuations. The latter effect has been discussed earlier in CHAPTER 5. During the charging process, the dust particles pile up charge as more and more electrons are attached to them. This variation in the charge state alters the number density of electrons for fixed number density of dust grains and ions, given by the charge neutrality relation $n_{e0} = (1 - Z_{d0}\eta)\, n_{i0}$, where in our calculation η $(= n_{d0}/n_{i0})$ is fixed as 10^{-5} . The charge state of the dust grain is chosen such that the number density of electrons ranges approximately from n_{i0} to zero. In the first limiting case, we have almost an electron-ion plasma while in the second it becomes a dust-ion plasma.

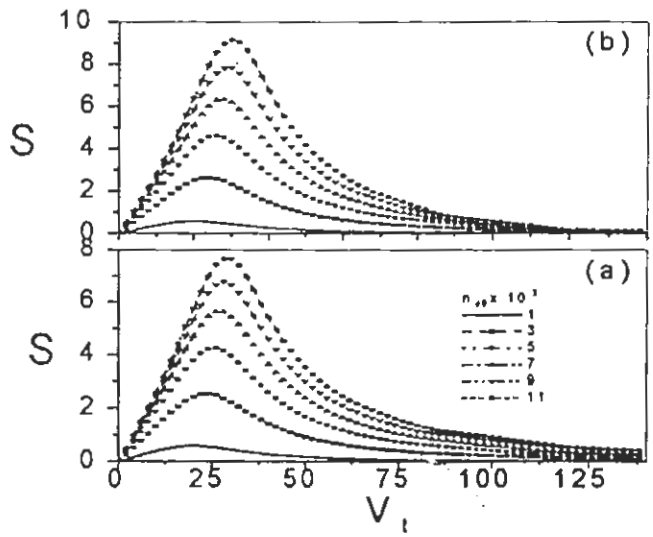

Figure 6-4: The energy loss per unit path length $(-dE/dx)$ versus test charge velocity V_t for different values of the dust number density n_{d0} $(10^3 < n_{d0} < 1.1 \times 10^4)$, with $Z_{d0} = 200$, while other parameters remain same as in Fig. (6.2).

We have numerically calculated the ES potential for different values of the dust charge state Z_{d0} $(10 < Z_{d0} < 10^5)$ and plotted it versus the normalized axial position ξ $(-60 < \xi < 60)$

in Fig.(6-1) by choosing different test charge velocities $V_t(= 10, 20, 60$ cm/s). The potential exhibits different behavior in different Z_{d0} value regimes. As the charge state increases in the lower regime $(10 < Z_{d0} < 10^3)$, the potential perturbation also increases. In the intermediate regime $(10^3 < Z_{d0} < 10^4)$, there is no detectable change in ϕ. For higher charge states $(Z_{d0} > 10^4)$, a decrease in ϕ is observed. Within each regime of Z_{d0}, ϕ shows almost the same behavior for different test charge velocities. However, the regimes themselves may change with test charge velocity, becoming lower for smaller velocities and vice versa. It is worth mentioning here that the charge state of the dust, Z_{d0}, increases at the expense of the electrons i.e., as Z_{d0} increases the electron number density is depleted. With an increase in Z_{d0}, contribution to ϕ from the electron plasma decreases and from the dust plasma increases. However, the two contributions are regime dependent: in the first regime $(10 < Z_{d0} < 10^3)$, the increase due to the dust plasma dominates the decrease due to the electron plasma, resulting in an overall increase in the potential perturbation. In the second regime $(10^3 < Z_{d0} < 10^4)$, the two contributions are nearly equal. In the third regime $(Z_{d0} > 10^4)$, the two contributions interchange their roles. Here, the loss in the potential perturbation (due to decrease in the number density of electron) is larger than the gain (due to increase of dust charge state).

The energy loss per unit path length is numerically calculated and plotted versus the test charge velocity for different dust charge states Z_{d0}. The results for $(60 < Z_{d0} < 210)$ with and without dust charge fluctuation are shown in Fig. (6.2). As is evident from the figure, higher the charge state of the dust, greater is the energy loss. However, this trend reduces considerably as one goes for higher Z_{d0}. When $Z_{d0} > 210$, the energy loss does not increase appreciably any more, becoming negligibly small beyond $Z_{d0} = 10^3$. The enhancement in the energy loss is self-explanatory by comparing the scale. It is worth mentioning to note here that we have used the fast dust-charge relaxation rate as $\nu_0 = 2.0 \times 10^{-5} \left(\omega_{pe}^2 + \omega_{pi}^2\right)^{1/2} / \omega_{pd}$.

6.4.2 Effect of the dust number density

The presence of dust particles alters the collective behavior of the electron-ion plasma, leading to dust ion acoustic (DIA) and dust acoustic (DA) waves due to static and mobile

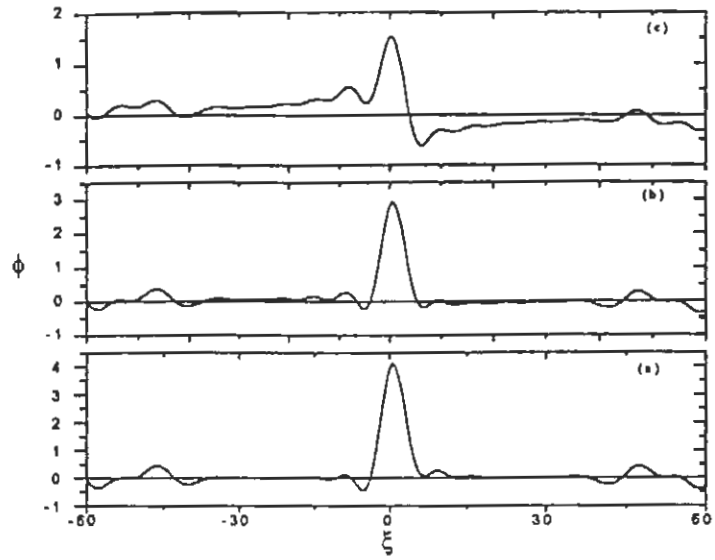

Figure 6-5: The normalized ES potential ϕ ($\times 10^{-5}$) versus normalized axial position $\xi\,(= z - V_t t)$ with the test charge velocity $V_t = 10$ cm/sec, $n_{d0} = 10^5\ cm^{-3}$, $Z_{d0} = 10^3$and the dust-neutral collision frequency (a) $\nu_{d0} = 0.0\ \omega_{pd}$, (b) $\nu_{d0} = 0.25\ \omega_{pd}$, (c) $\nu_{d0} = 0.5\ \omega_{pd}$, while other parameters are the same mentioned in the text.

dust grains, respectively. The number of dust particles varies from very few to a very large value [82]. So, it is worth while to simulate the results for different number densities of the dust particles. In Fig. (6.3), we present the numerically calculated ES potential for $10^2 < n_{d0} < 6 \times 10^3$ against the normalized axial position ξ, keeping other parameters the same as in Fig. (6-1). The results for the energy loss per unit path length against the normalized test charge velocity are presented in Fig. (6-4) for $10^3 < n_{d0} < 11 \times 10^3\ cm^{-3}$.

From Fig.(6-3), we observe that an increase in the dust number density n_{d0} in the range $10^2 < n_{d0} < 6 \times 10^3\ cm^{-3}$, reduces ϕ for test charge velocity $V_t < 50$ cm/s.

For $V_t \approx 20$ cm/s, the wake field behind the moving test charge shifts slightly ahead of the test charge. For higher values ($V_t > 50$ cm/s), as dust number density increases, the amplitude of ϕ first increases around the origin and then decreases, having (weakly damped large wavelength) wake field extended up to several Debye lengths as shown in Fig. 6.3 (c). For this range of velocity V_t, the potential perturbation is no longer a Debye Hückel potential. At this stage, nonlinear effects have set in, for which further analytical work is

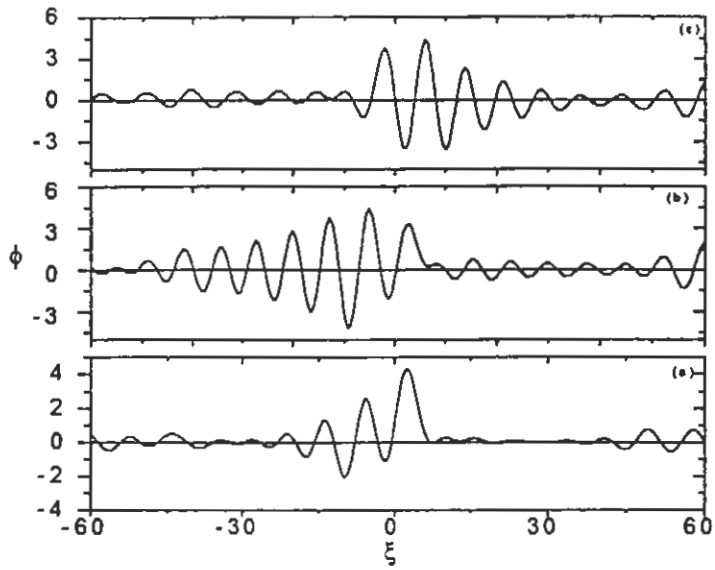

Figure 6-6: The same as Fig. (6.5), except the test charge velocity is $V_t = 20$ cm/sec.

needed.

Enhancement in the energy loss curve is observed for higher values of dust number densities in the range $10^3 > n_{d0} > 11 \times 10^3\ cm^{-3}$ for $Z_{d0} = 200$. For $n_{d0} > 10^4\ cm^{-3}$, the energy loss curve saturates, signifying that the dust plasma has acquired a state in which the effect of electrons is completely washed out and that the plasma has only ion–dust components. These results are further modified due to dust-neutral collisions and charge fluctuations, are discussed in the next section.

6.4.3 Effect of the dust-neutral collision frequency

We have numerically solved Eqs.(6.6) and (6.14) for the ES potential and the energy loss, respectively, taking some typical parameters as $T_d = 0.1\ eV$, $T_i = 0.3\ eV$, $T_e = 2.0\ eV$, $n_{i0} = 10^8\ cm^{-3}$and $m_d = 10^8 m_p$, where m_p is the mass of proton.

We then plot ϕ against the normalized axial position $\xi\ (= z - V_t t)$ for different values of the normalized collision frequencies $0.0 \leq \nu_{d0} \leq 0.5$, using test charge velocity $V_t = 10$ cm/s in Fig.(6-5) and $V_t = 20$ cm/s in Fig.(6-6). The collisions are observed to modify the shape of the Debye-Hückel potential for the lower test charge velocity ($V_t <$ dust sound

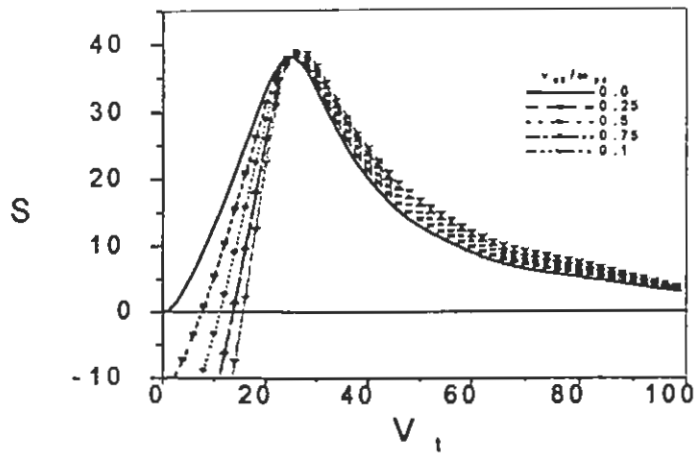

Figure 6-7: The energy loss per unit path length S versus test charge velocity for dust neutral collision frequency ν_{d0} $(0 \leq \nu_{d0} \leq \omega_{pd})$, while other parameters remain the same as in Fig. (6.1).

speed C_d). The potential takes on negative values when the collision frequency becomes large. Collisions also pronounce the wake field excited by the *DAW* and it overshoots the test charge for higher collision frequencies.

For subsonic motion of the particles, the collisions change the screening properties of the plasmas. When $\nu_{d0} \gg \mathrm{K} \cdot \mathrm{V}_{td} \gg \mathrm{K} \cdot \mathrm{V}_t$ or roughly $\xi \gg \lambda_m \gg V_t/\nu_{d0}$, then the far-field potential falls slowly as compared with collisionless case. In the collision dominated case the far-field potential varies as $1/\xi^2$ instead of $1/\xi^3$ for collisionless plasma[83]. In the other limit $\nu_{d0}\mathrm{K} \cdot \mathrm{V}_t \gg K^2 v_{td}^2$, then the test charge is no more shielded and consequently have a Coulomb type potential [see e.g., Fig.(6-5)b]. Physically, this result may be explained by the fact that due to relatively high speed of the test charge and high collision frequency of the dust particles, the latter are unable to response locally to the presence of the test charge. When the mean free path λ_m $(= v_{td}/\nu_{d0})$ is comparable to the effective screening length λ_{eff} $(= V_t/\omega_{pd})$ or even large, then the far-filed potential falls off less rapidly and when $V_t = C_d$ (the dust sound speed), the wake filed in the tail of the test charge will falls of slowly as compared with collisionless plasma. This means that the wake field is more pronounced and damps slowly as can be seen from Fig.(6-6).

The calculation of the ES potential shows that there is a non-Coulombic potential besides

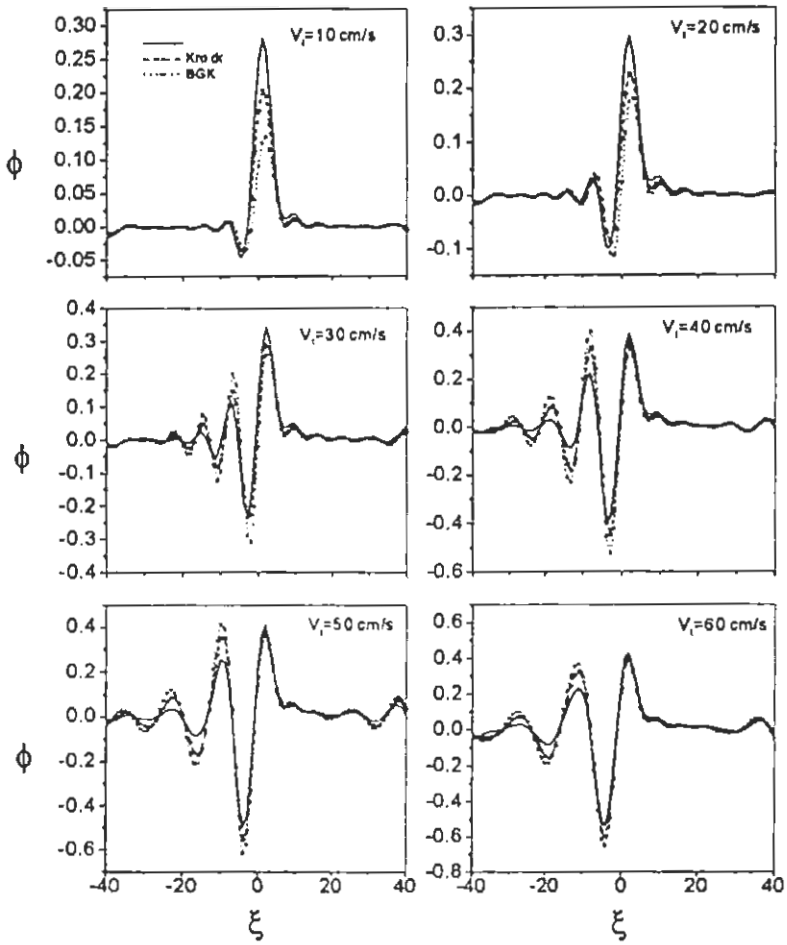

Figure 6-8: The normalized ES potential ϕ ($\times 10^{-5}$) versus the normalized axial position $\xi\,(= z - V_t t)$ without collisions (solid line), with Krook collisions (dashed line) and BGK collisions (dotted line) $\nu_{d0} = 0.2\ \omega_{pd}$, and the test charge velocity (a) $V_t = 10$ cm/s (b) $V_t = 20$ cm/s (c) $V_t = 30$ cm/s (d) $V_t = 40$ cm/s (e) $V_t = 50$ cm/s (f) $V_t = 60$ cm/s(c), with $n_{i0} = 10^9\ cm^{-3}$, $n_{d0} = 10^5\ cm^{-3}$; $T_e = 2.0$ eV;$T_i = 0.3$ eV;$T_d = 0.03$ eV; $Z_{d0} = 10^3$;$n_{d0} = 10^4$.

the usual Debye screening potential. When the test charge velocity is comparable to the phase velocity of the DAW, a wake field in the trail of test charge is produced. This wake field is further pronounced when dust-neutral collisions are incorporated. Physically, the test charge particle polarizes the medium by attracting positive ions that are involved in the collective behavior of the DAW. An excess of positive ions attract the neighboring dust particles. When the test particle velocity is close to the phase velocity of dust acoustic wave, the potential behind the test charge forms an oscillatory wake field. This wake field is weakly damped and persists up-to several Debye lengths. Due to dust-neutral collisions the amplitude of this wake field increases as a result of trapping of the ions in the wake field and due to the absence of linear damping caused by electron and ion plasma.

To investigate the energy loss, we have numerically solved Eq.(6.14) using the dielectric response function which incorporates the BGK collisions. The results are plotted against the normalized test charge velocity for different collision frequencies in Fig. (6-7). For a given collision frequency, there is a critical value of the test charge velocity V_c, below which the test charge gains energy instead of loosing. Which means that all particles with $V_t < V_c$ will gain energy and will thus accelerate. The value of the critical velocity depends upon the collision frequency and is observed to shift upward as the collision frequency increases. In other words, the higher the collision frequency, the greater will be the acceleration. The maximum energy loss rate occurs when the test charge velocity becomes comparable to the phase velocity of the dust acoustic wave C_d. The collisions however, only slightly shift the maximum towards the right. It is also observed that the energy loss rate is reduced when $V_c < V_t < C_d$, but increases when $V_t > C_d$.

Due to dust-neutral collisions, a critical test charge velocity is identified below which the test charge gains energy instead of losing. This critical velocity depends upon the dust-neutral collision frequency. It shows that for test charge velocities smaller than the thermal velocity of dust particles, the test charge particle will be accelerated up to the temperature of the surrounding plasma. This exhibits the fact that subsonic dust particles can absorb phonon rather than emit them[88] which is the well known acoustic Cherenkov effect. These results are useful to understand the wave phenomenon produced in a partially ionized dusty plasma in which dust-neutral collisions play an important role. Uptill now we have only

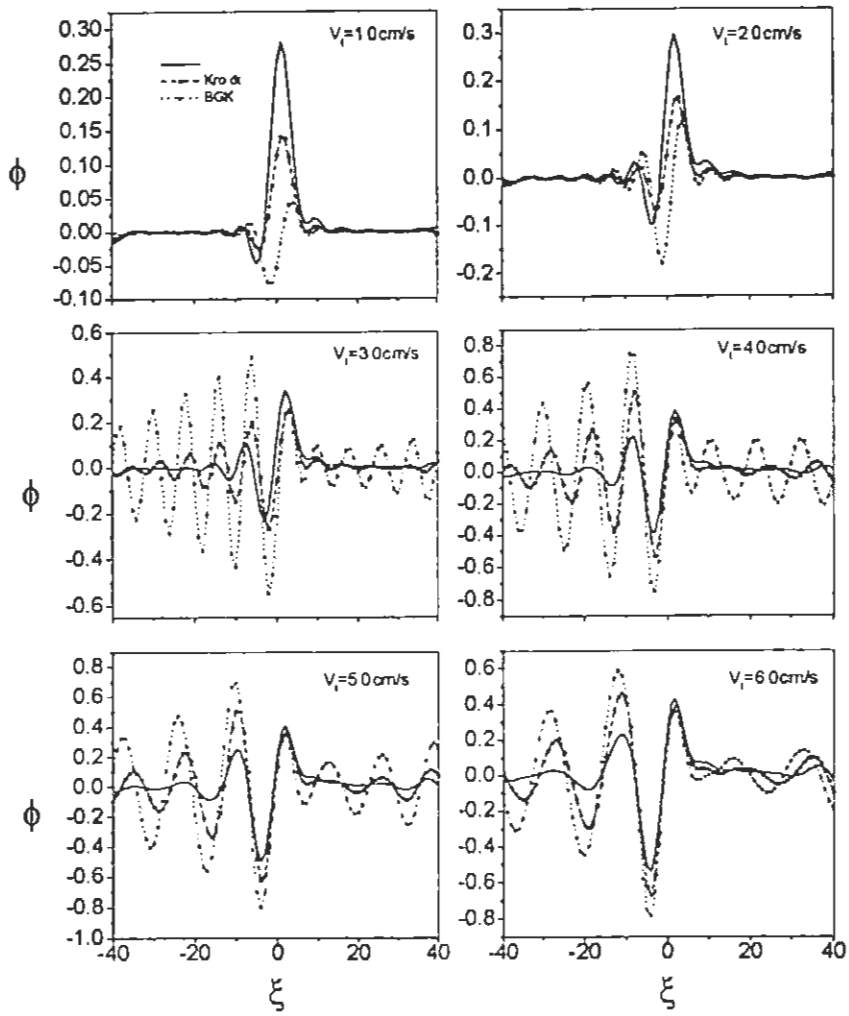

Figure 6-9: The same as Fig. (6.5), except the dust-neutral collision frequency $\nu_{d0} = 0.4$ ω_{pd}.

discussed the collision using BGK collisional operator.

In our calculation we have used the BGK and Krook collision operators for the calculations of the dielectric response function and their effects are discussed below.

We have numerically solved (6.6) for the ES potential (ϕ) by inserting the dielectric response function from (6.11) for Krook type collisions and from (6.13) for BGK type collisions. We then plot ϕ against the normalized axial position $\xi\,(= z - V_t t)$ for different values of the test charge velocities with a fixed value of the normalized collision frequencies $\nu_{d0} = 0.2\ \omega_{pd}$ in Fig.(6-8) and $\nu_{d0} = 0.4\ \omega_{pd}$ in Fig.(6-9). The collisions are observed to modify the shape of the Debye-Hückel potential for the lower test charge velocity ($V_t <$ dust sound speed C_d). The potential takes on negative values when the collision frequency becomes large. Collisions also pronounce the wake field (excited by the DAW) so much so that the wake field overshoots the test charge for higher collision frequencies. Moreover, fast collisions are observed to stabilize the non-linear (transient) effects produced by supersonic motion of the test charge leading to a weakly damped wake field of large wavelength.

Comparing the two models, we find that for the subsonic motion of the test charge, the BGK model is observed to reduce the amplitude of ϕ around the origin more than the Krook model . However, for the sonic motion, the BGK collisions pronounce the wake field more. This wake field is weakly damped and has greater wavelength with the higher test charge velocity [see Fig. (6-9) d].

To investigate the energy loss, we have numerically solved (6.14) using the dielectric response function which incorporates the BGK and Krook collisions. The results are plotted against the normalized test charge velocity for different collision frequencies without and with dust-charge fluctuations in Fig.(6-10) and in Fig.(6-11) respectively. It is observed that for subsonic or super-sonic motion of the test charge particle energy loss rate is large for BGK collisional model than Krook model.

Dust charge fluctuations are observed to enhance the energy loss for both the subsonic and sonic test charge particles. Collisions, however, enhance the energy loss rate for only supersonic test charge particles. Note that we have used a relatively fast charge relaxation rate ($\nu_0 = 10^{-4}\left(\omega_{pe}^2 + \omega_{pi}^2\right)^{1/2}/\omega_{pd}$.) in the present calculation so as to study the effect of dust charge fluctuations and a detailed discussion of which is given in CHAPTER 5.

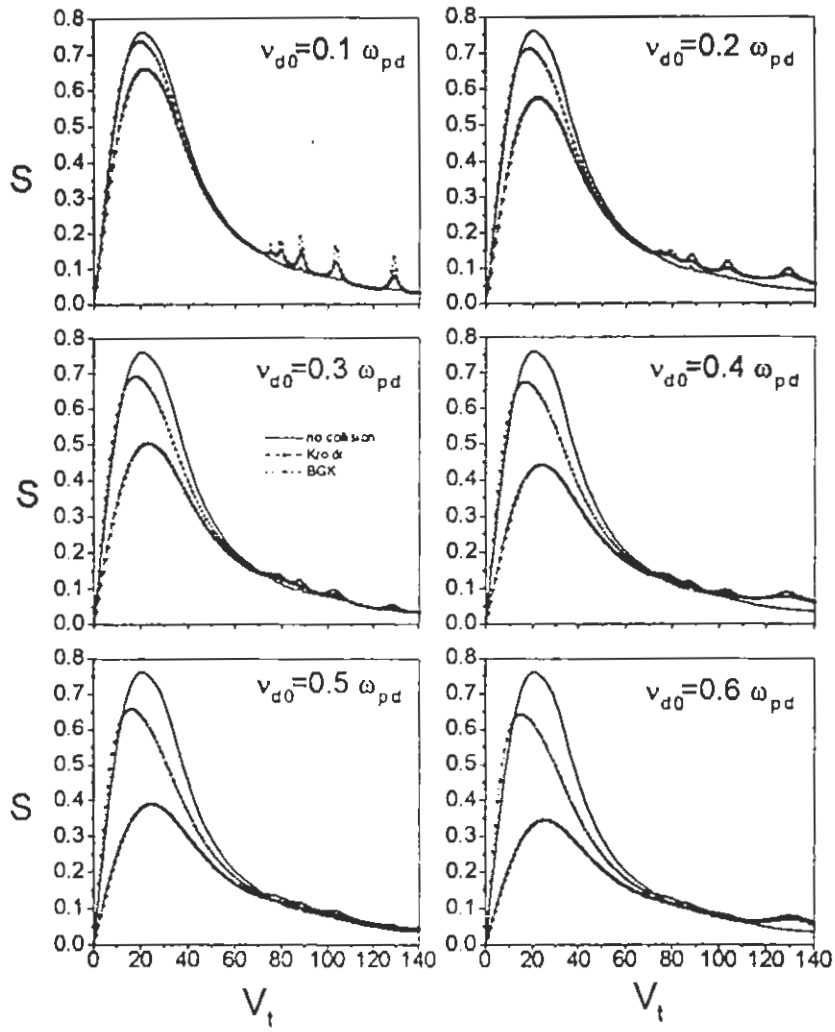

Figure 6-10: The energy loss per unit path length $(-dE/dx)$ versus test charge velocity V_t, without collisions (solid line), with Krook collisions (dashed line) and BGK collisions (dotted line), other parameters remain the same as in Fig. (6.5).

6.5 Summary and conclusions

We have presented a numerical evaluation of the potential due to a test particle moving with a uniform speed V_t through a dusty plasma, whose constituents are electrons, singly ionized positive ions, negatively charged micron-size dust particles and a sufficient amount of neutrals, taking into account the dusty dielectric response which includes collisions. The energy loss per unit path length of the test particle has also been calculated by knowing the force that the test particle experiences in its own induced field. In our analysis, we have assumed that all the plasma particles are point charges and that all the dust particles have the same mass and the same equilibrium charge. This assumption is quite valid under the condition $a \ll \lambda_D \ll \lambda_{mfp}$, where a is the size of the dust particle, λ_D the effective Debye length, and λ_{mfp}, the collision mean–free–path. Collisional effects included are based on the BGK and Krook models. While the Krook model is rather crude and only changes the wave frequency ω to $\omega + i\nu_{do}$, the BGK collision operator introduces nontrivial effects.

The calculation of the ES potential shows that there is a non-Coulombic potential besides the usual Debye screening potential. When the test charge velocity is comparable to the phase velocity of the DAW, a wake field in the trail of test charge is produced. This wake field is further pronounced when dust-neutral collisions are incorporated. Physically, the test charge particle polarizes the medium by attracting positive ions that are involved in the collective behavior of the DAW. An excess of positive ions attract the neighboring dust particles. When the test particle velocity is close to the phase velocity of dust acoustic wave, the potential behind the test charge forms an oscillatory wake field. This wake field is weakly damped and persists up-to several Debye lengths. Due to dust-neutral collisions the amplitude of this wake field increases as a result of trapping of the ions in the wake field and due to the absence of linear damping caused by electron and ion plasma. For very large test charge velocities, non-Coulombic effects behind the test particle are stabilized due to collisions but are converted to wake field due to dust charge fluctuations.

It is observed that for test charge velocities smaller than the thermal velocity of dust particles, the test charge particle will be accelerated up to the temperature of the surrounding plasma. This exhibits the fact that subsonic dust particles can absorb phonon rather than

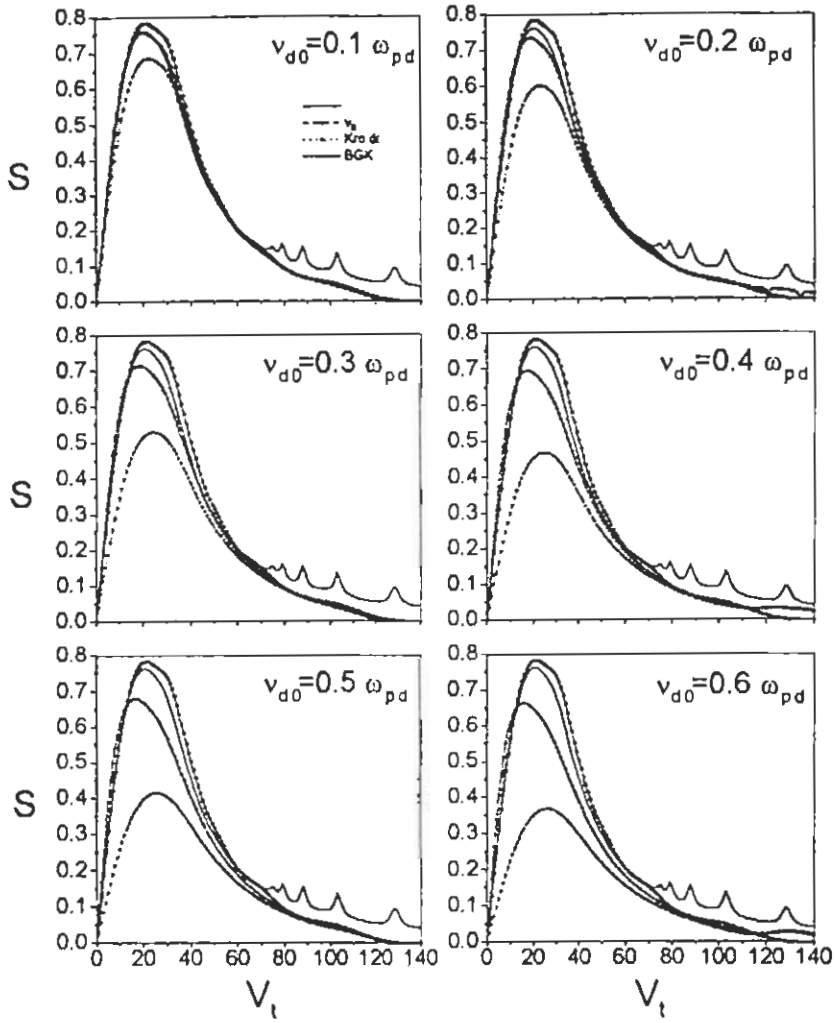

Figure 6-11: The same as Fig. (6.10) except for the dust charge fluctuations

emit them[88] which is the well known acoustic Cherenkov effect. Moreover, the effects of the dust charge state and the dust number density are also investigated. These results are useful to understand the wave phenomena produced in a partially ionized dusty plasma in which dust-neutral collisions and dust charge fluctuations play an important role.

Bibliography

[1] N. Bohr, K. Dan, Vidensk, Selsk., Mat.-Fys. Medd. **18**, No. 8 (1948).

[2] N. R. Arista, Phys. Rev. B **18**, 1 (1978).

[3] T. Peter and Mayer-ter-Vehn, Phys. Rev. A **43**, 1998 (1991).

[4] E. M. Bringa and N. R. Arista, Phys. Rev. E **52**, 3010 (1995); *ibid.* **54**, 4101 (1996).

[5] Proceeding of the Informal Workshop on the "*Penetration of Charged Particles in Matter Under Extreme Conditions*", New York University, January 1980 (unpublished).

[6] N. Arista and W.Brandt, Phys. Rev. A 23,1898(1981).

[7] L. Spitzer, Jr., *Physics of Fully Ionized Gases* (Interscience, New York, 1962).

[8] S. Chandrasekhar, Astrophys. J **93**,285(1941).

[9] M. Gryzinski, Ohys. Rev. **107**,1471(1957).

[10] S. T. Butler and M.J. Buckingham, Phys. Rev. **126**, 1(1962).

[11] G. Zwicknagel and C. Deutsch, Phys. Rev. E 56, 970 (1997).

[12] C. Deutsch, Laser Part. Beams 8, 541 (1990) and references therein.

[13] heavy ion pump laser

[14] J. J. Duderstadt and G. A. Moses, *Inertial Confinement Fusion*, Wiley & Sons, New York, 1982.

[15] J. H. Chu, J. B. Du, and Lin I., J. Phys. D 27, 296 (1994).

[16] C. K. Goertz, Rev. Geophys. **27**, 271 (1989).

[17] T. G. Northrop, Physica Scripta **45**, 475 (1992).

[18] P. K. Shukla, in *The Physics of Dusty Plasmas*, Editors: P. K. Shukla, D. A. Mendis, and V. W. Chow (World Scientific, Singapore, 1996), p. 107.

[19] N. N. Rao, P. K. Shukla, and M. Y. Yu, Planet. Space Sci. **38**, 543 (1990).

[20] P. K. Shukla and V. P. Silin, Phys. Scripta **45**, 508 (1992).

[21] M. Rosenberg, Planet. Space Sci. **41**, 229 (1993).

[22] R. K. Varma, P. K. Shukla, and V. Krishan, Phys. Rev. E **47**, 3612 (1993).

[23] F. Melandsø, T. K. Aslaksen, and O. Havnes, Planet. Space Sci. **45**, 1142 (1993).

[24] A. Barkan, R. L. Merlino, and N. D'Angelo, Phys. Plasmas **2**, 3563 (1995); C. Thompson, A. Barkan, N. D'Angelo, and R. L. Merlino *ibid.* **4**, 2331 (1996).

[25] A. Barkan, N. D'Angelo, and R. L. Merlino, Planet. Space Sci. **44**, 239 (1996).

[26] H. R. Prabhakara and V. L. Tanna, Phys. Plasmas **3**, 1212 (1996).

[27] M. R. Jana, A. Sen, and P. K. Kaw, Phys. Rev. E **48**, 3930(1993).

[28] M. H. Nasim, P. K. Shukla, and G. Murtaza, Phys. Plasmas, **6**,1409(1999).

[29] B. P. Pandey, K. Avinash and C. B. Dwivedi Phy. Rev. E, **49**, 5599(1994).

[30] D. Pines and D. Bohm, Phys. Rev. **85**, 338(1952).

[31] A. G. Sitenko, *Electromagnetic Fluctuations in Plasma* (Academic, New York, 1967).

[32] J. Neufeld and R. H. Ritchie, Phys. Rev. **98**, 1632 (1955).

[33] J. R. Sanmartin and S. H. Lam, Phys. Fluids **14**, 62 (1971).

[34] L. Chen, A. B. Langdon and M. A. Lieberman, J. Plasma Phys. **9**, 311 (1973).

[35] N. R. Arista and V. H. Ponce, J. Phys. C **8**, L188(1975).

[36] N. R. Arista, Phys. Rev. B **18**, 1 (1978).

[37] W. Brandt, A. Ratkowski, and R. H. Ritchie, Phys. Rev. Lett. **33**, 1325 (1974).

[38] D. S. Gemmell, J. Remillieux, J. C. Poizat, M. J. Gaillard, R. E. Holland, and Z. Vager, Phys. Rev. Lett. **34**, 1420 (1975).

[39] G. Basbas and R. H. Ritchie, Phys. Rev. A 25, 1943 (1982).

[40] M. H. Nasim, A. M. Mirza, M. S. Qaisar, G. Murtaza, and P. K. Shukla, Phys. Plasmas **5**, 3581(1998).

[41] M. H. Nasim, M. S. Qaisar, Arshad M. Mirza, , and G. Murtaza, "*Energy loss of a dust grain in dusty plasma*" appear in the "*Proc. 7th National Symposium on Frontiers in Physics*", Quaid-i-Azam University , Islamabad, Pakistan, 19-21 November, 1998.

[42] M. H. Nasim, G. Murtaza and Arshad M. Mirza, "*Anisotropy in the energy loss of charged projectiles in plasmas*", Phys. Plasmas, 2000 (submitted to).

[43] M. H. Nasim, Arshad M.Mirza, G.Murtaza and P. K. Shukla, Physica Scripta, 59, 379-388(1999).

[44] M. H. Nasim, M. S. Qaiser, Arshad M. Mirza, G. Murtaza and P. K. Shukla, "*Energy loss of a test charge in partially ionized dusty plasma*", Phys. Plasmas, **7**, number 2, pp 2000

[45] M. H. Nasim, Arshad M. Mirza, G. Murtaza and P. K. Shukla, "Collisional effects on the *energy loss of a test charge in dusty plasma*", Physica Scripta, 2000, (appear in).

[46] S. Ichimaru, *Basic Principles of Plasma Physics: A Statistical Approach* (Benjamin, Reading, 1973).

[47] N. A. Krall and A. W. Trivelpiece, *Principles of Plasma Physics* (McGraw Hill, New York, 1973).

[48] N. Rostoker Nucl. Fusion **1**, 101(1960).

[49] T. Peter, J. Plasma Phys. **44**, 269(1990).

[50] P. Debye and E. Hückel, Physik. Z. **24**,185(1923).

[51] N. D'Angelo, A. Barkan and R. L. Merlino, in *The Physics of Dusty Plasmas*, Editors: P. K. Shukla, D. A. Mendis, and V. W. Chow (World Scientific, Singapore, 1996), p. 93.

[52] H. M. Thomas and G. E. Morfill, in *The Physics of Dusty Plasmas*, Editors: P. K. Shukla, D. A. Mendis, and V. W. Chow (World Scientific, Singapore, 1996), p. 199.

[53] F. Melandsø Physica Scripta, **45**, 515 (1992).

[54] W. Brandt, A. Ratkowski and R. H. Ritchie, Phys. Rev. Lett. **33**, 1325(1974).

[55] N. R. Arista and V. H. Ponce,J. Phys. C **8**, L188(1975).

[56] W. Brandt, and R. H. Ritchie, Nucl. Instrum. Methods **132**, 43(1976).

[57] C. Deutsch and N. A. Tahir, Phys. Fluids B 4, 3735(1992).

[58] C. Deutsch et al. Fusion Technology **29**, 306(1996).

[59] C. Deutsch, P. fromy, and HG. Zwicknangel, Laser Particle Beams, **14**, 699(1996).

[60] J. D Avanzo and M. Lontano Phys. Rev. A, **45**, 6126(1992).

[61] J. D Avanzo, M. Lontano and P. F. Bortgon Phys. Rev. E, **47**, 3574(1993).

[62] M. Lontano and F. Raimond, Phys. Rev. E, **51**, R2755(1995).

[63] N. Otani and A. Bhattacharjee, Phys. Rev. Lett. **78**, 1468 (1997).

[64] V. N. Tsytovich, U. de Angelis, R. Bingham, and D. Resendes, Phys. Plasmas **4**, 3882 (1997).

[65] N. D'Angelo, A. Barkan and R. L. Merlino, in *The Physics of Dusty Plasmas*, Editors: P. K. Shukla, D. A. Mendis, and V. W. Chow (World Scientific, Singapore, 1996), p. 93.

[66] H. M. Thomas and G. E. Morfill, in *The Physics of Dusty Plasmas*, Editors: P. K. Shukla, D. A. Mendis, and V. W. Chow (World Scientific, Singapore, 1996), p. 199.

[67] C. M. C. Nairn, B. M. Annaratone and J. E. Allen, in *The Physics of Dusty Plasmas*, Editors: P. K. Shukla, D. A. Mendis, and V. W. Chow (World Scientific, Singapore, 1996), p.1.

[68] J. Goree, Plasma Sources Sci. Techonl., **3**, 400(1994).

[69] J. R Bhatt and B. P. Pandey, Phys Rev. E **50**, 3980 (1994).

[70] F. Verheest, P. K. Shukla, N. N. Rao and P. Meuris, J. Plasma Phys. **58** 163 (1997).

[71] G. Praburam and J. Goree, Phys. Plasmas **3**, 1212 (1996).

[72] R. C. Hazelton and E. J. Yadlowsky IEEE Trans. Plasma Sci. **22**, 91 (1994).

[73] S. J. Choi and M. J. Kushner IEEE Trans. Plasma Sci. **22**, 138 (1994).

[74] F. Melandsø , Phys. Plasmas **3**, 3890 (1996).

[75] S. V. Singh and N. N. Rao and R. Bharuthram, Phys. Plasmas **5**,2477(1998).

[76] P. Meuris and F. Verheest, in *The Physics of Dusty Plasmas*, Editors: P. K. Shukla, D. A. Mendis, and V. W. Chow (World Scientific, Singapore, 1996), p. 159.

[77] P. K. Shukla, M. R. Amin, and G. E. Morfill, Phys. Scr., **59**, 389(1999).

[78] M. Rosenberg, and G. Kalman, Phys. Rev. E **56**, 7166 (1997).

[79] C. Uberoi, and Ajanta Datta, Phys. Plasmas, **5**, 4149(1998).

[80] A. A. Shaikh, A. C. Das, and V. B. P. Agrawal, Phys. Scr., **59**, 458(1999).

[81] A. V. Ivlev, D. Samsonov, J. Goree, G. Morfill, and V. E. Fortov, Phys. Plasmas, **6**, 741(1999).

[82] P. K. Shukla, and M. Rosenberg, Phys. Plasmas, **6**, 1038(1999).

[83] L. Stenflo, M. Y. Yu, and P.K. Shukla, Phys. Fluids **16**, 450 (1973).

[84] B. S. Tanenbaum, Plasma Physics, (McGraw-Hill, New York 1967)p. 184.

[85] P.L. Bhatanagar, E. P. Gross, and M. Krook, Phys. Rev. **94**, 511(1954).

[86] P. C. Clemmow, and J. P. Dougherty, "*Electrodynamics of Prticles and Plasmas*" (Addison-INC, 1961).

[87] D. B. Fried and S. D. Conte, *The Plasma Dispersion Function*, (Acedemic Press, New York, 1961).

[88] M. Luft, T. Meyer, W. D. Kraeft, H. H. Brouwer, P. P. J. M. Schram and B. Strege, Contrib. Plasma Phys. **30**, 369(1990).

```
*********************************************************
*     PROGRAM TO CALCULATE POTENTIAL                    *
*     By Using KROOK and BGK collisional operator       *
*                                                       *
*        &                                              *
*                                                       *
*     DUST CHARGE PERTURBATION (IF NECESSARY)           *
*********************************************************
      Real k1,k2,mu,k,kde,kdi,kdd,KD
      Real Lde,Ldi,Ldd,me,Mi,Md
      Real ni,ne,nd,NDe,NDi,NDd
      Real s(1100,11),kd1(11),ex1(1100)
c
      COMMON /k/k
      COMMON /mu/mu
      COMMON /bet/bet
      COMMON /x/x
      COMMON /ro/ro
      COMMON /z/z                        !Normalized charge state
      COMMON /fd/fd
      COMMON /fie/fie
      COMMON /vp/vp
      COMMON /vd/vd                      !Normalized projectile velocity
      COMMON /v0/v0                      !Normalized charge relaxation
      COMMON /KD/KD
      COMMON /bgk/bgk
      COMMON /vtd/vtd
      COMMON /vte/vte
      COMMON /vti/vti
c
      parameter(PI=3.14159265)
      OPEN(1,file='Fig5.dat',status='unknown')
      OPEN(2,file='Fig5.par',status='unknown')
c
c.. initialize the values for variations........
c
      Zd  = 1.0E3
      Zp  = 1.0E3
      eta = 1.0E-5
      tes = eta*Zd*Zd
      if(tes.lt.1.or.tes.gt.140)print*,' eta zd incorrect',tes
c-------------------------------------------------
      Te  = 2.0
      Ti  = 0.3
      Td  = 0.03
      ni  = 1.0E9            !ion number density
      ne  = (1-Zd*eta)*ni    !electron number density
      nd  = ni*eta           !dust number density
      ne=ni
c-------------------------------------------------
      eV  = 11600
c  Debye lengths in cm  ......
      Lde = 743*sqrt(Te/ne)
      Ldi = 743*sqrt(Ti/ni)
      Ldd = 743*sqrt(Td/nd)/Zd
c..masses are in energy units.........
      c  = 3.0E10
      me = 0.51E6/(c*c)
```

```
      Md = 1836*1.0E8*me      !md=10**10 mp
      Mi = 1836*me
c..Velocities are in cm/s.........
      vte = sqrt(Te/me)
      vtd = sqrt(Td/Md)
      vti = sqrt(Ti/Mi)
      Ci  = sqrt(Te/Mi)
      Cd  = sqrt(Te/Md)
c....Debye wave numbers..............
      kde  = (1/6.9)*sqrt(ne/(Te*eV))
      kdi  = (1/6.9)*sqrt(ni/(Ti*eV))
      kdd  = (1/6.9)*sqrt(nd*Zd*Zd/(Td*eV))
c-.. Plasma frequency in rad/s.........
      wpe  = 5.64e4*sqrt(ne)
      wpi  = 1.32e3*sqrt(ni)
      wpd  = 1.32e3*sqrt(nd)*zd/sqrt(md/mi)
      test2=0.5*wpd/pi
      if(test2.lt.1.or.test2.gt.100)print*,'freq. incorrect',test2
c... Number of particle in Debye sphere......
      NDe  = ne*lde**3
      NDi  = ni*ldi**3
      NDd  = nd*ldd**3
      IF(NDD.LT.1.0)PRINT*,'NDd is incorrect',ndd
c...Coupling parameter.................
      e     =4.8032E-10                    !electronic charge in cgs
      d     = (3/(4*pi*nd))**0.33333
      Gd    = zd*zd*e*e/(Td*d)
      Z     = Zp/NDe
c....neutral plasma collision........
      eLd  = sqrt(Ldd*Ldd+Lde*Lde+Ldi*Ldi)
      a    = 1.0E-1*eLd
c      a    = 5.0E-2                      !POP 3(8),3176(1996)
      dn   = 1.0E-1*Nd
c      Fd0   = PI*a*a*Vtd*dn
      Fd0  = 1.0E-4*wpd
      Fi   = PI*a*a*Vti*dn*1.0E-10
      Fie  = SQRT(wpe*wpe+wpi*wpi)        !Eff.charge relaxation rate
      Fie  = 2.0E-5*Fie/wpd
c.............................
      write(2,101)z,zd,eta,d,Gd,
     +   Te,Ti,Td,me,Mi,Md,Vte,Vti,Vtd,ci,cd
      write(2,102)ne,ni,nd,NDe,NDi,NDd,wpe,wpi,wpd,
     +   lde,ldi,ldd,kde,kdi,kdd
      write(2,203)a,dn,fd,fi,eld
c     write(*,203)a,dn,fd,fi,eld
c-----parameters are normalized-----------
c     vd=mu*vp/vtd
      v0=fie
      KD=SQRT(KDe*KDe+KDi*KDi)/KDd
      ro   = 0
      i    = 0
c.. limits of k - integration
      k1 = 0
      k2 = 1.0
      write(*,900)
900   format(1x, 'Enter min & max.value of test velocity  ',$)
      read(*,*)vdm,vdx
      vdi=(vdx-vdm)/2.0
```

```
*****************************************************************
      write(*,901)
901   format(1x, 'Enter norm. collision frequency ',$)
      read(*,*)fd1
      fd=fd1
      do 111 vp1=vdm,vdx,vdi
      vp=vp1/vtd                ! vp is normalized
c
      Do 100 bgk=0,2.0,1.0      !BGK=0 ; no collision
c                               !BGK=1 ; Krook's model
      fd=fd1                    !BGK=2 ; BGK model
      if (bgk.eq.0.0)fd=0
c
      bet     =1.0
      i       =i+1
      j       = 0
      ex1(j)  = 0
      KD1(i)  = vp1
      print*,i,vp1,vtd,vp,kd
c---------------------------------------
c
      do 10 x =-40,40,1
c---------------------------------------
      j      = j+1
      ex1(j) = x
c----------------------------------
      call quad2d(k1,k2,s1)
c----------------------------------
      s(j,i) = s1
c     print*,s(j,i)
c
10      continue
100     continue
111     continue
c
      write(1,103)(kd1(m),m=1,i)
      do l = 1,j
c     write(*,202)ex1(l),(s(l,m),m=1,i)
      write(1,202)ex1(l),(s(l,m),m=1,i)
      enddo
c*************************************************************
101     format(
     + 1x,'Charge state of Projectile  ( Zp/NDe) = ',1pe13.4,/
     + 1x,'Charge state of Dust         ( ZD )   = ',1pe13.4,/
     + 1x,'Ratio of nd/ni               ( eta)   = ',1pe13.4,//

     + 1x,'Spacing between the dust par  ( d )   = ',1pe13.4,/
     + 1x,'Coupling parameter for dust   ( Gd )  = ',1pe13.4,//

     + 1x,'Temperature of electron     ( Te )    = ',1pe13.4,' eV',/
     + 1x,'Temperature of ion          ( Ti )    = ',1pe13.4,' eV',/
     + 1x,'Temperature of dust         ( Td )    = ',1pe13.4,' eV',//

     + 1x,'Mass  of   electron         ( me )    = ',1pe13.4,' ev',/
     + 1x,'Mass of ion                 ( Mi )    = ',1pe13.4,' ev',/
     + 1x,'Mass of dust                ( Md )    = ',1pe13.4,' ev',//

     + 1x,'Thermal velocity of ele     ( Vte)    = ',1pe13.4,' cm/s',/
```

```
     + 1x,'Thermal velocity of ion     ( Vti)    = ',1pe13.4,' cm/s',/
     + 1x,'Thermal velocity of dust    ( Vtd)    = ',1pe13.4,' cm/s',/
     + 1x,'Ion sound speed             ( Ci )    = ',1pe13.4,' cm/s',/
     + 1x,'Dust sound speed            ( Cd )    = ',1pe13.4,' cm/s',//
     +  )
102     format(
     + 1x,'Number density of electron  ( ne )    = ',1pe13.4,'cm(-3)',/
     + 1x,'Number density of ions      ( ni )    = ',1pe13.4,'cm(-3)',/
     + 1x,'Number density of dust      ( nd )    = ',1pe13.4,'cm(-3)',//

     + 1x,'Electrons in Debye sphere   ( NDe )   = ',1pe13.4,/
     + 1x,'Ions in Debye sphere        ( NDi )   = ',1pe13.4,/
     + 1x,'Dust part in Debye sphere   ( NDd )   = ',1pe13.4,//

     + 1x,'Plasma freq. for electron   ( Wpe )   = ',1pe13.4,'cm(-3)',/
     + 1x,'Plasma freq. for ions       ( Wpi )   = ',1pe13.4,'cm(-3)',/
     + 1x,'Plasma freq. for dust       ( Wpd)    = ',1pe13.4,'cm(-3)',//

     + 1x,'Debye length for electron   ( Lde )   = ',1pe13.4,' cm  ',/
     + 1x,'Debye length for ions       ( Ldi )   = ',1pe13.4,' cm  ',/
     + 1x,'Debye length for dust       ( Ldd )   = ',1pe13.4,' cm  ',//

     + 1x,'wave number for electron    ( Kde )   = ',1pe13.4,'cm(-1)',/
     + 1x,'Wave number for ions        ( Kdi )   = ',1pe13.4,'cm(-1)',/
     + 1x,'Wave number for dust        ( Kdd )   = ',1pe13.4,'cm(-1)',//
     + //)
203     format(
     + 1x,'Size of dust grain           ( a )    = ',1pe13.4,' cm ',/
     + 1x,'Density of neutral dust      (  dn )  = ',1pe13.4,'cm (-3)',/
     + 1x,'Dust neytral frequency       ( Fd )   = ',1pe13.4,' s(-1)',/
     + 1x,'Ion neytral frequency        ( Fi )   = ',1pe13.4,' s(-1)',/
     + 1x,'Effective Debye length        (eLd)   = ',1pe13.4,' cm ')
c
104     format(1x,6(1pe11.3,1x))
105     format(7x,'vp',9x,'AK2e',8x,'Ak2i',8x,'Ak2d',8x,'K1',8x,'k2')
202       format(1x,f7.3,11(1pe11.3))
103     format(1x,'  exi  ',11(1pe10.3,1x))
      print*,fie,wpe,wpi,wpd
c     pause
      end
c
c-----------------------------------------------
c
      SUBROUTINE quad2d(k1,k2,ss)
      Real k1,k2,ss
c
c
      COMMON /k/k
      COMMON /mu/mu
      COMMON /bet/bet
      COMMON /x/x
      COMMON /ro/ro
      COMMON /z/z                       !Normalized charge state
      COMMON /fd/fd
      COMMON /fie/fie
      COMMON /vp/vp
      COMMON /vd/vd                     !Normalized projectile velocity
      COMMON /v0/v0                     !Normalized charge relaxation
```

```
      COMMON /KD/KD
      COMMON /bgk/bgk
c
      EXTERNAL h
      call qgausx(h,k1,k2,ss)
      return
      END
**************************************************
c   function to define integrand of potential     *
c                                                  *
      FUNCTION f(yy)                               *
**************************************************
      External bessj0
      external ff1,ff2
      Real k,mu,KD
      COMPLEX DIEL,DISD,FUN,EOT,q1,q2,w,at
      parameter(PI=3.14159265)
c
c
      COMMON /k/k
      COMMON /mu/mu
      COMMON /bet/bet
      COMMON /x/x
      COMMON /ro/ro
      COMMON /z/z                    !Normalized charge state
      COMMON /fd/fd
      COMMON /fie/fie
      COMMON /vp/vp
      COMMON /vd/vd                  !Normalized projectile velocity
      COMMON /v0/v0                  !Normalized charge relaxation
      COMMON /KD/KD
      COMMON /zz1/zz1
      COMMON /zz2/zz2
      COMMON /bgk/bgk
c.........................................
      mu=yy
      aa=0
      eot=CMPLX(0,1.0)
      vd=mu*vp
c-----------------------------------------------
      CALL G1(ff1,aa,vd,ar1)      !vd Vp/Vtd
      CALL G1(ff2,aa,fd,ar2)      !fd is collision frequency
      q1=CMPLX(ar1,ar2)           !complex integration exp(-q2*q2)
      q2=CMPLX(vd,fd)
      W=CEXP(-q2*q2)*(2.0*q1+CMPLX(0.0,SQRT(PI)))
      DISD=(1.0-q2*w)
      if(bgk.eq.2.0)DISD=(1.0-q2*w)/(1+eot*fd*w)
c-----------------------------------------------
      DIEL=K*K+KD*KD+DISD-eot*bet/CMPLX(vd,v0)
c     DIEL=K*K+KD*KD+DISD
      at=CMPLX(COS(k*mu*x),Sin(-k*mu*x))
      fun=k**2*at*(1/DIEL)
      f=real(fun)
c     print*,bet,eot*bet/CMPLX(vd,v0)
      return
      END
c ************************
      function ff1(az1)
```

```
c
c
      Real k,mu
      COMMON /k/k
      COMMON /mu/mu
      COMMON /bet/bet
      COMMON /x/x
      COMMON /ro/ro
      COMMON /z/z                          !Normalized charge state
      COMMON /fd/fd
      COMMON /fie/fie
      COMMON /vd/vd                        !Normalized projectile velocity
      COMMON /v0/v0                        !Normalized charge relaxation
      COMMON /KD/KD
      COMMON /zz1/zz1
      COMMON /bgk/bgk
      COMMON /vtd/vtd
      COMMON /vte/vte
      COMMON /vti/vti
c
      zz1=az1
c     q2=CMPLX(vd*mu,fd)
      ff1=EXP(zz1*zz1-fd*fd)*COS(2.*zz1*fd)
      return
      end
c *************************
      function ff2(az2)
c
c
      Real k,mu
      COMMON /k/k
      COMMON /mu/mu
      COMMON /bet/bet
      COMMON /x/x
      COMMON /ro/ro
      COMMON /z/z                          !Normalized charge state
      COMMON /fd/fd
      COMMON /fie/fie
      COMMON /vd/vd                        !Normalized projectile velocity
      COMMON /v0/v0                        !Normalized charge relaxation
      COMMON /KD/KD
      COMMON /zz2/zz2
      COMMON /bgk/bgk
      COMMON /vtd/vtd
      COMMON /vte/vte
      COMMON /vti/vti
c
      zz2=az2
c     q2=CMPLX(vd*mu,fd)
      ff2=EXP(-zz2*zz2+vd*vd)*COS(2.*zz2*vd)
      return
      end

*******************************************************

      FUNCTION h(xx)
      Real xx,mu1,mu2,k,mu,kd
      EXTERNAL f
```

```
c
c
      COMMON /k/k
      COMMON /mu/mu
      COMMON /bet/bet
      COMMON /x/x
      COMMON /ro/ro
      COMMON /z/z                          !Normalized charge state
      COMMON /fd/fd
      COMMON /fie/fie
      COMMON /vd/vd                        !Normalized projectile velocity
      COMMON /v0/v0                        !Normalized charge relaxation
      COMMON /KD/KD
      COMMON /bgk/bgk
c
      mu1(k)=0.0
      mu2(k)=1.0
      k=xx
      call qgausy(f,mu1(k),mu2(k),ss)
       h=ss
      return
      END
c
c*******************************************************
c                                                      *
c     end of user  supplied subroutines                *
c                                                      *
c*******************************************************
c
      SUBROUTINE qgausx(func,a,b,ss)
c-----------------------------------------------
      REAL a,b
      EXTERNAL func
      REAL dx,xm,xr,w(5),x(5)
      SAVE w,x
      DATA w/.2955242247,.2692667193,.2190863625,.1494513491,
     *.0666713443/
      DATA x/.1488743389,.4333953941,.6794095682,.8650633666,
     *.9739065285/
c
c--- initialize the return variable.........
      ss=0.0
c
      xm=0.5*(b+a)
      xr=0.5*(b-a)
      do 11 j=1,5
      dx=xr*x(j)
      ss=ss+w(j)*(func(xm+dx)+func(xm-dx))
11    continue
      ss=xr*ss
      return
      END
c-----------------------------------------------
      SUBROUTINE qgausy(func,a,b,ss)
      REAL a,b
      EXTERNAL func
      INTEGER j
      REAL dx,xm,xr,w(5),x(5)
```

```
      SAVE w,x
      DATA w/.2955242247,.2692667193,.2190863625,.1494513491,
     *.0666713443/
      DATA x/.1488743389,.4333953941,.6794095682,.8650633666,
     *.9739065285/
c
c--- initialize the return variable.........
      ss=0.0
c
      xm=0.5*(b+a)
      xr=0.5*(b-a)
      do 11 j=1,5
      dx=xr*x(j)
      ss=ss+w(j)*(func(xm+dx)+func(xm-dx))
11    continue
      ss=xr*ss
      return
      END
c-----------------------------------------------
      FUNCTION bessj0(x)
      REAL bessj0,x
      REAL ax,xx,z
      DOUBLE PRECISION p1,p2,p3,p4,p5,q1,q2,q3,q4,q5,r1,r2,r3,r4,r5,r6,
     *s1,s2,s3,s4,s5,s6,y
      SAVE p1,p2,p3,p4,p5,q1,q2,q3,q4,q5,r1,r2,r3,r4,r5,r6,s1,s2,s3,s4,
     *s5,s6
      DATA p1,p2,p3,p4,p5/1.d0,-.1098628627d-2,.2734510407d-4,
     *-.2073370639d-5,.2093887211d-6/, q1,q2,q3,q4,q5/-.1562499995d-1,
     *.1430488765d-3,-.6911147651d-5,.7621095161d-6,-.934945152d-7/
      DATA r1,r2,r3,r4,r5,r6/57568490574.d0,-13362590354.d0,
     *651619640.7d0,-11214424.18d0,77392.33017d0,-184.9052456d0/,s1,s2,
     *s3,s4,s5,s6/57568490411.d0,1029532985.d0,9494680.718d0,
     *59272.64853d0,267.8532712d0,1.d0/
      if(abs(x).lt.8.)then
      y=x**2
      bessj0=(r1+y*(r2+y*(r3+y*(r4+y*(r5+y*r6)))))/(s1+y*(s2+y*(s3+y*
     *(s4+y*(s5+y*s6)))))
      else
      ax=abs(x)
      z=8./ax
      y=z**2
      xx=ax-.785398164
      bessj0=sqrt(.636619772/ax)*(cos(xx)*(p1+y*(p2+y*(p3+y*(p4+y*
     *p5))))-z*sin(xx)*(q1+y*(q2+y*(q3+y*(q4+y*q5)))))
      endif
      return
      END
c*****************************************************************
      SUBROUTINE g1(func,a,b,ss)
c   subroutine use for integration
      REAL a,b
      EXTERNAL func
      INTEGER j
      REAL dx,xm,xr,w(5),x(5)
      SAVE w,x
      DATA w/.2955242247,.2692667193,.2190863625,.1494513491,
     *.0666713443/
      DATA x/.1488743389,.4333953941,.6794095682,.8650633666,
```

Chapter 7

Summary and Conclusions

This chapter summarizes the results of whole work in this task and conclusions drawn from them. Suggestions for further exploration of the subject are also outlined.

In this thesis, we have studied the potential perturbations caused by a test charge and cosequently the energy loss as it propagates through a multi-component dusty plasmas within the framework of dielectric theory. The dusty plasma, consists of electrons, singly charged positive ions, and extremely massive, micron size negatively charged dust particles with a small fraction of neutral dust. The dust charge is a time dependent variable and fluctuates about its equilibrium value. The amount of dust charge fluctuation depends upon the nature of the plasma. In our calculations we have treated the dust charge both as a constant and a dynamic variable. Moreover, only the dust-neutral collisions are incorporated.

Our numerical calculations show that the electrostatic potential is Debye-Hückel when the test charge velocity is greater than the dust thermal speed ($V_t \geq v_{td}$) and becomes Coulomb type when the test charge velocity grows bigger i.e., $V_t \gg v_{td}$ When the test charge velocity is comparable to the phase velocity of the dust acoustic (DA) speed ($V_t \simeq C_D$), a strong wake field in the trail of test charge appears. This wake field is weakly damped and persists up to several Debye lengths. Further, the wake-field is anisotropic with respect to the axial and radial directions, being stronger behind the trail of the test charge. Cosequently, the effective shielding length λ_{eff} ($\approx V_t/\omega_{pd}$) is greater than the Debye length λ_D ($= V_{td}/\omega_{pd}$) behind the test charge. Physically, the test charge particle polarizes the medium by attracting positive ions that are involved in the collective behavior of the DA waves.

The study has been extended to two projectiles moving with the same velocity but with a time lag (τ). Two cases are considered here (i) the two projectiles moving one behind the other along same direction (ii) they are moving in parallel direction with some separation. The separation distance (R) is an important parameter. It is observed that as long as R remains less than λ_D, the two projectiles behave as a single projectile with charge almost equal to the sum of the charges of the two projectiles. When R is very large ($\rightarrow \infty$), the motion of the two projectiles is completely uncorrelated. There is anisotropy in the energy loss rate. The total energy loss is large for collinear projectiles than the parallel, keeping the same separation. For large separations, the anisotropy becomes negligible. It is further noted that the inclination angle of the two projectiles with the direction of projectile motion is important. The energy loss rate depends upon the angle of inclination of the projectiles with their separation vector R. Maximum energy loss occurs for zero inclination i.e., the projectiles are collinear, and energy loss becomes smaller and smaller as we increase the angle and reaching its minimum value for 90^0 angle of inclination.

The study is further extended by incorporating the dust charge fluctuations. We find that the dust charge relaxation rate is a crucial parameter. For slow charge relaxation rate ($\nu_0 < \omega_{pd}$) , a potential well is formed by the slowly moving test charge ($V_t \simeq 0$), when a shielded potential occurs for fast moving test charge. It is worth mentioning that this shielded potential is on the negative side of the axial direction. This result is further supported when we calculate the energy loss rate. In this case the test charge gains energy instead of losing for all the test charge velocities. For fast charge relaxation rate, an increase in the potential perturbation is observed and cosequently an enhancement in the energy loss rate, compared to the case with no charge fluctuations. Moreover, for ($\nu_0 > \omega_{pd}$), some waves are excited showing peaking trend in the energy loss rate. These modes are damped when ν_0 is very large. More discussion can be found on page 56.

Finally, we have studied the effect of dust-neutral collisions by using Krook and BGK type collisional operators. When the dust-neutral collision frequency (ν_{d0}) is very large, the far-field potential falls slowly as compared with collisionless case. It means that the wake-filed (excited by DA waves) is more pronounced having large amplitude, extended upto several Debye lengths. In other words, the amplitude of this wake field becomes large due

to trapping of the opposite polarity charges. In the negative side of the wake filed, positive ions are trapped and vice versa. A critical test charge velocity is found below which the test charge gains energy and will be accelerated up to the ambient plasma temperature. This exhibits the fact that the subsonic dust particles ($V_t < C_D$) can absorb phonon rather than emit them. The effect of equilibrium dust charge state, the dust number density are also investigated.

Finally, we should incorporate some suggestions for further extension in this work. In this thesis, the equilibrium dust charges are assumed to be the same and all the dust particles are point particles. But in reality it is not always true. The dust particles have different sizes and having different charges. The effect of dust size distribution on the energy loss must be studied. Moreover, the dust particles are very massive and are of micron size, the gravitational potential becomes significant and can not be ignored. The gravitational effect on the energy loss should also be investigated. We have used Krook and BGK collisional operators to incorporate the dust-neutral collisions. These models do not conserve energy. It is recommended that more sophisticated collisional operators should be used and compared with our results. We have only considered the electrostatic case, a natural extension of the work is to consider the electromagnetic case for a magnetized dusty plasma.

```
     *.9739065285/
c
c--- initialize the return variable.........
      ss=0.0
c
      xm=0.5*(b+a)
      xr=0.5*(b-a)
      do 11 j=1,5
      dx=xr*x(j)
      ss=ss+w(j)*(func(xm+dx)+func(xm-dx))
11    continue
      ss=xr*ss
      return
      END
*************************************************************
```